(12)

TGAL-86-6

MULTICHANNEL DECONVOLUTION OF P WAVES AT SEISMIC ARRAYS AND THREE COMPONENT STATIONS

Z.A. Der, A.C. Lees, R.H. Shumway, T.W. McElfresh, and M.E. Marshall
Teledyne Geotech Alexandria Laboratories
314 Montgomery Street
Alexandria, Virginia 22314-1581

OCTOBER 1986

ANNUAL TECHNICAL REPORT:
ARPA ORDER NO: 4511
PROJECT TITLE: Source Time Function Deconvolution
CONTRACT: F08606-86-C-0006

Approved for Public Release; Distribution Unlimited.

Prepared for:
DEFENSE ADVANCED RESEARCH PROJECTS AGENCY
1400 Wilson Boulevard
Arlington, VA 22209

Monitored By:
AFTAC/TGR
PATRICK AFB
FLORIDA 32925-6001

UNCLASSIFIED

SECURITY CLASSIFICATION OF THIS PAGE

A184 45

REPORT DOCUMENTATION PAGE

Form Approved
OMB No. 0704-0188
Exp. Date: Jun 30, 1986

1a REPORT SECURITY CLASSIFICATION Unclassified	1b RESTRICTIVE MARKINGS
2a SECURITY CLASSIFICATION AUTHORITY	3 DISTRIBUTION / AVAILABILITY OF REPORT Approved for public release; Distribution is unlimited.
2b DECLASSIFICATION / DOWNGRADING SCHEDULE	
4 PERFORMING ORGANIZATION REPORT NUMBER(S) TGAL-86-6	5. MONITORING ORGANIZATION REPORT NUMBER(S)
6a NAME OF PERFORMING ORGANIZATION Teledyne Geotech Alexandria Laboratories 6b OFFICE SYMBOL (If applicable)	7a. NAME OF MONITORING ORGANIZATION AFTAC/TGR
6c. ADDRESS (City, State, and ZIP Code) 314 Montgomery Street Alexandria, Virginia 22314-1581	7b. ADDRESS (City, State, and ZIP Code) Patrick Air Force Base Florida 32925-6001
8a. NAME OF FUNDING / SPONSORING ORGANIZATION DARPA 8b OFFICE SYMBOL (If applicable) GSD	9. PROCUREMENT INSTRUMENT IDENTIFICATION NUMBER F08606-86-C-0006
8c. ADDRESS (City, State, and ZIP Code) 1400 Wilson Boulevard Arlington, Virginia 22209	10. SOURCE OF FUNDING NUMBERS PROGRAM ELEMENT NO. 62714E; PROJECT NO.; TASK NO.; WORK UNIT ACCESSION NO.

11. TITLE (Include Security Classification)

Multichannel Deconvolution of P Waves at Seismic Arrays and Three Component Stations

12. PERSONAL AUTHOR(S)

Z.A. Der, A.C. Lees, R.H. Shumway, E. Smart, T.W. McElfresh, and M.E. Marshall

13a. TYPE OF REPORT	13b. TIME COVERED	14. DATE OF REPORT (Year, Month, Day)	15. PAGE COUNT
Annual Report	FROM 10/1/85 TO 10/1/86	1986 October 30	117

16. SUPPLEMENTARY NOTATION

17. COSATI CODES			18. SUBJECT TERMS (Continue on reverse if necessary and identify by block number)
FIELD	GROUP	SUB-GROUP	
08	11		
17	10		

19. ABSTRACT (Continue on reverse if necessary and identify by block number)

The results of a new multichannel deconvolution method, applied to array recordings and three component station networks for teleseismic P waves, are presented and interpreted in terms of possible surface reflections and other arrivals from the Nevada Test Site (NTS), Novaya Zemlya, and Eastern Kazakh Test Site (EKTS) nuclear explosions. The deconvolution method utilizes the well known fact that P wave spectra can be decomposed into source and receiver spectral factors. The source functions obtained in the deconvolution process provide a better picture of the nature of explosion source time functions, and in particular of the presence or lack of secondary arrivals following the P wave such as pP or spall. The presence of such secondary arrivals and their effects on the first cycle of the P wave are very important in yield estimation. For most events at the eastern part of EKTS the source time functions appear to contain a pP arrival but they also show later, unexplained arrivals and other complexities. At other test sites often there are no clearly identifiable pP phases in the deconvolved traces. Joint

→ next page

20 DISTRIBUTION / AVAILABILITY OF ABSTRACT ☒ UNCLASSIFIED/UNLIMITED ☐ SAME AS RPT. ☐ DTIC USERS	21. ABSTRACT SECURITY CLASSIFICATION UNCLASSIFIED
22a. NAME OF RESPONSIBLE INDIVIDUAL Dr. Dean Clauter	22b. TELEPHONE (Include Area Code) (305) 494-5263 22c OFFICE SYMBOL TGR

DD FORM 1473, 84 MAR

83 APR edition may be used until exhausted
All other editions are obsolete

SECURITY CLASSIFICATION OF THIS PAGE
UNCLASSIFIED

(19. Continued)

deconvolution of central EKTS data using all AWRE arrays indicated strong azimuthal asymmetries in the body wave radiation. Deconvolutions of NTS events were considerably degraded by the limited signal bandwidth due to strong mantle attenuation under this test site. The site functions are also complex in most cases. Site and source effects contribute about equally to the energy observed in the P codas of the events analyzed. During the second year of this project, we will deconvolve several additional data sets, apply the deconvolution technique to three-component data, use the amplitude and area of the deconvolved source time functions to develop improved estimates of yield, and assess the combined influence of Q and pP on yield at the various test sites.

SUMMARY

The results of a new multichannel deconvolution method, applied to array recordings and three component station networks for teleseismic P waves, are presented and interpreted in terms of possible surface reflections and other arrivals from the Nevada Test Site (NTS), Novaya Zemlya, and Eastern Kazakh Test Site (EKTS) nuclear explosions. The deconvolution method utilizes the well known fact that P wave spectra can be decomposed into source and receiver spectral factors. The source functions obtained in the deconvolution process provide a better picture of the nature of explosion source time functions, and in particular of the presence or lack of secondary arrivals following the P wave such as pP or spall. The presence of such secondary arrivals and their effects on the first cycle of the P wave are very important in yield estimation. For most events at the eastern part of EKTS the source time functions appear to contain a pP arrival but they also show later, unexplained arrivals and other complexities. At other test sites often there are no clearly identifiable pP phases in the deconvolved traces. Joint deconvolution of central EKTS data using all AWRE arrays indicated strong azimuthal asymmetries in the body wave radiation. Deconvolutions of NTS events were considerably degraded by the limited signal bandwidth due to strong mantle attenuation under this test site. The site functions are also complex in most cases. Site and source effects contribute about equally to the energy observed in the P codas of the events analyzed. During the second year of this project, we will deconvolve several additional data sets, apply the deconvolution technique to three-component data, use the amplitude and area of the deconvolved source time functions to develop improved estimates of yield, and assess the combined influence of Q and pP on yield at the various test sites.

(THIS PAGE INTENTIONALLY LEFT BLANK)

TABLE OF CONTENTS

LIST OF FIGURES

LIST OF TABLES

INTRODUCTION

The determination of the effect of surface reflection and other secondary arrivals on the estimated yields of nuclear explosions has been a major problem in nuclear monitoring work. The major philosophical issues in such work are the following:

a) Are the explosion source functions simple superpositions of P and pP pulses or are more complex source time histories appropriate? Much of the previous work on P waveforms simply assumed the validity of the P+pP models and proceeded to fit the model to determine pP amplitudes and delay times.

b) Can we predict the effect of the secondary arrivals on the yields estimated from time domain measurements on the first cycle of the P wave signal? This depends on the resolvability of secondary arrivals and their physical interpretation.

c) What is the effect of these secondary arrivals on frequency domain measures of yield?

d) What are the limitations imposed by Q and the noise on the time resolution in separating multiple arrivals? Clearly, it is not possible to resolve pP delay times of a few tenths of a second along low Q paths.

e) And, in general, what processes, e.g. Q, scattering, near source and receiver wave conversions, spall, Rayleigh-to-P conversions, etc., determine the waveforms and spectra of teleseismic P waves?

In this progress report we present results of the application of a new maximum-likelihood iterative deconvolution technique which is designed to help resolve the above questions. The method is based on the factoring of P wave spectral matrices, consisting of recordings of multiple events at common test sites and using a common set of array sensors, into site and source related factors. The method has its roots in several previously proposed deconvolution techniques.

First, we discuss previous work in estimating pP times and amplitudes and previously developed deconvolution methods. Then we outline the maximum likelihood multichannel

deconvolution algorithm and present the results of deconvolutions of data from nuclear explosions at Pahute Mesa and Yucca Flats at the Nevada Test Site (NTS), at the Soviet Eastern Kazakh Test Site (EKTS), Novaya Zemlya, and the French Sahara test sites. The deconvolutions are interpreted in terms of the presence and characteristics of pP, the presence and complexity of other secondary arrivals and of the P wave coda, and azimuthal variations in the source-time function. We find that explosion source time functions, while they generally appear to contain a phase that is readily ascribable to pP, also contain a number of other arrivals. Both source and site terms appear to contribute to the presence of P coda.

BACKGROUND

One of the fundamental problems that motivate research on pP is the possible effects of such secondary arrivals on estimated yields. Assuming that m_b is used for deriving yields through some m_b-yield formula, a complex interaction of Q, source scaling, and pP interference will affect the measured m_b which can be modeled by synthetic simulation of the waveforms. For this we need reliable estimates of Q, source waveforms, and pP parameters derived from the data.

In much of the early work it was assumed that P waves are composed of P and pP pulses possibly convolved with some site-related transfer function. Therefore, a variety of methods have been proposed for estimating pP times and amplitudes. Spectral methods (Cohen 1970, 1975; Shumway and Blandford 1978) attempt to make use of the spectral modulation due to pP. In the case of complex site related modulation of P wave spectra, the spectral minima due to any, even solitary, pP arrival besides the direct P, may be completely disguised, thus making the interpretation of spectral minima difficult. Interpretation of power spectra in terms of multiple arrivals is totally nonunique since the phase information is lost and an infinite number of pulse sequences, derivable from each other by dispersive, all-pass filters (Robinson and Treitel 1980), may yield identical power spectra.

Direct modeling of narrow frequency band P waveforms was also frequently used for the determination of various source and path parameters in seismology (Burdick and Helmberger 1979, Bache 1982). It appears, however, that too high values of the attenuation parameter t^*_P were used in much of the past work and the results are not acceptable. This was also pointed out by Douglas (1986). Moreover, it has been shown by Cormier (1982) that in the case of explosion P waves, such waveform fits are highly nonunique because the attenuation parameter t^*, pP times and amplitudes, and the various source related parameters strongly trade off

against each other. Generally speaking, waveform fits are not satisfactory substitutes for deconvolutions which make use of the total information in seismic signals more efficiently and take advantage of the high dynamic range and consequently, the broad signal bandwidth provided by modern digital recording systems.

Another approach that has been proposed involves cross-equalization (or as the authors call it, "intercorrelation") of narrow band short period waveforms (Mellman and Kaufman 1981; Lay et al 1984 a,b). This method produces "pseudo-pP" delay times and amplitudes, i.e. the best fits to simple P+pP models. Since the results are not deconvolutions in the true sense they do not prove the existence or correctness of such models. (Lay et al 1984 a,b; Mellman et al 1984). However, it is easy to prove by simple simulations that very good cross-equalization (intercorrelation) of pairs of P wavetrains is possible with narrow band data, even if the wavetrains are considerably more complex than P+pP combinations. Moreover, interevent spectral amplitude ratios, which should be of the form

$$\frac{1 - \alpha_1 e^{-i\omega\tau_1}}{1 - \alpha_2 e^{-i\omega\tau_2}} \tag{1}$$

(because the site factors should cancel), cannot be fitted by any reasonable values of α_1 α_2, τ_1 or τ_2, where the α's and τ's are the pP amplitudes and delay times respectively. The forms of the spectral ratios computed from data are quite complex, indicating complex sequences of arrivals from the source regions (Der et al 1986b).

As a general comment, it may be stated that all proposed techniques seem to work quite well with synthetic data that conform to the proposed signal model. The problem is that it is rarely attempted to verify from the data that the underlying models are valid. Based on present knowledge, however, we cannot even be sure that pP arrivals exist in most P waves from nuclear explosions. For example, the spectral modulations introducing pP "nulls" in the spectra

are very rarely observed and often the associated "pP" lag times are unreasonably long. Moreover, it seems certain, that along some low Q paths a short pP delay time is not resolvable, and thus no usable pP "correction" may be derivable from the data.

Time domain methods for estimating pP times and amplitudes include various deconvolution schemes (Marshall 1972; Bakun and Johnson 1973; Kemerait and Sutton 1982; Israelson 1983) which generally preserve the phase information and do not depend on the simple P+pP model. Least squares (l_2 norm) deconvolution models work well, but those that use the l_1 norm (Levy and Fullagar 1981; Mellman et al 1984) were shown by Jurkevics and Wiggins (1984) to result in erroneous deconvolutions as judged by synthetic simulations. Deconvolution methods belong to the general type of "appraisal" methods, borrowing the terminology of Oldenburg (1981), in which we attempt to establish, from the data, signal models and to measure their parameters, as contrasted to the "direct modeling" waveform methods that attempt to fit the data to some *a priori* model without any attempt to verify its validity.

The purpose of the deconvolution methods is to transform the complex wavelets constituted from the attenuation operator, instrument, and, in some methods, the estimate of the source wavelet and/or the site function, into something resembling a delta function which can directly be recognized in the output by visual inspection (Figure 1). Preferably, we also strive to decrease the length of the wavelet, i.e. increase the time resolution. However, in practice it is impossible to obtain exact delta functions by deconvolution because of the bandwidth limitations in the signals, the fact that large explosions often do not contain enough high frequency energy, and the ever present background noise, and we must be satisfied with approximations to the delta function such as broader pulses resembling sin(x)/x functions. The resulting pulse is often broader that one would desire and small pP delay times may not always be resolvable. However, such limitations are fundamental in nature, inherent in the uncertainty principle, and

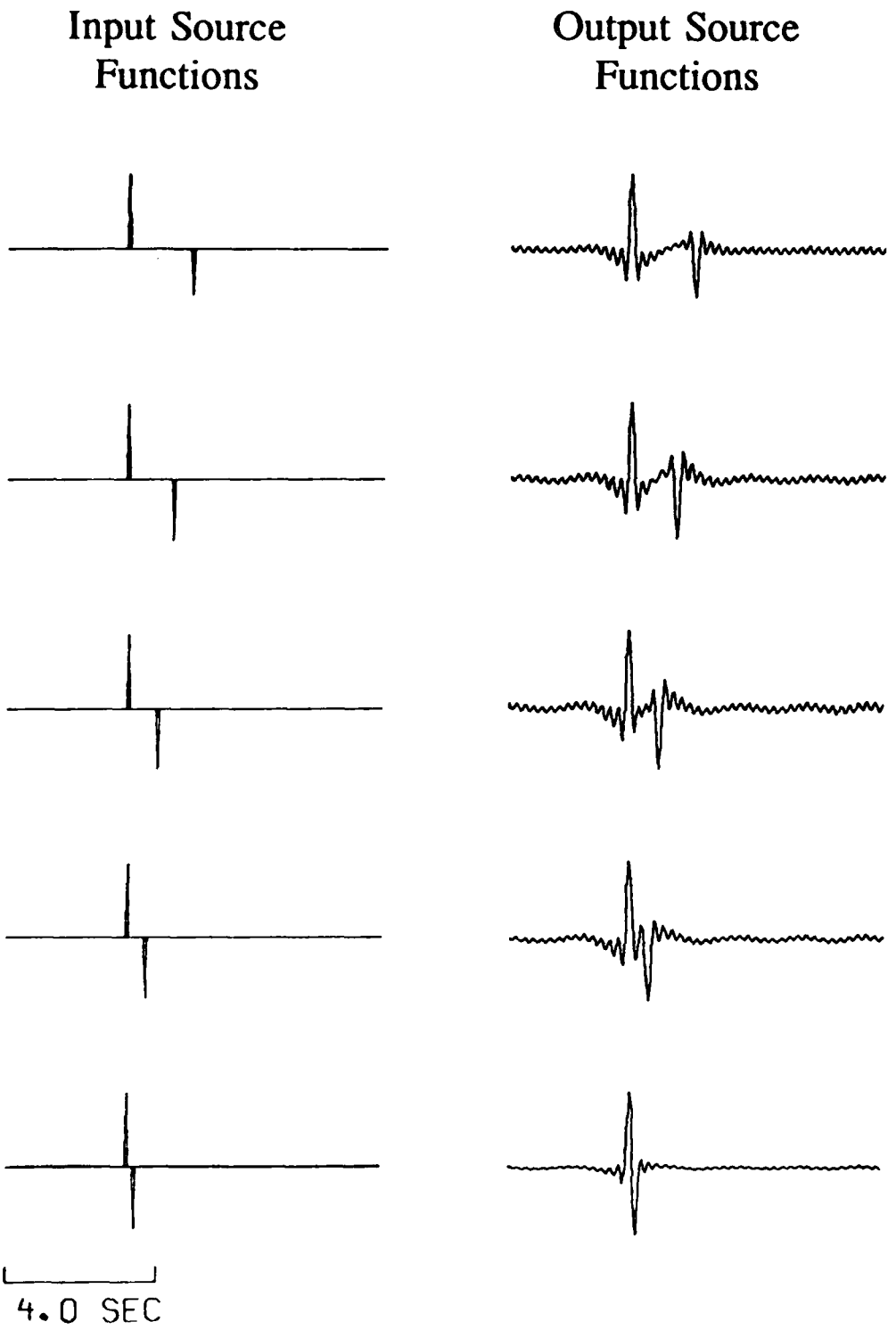

Figure 1. Band-limited deconvolution results for synthetic data. Input spike sequences for a range of pP times are shown on the left and the deconvolution output is shown on the right.

constitute a limit to the applicability of the seismic method which cannot be overcome. If the pP delay time is smaller that the width of the resolution kernel, deconvolution will yield progressively smaller amplitudes in the deconvolved P+pP waveforms with decreasing pP delay times without seeing any decrease between the positive and negative peak distances commonly used to estimate pP delay times. This problem is illustrated in Figure 2. Of course, for actual nuclear explosions there is a lower limit to the pP delay time, assuming everything to be linear. This is imposed by the minimum depth of containment in the rocks in question. Moreover, at very shallow depth the pP phase is expected to disappear, such for cratering explosions. If the pP arrival can be resolved in the deconvolutions the most logical approach is to use some measure of the energy in the first positive pulse of the deconvolved record to estimate yield without ever estimating m_b. This approach was followed by Douglas (1986) and should be preferable to estimating yields from m_b. The advantage of the maximum likelihood multichannel deconvolution method discussed in this paper is that it assumes little about the nature of the source and site factors, and it exploits the factorable nature of P wave spectra which is verified subsequently in each case by the reconstruction of the original data.

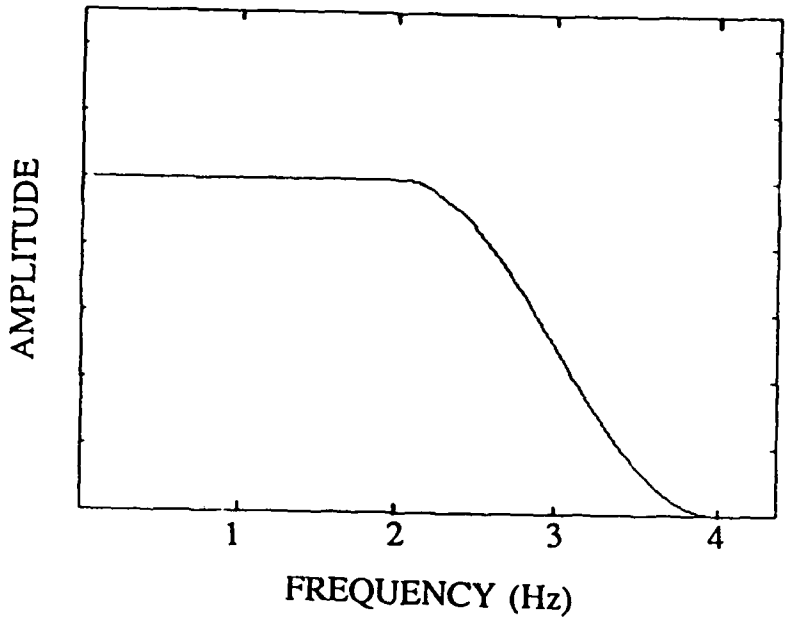

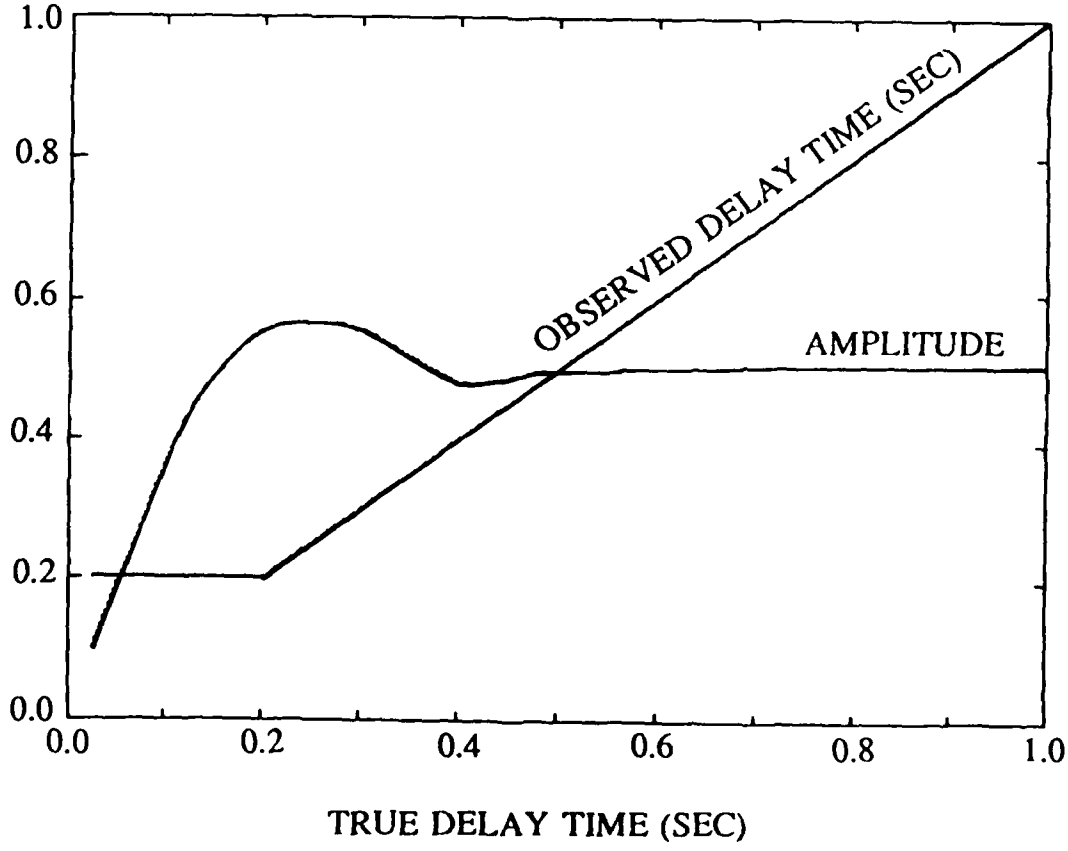

Figure 2. (Top) The spectral band of the P and pP wavelet used in the simulations. (Bottom) Estimated pP delay times and peak-to-peak amplitudes for band limited deconvolutions as functions of true pP time delay (horizontal axis).

DESCRIPTION OF THE DECONVOLUTION METHOD

A major advance in the understanding of the structure of teleseismic P waves was the finding by Filson and Frasier (1972) that P wave amplitude spectra from a set of events observed at a narrow range of azimuths at multiple array sites may be factored as

$$Y_{ij}(\omega) = R_i(\omega)\, S_j(\omega)\ , \qquad (2)$$

where $Y_{ij}(\omega)$ are the P wave spectra, $S_j(\omega)$ are source factors, and $R_i(\omega)$ are factors appropriate to the receiver sites. The validity of this equation has been verified for a number of seismic arrays as well as more widely separated receivers (Lundquist et al 1980) and the idea was also exploited for deriving "relative receiver functions", which are time domain representations of intersite transfer functions (Lundquist et al 1980) including Q effects. This model simply states the factorability of the spectral matrix without assuming any model such as P+pP as mentioned above. The source factors should include all features that associate with a given source, such as source pulse shape (if not factored out), the P, pP, and spall arrivals, and scattered P waves generated near the source, such as Rayleigh-to-P conversions (Greenfield 1971). The site factors include peculiarities due to the geology near the particular sensor in the array, such as P-to-Rayleigh conversions on local topography, i.e. anything that determines the features in P waveforms peculiar to a sensor location. The two factors together, as we shall show below, define most of the details in the observed P waveforms that can be associated with either the given source or recording site provided that the factorability condition as defined by equation (2) is satisfied for the given data set.

In this paper we talk of "receiver factors" and "source factors" in order to make the distinction from the related concept, the "relative receiver functions", which also incorporate some additional assumptions (Hart et al 1979), such as the maximum "spikiness" condition (Wiggins

1978), which is not required by the physics of the problem. We separate the Q operator, the instrument, and the source wavelet from the "source factor" and combine these in an assumed known source wavelet, A_j. Thus, $S_j(\omega) = A_j(\omega)X_j(\omega)$ where $A_j(\omega)$ is the spectrum of the combined source wavelet, instrument, and Q. This way the "source factor", $X_j(\omega)$, is a Fourier transform of a spike sequence associated with the radiation from a source and the "receiver factor", $R_i(\omega)$, is the Fourier transform of the site transfer function. Since the receiver factors strongly depend on the azimuths and distances of the sources, they may be assumed to be constant for a given sensor only for limited source regions.

If we have N receivers (sites) and M sources, we may describe (N x M) P wave spectra (or time series) in terms of N + M factors; there is thus a considerable degree of redundancy in the problems with N and M sufficiently large. This helps us to separate the $R_i(\omega)$ from the $X_j(\omega)$. This cannot be achieved uniquely, however, unless something is known *a priori* about the properties of each. Otherwise, common spectral factors can be assigned to either the source or receiver factors, or canceling, reciprocal factors may be assigned to both the receiver and source factors as indicated below:

$$Y_{ij}(\omega) = [R_i(\omega)\ F(\omega)]\ [F^{-1}(\omega)\ X_j(\omega)]\ A_j(\omega) \qquad (3)$$

This is the most dangerous aspect in any simultaneous determination of source and site factors. Fortunately, if we estimate the source factors first by averaging over receiver sites we may expect that in the first step the site effects will be approximately averaged out. This is based on the, quite reasonable, assumption that the site factors will tend to be quite random and dissimilar at the various array sensors. In the following steps the factors are refined without too much change and thus the chances of introducing major distortion into the estimated source and site spike sequences is thus minimized.

Since all P wave signals are embedded in the noise background it is desirable that the deconvolution-factoring process is optimized in some sense with respect to the noise i.e., we are trying to find some compromise between the resolution and the S/N ratio. Thus, although the original derivation of Shumway (1984) includes weighting with respect to noise spectra, in this work we do not maximize the S/N ratio in order to increase the time resolution of the deconvolution.

The detailed derivation of the maximum likelihood multichannel deconvolution method is given in Der et al (1983) and Shumway and Der (1985). Only the key formulas are repeated here:

$$\hat{X}_j = \frac{\sum_i \overline{A_j}\,\overline{R_i}\,Y_{ij}}{\sum_i |A_j|^2 |R_i|^2 + \theta_j} \quad \text{where } \theta_j = \frac{P_n}{P_{x_j}}, \tag{4}$$

$$\sigma_j^2 = P_n \left[\sum_i |A_j|^2 |R_i|^2 + \theta_j\right]^{-1}, \quad \text{and} \tag{5}$$

$$\hat{R}_i = \frac{\sum_j \overline{A_j}\,\overline{\hat{X}_j}\,Y_{ij}}{\sum_j |A_j|^2 \left[|\hat{X}_j|^2 + \sigma_j^2\right]}, \tag{6}$$

where

Y_{ij} data

A_j source wavelet spectrum

R_i receiver spike response

X_j source spike sequence

θ adjustable N/S ratio

P_n noise power spectrum

P_z initial signal power

σ_j^2 effective noise power in second step

and an overbar denotes the complex conjugate. The i's correspond to the individual receiver sites and the j's to the individual sources. Equations 4 through 6 are very similar to those presented by Oldenburg (1981) and Oldenburg et al (1981), and are essentially multichannel versions of the same. The term θ corresponding to the signal-to-noise ratio performs the same function as in Oldenburg's (1981) formulas. It is apparent from Equation (4) that the procedure is also similar, in computational approach, to the iterative beaming method (Blandford et al 1973) in which the previous estimates of the two interfering signals are iteratively estimated in each step.

The deconvolution is done in the frequency domain. The first step is to factor out the "known" spectra, $A_j(\omega)$, consisting of t^*, the instrument response, and the source function (a von Seggern and Blandford (1972) explosion source wavelet). Since we are working with small source and receiver arrays, we assume that the attenuation parameter t^*_P is the same for all source-receiver pairs and that all instruments have the same response. At the start of the iteration process the source and site functions are each initialized to an impulse in the time domain.

The iteration starts with the estimation of the source factors by deconvolving the source pulse and stacking these deconvolutions over the available sites. This is intuitively the most reasonable first step because we expect the site-generated pulse sequences to be more random than the source-related ones and thus they may be easier to average out by stacking. The flow diagram of the iterations is depicted in Figure 3. After several iterations, each source factor will contain the contribution appropriate to the particular source at all receivers including the

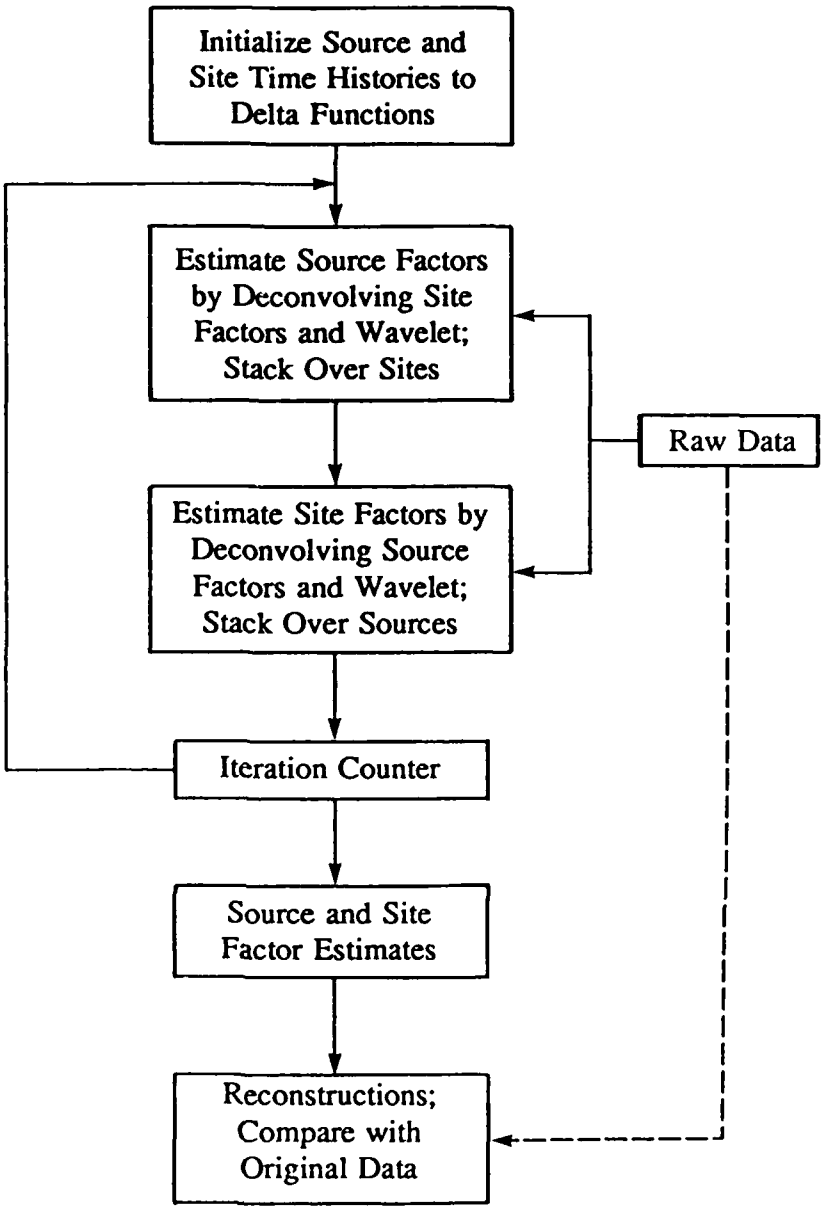

Figure 3. Flow diagram of the multichannel deconvolution process. In the center, the second and third boxes from the top correspond to Equations (4) and (6) in the text, respectively.

source pulse, pP, and spall (in the case of explosion sources) arrivals, and any scattering contributions that may be associated with a particular source.

Each site factor will contain the contribution of that site to the seismogram, mostly the random scattering effects attributable to the structure near the receiver. The site factors are of high frequency in character to compensate for the partial whitening of the spectra in estimating the source time functions (Figures 4 and 5). In order to see what effects these have on the coda one has to extract the low frequency part of them by band-pass filtering (Figure 6). The approximately Sinc(x) shaped resolution kernels characterizing the attainable resolution with the given bandwidth are also byproducts of the iterative process (see Shumway and Der 1985).

As a final test, the results are checked by reconstructing each input trace from the convolution of the appropriate source and site terms and the wavelet consisting of the von Seggern and Blandford source pulse, t^*, and instrument response. In most cases the reconstructions and the original traces are very similar (Figures 7 and 8). The differences between the original and reconstructed seismograms can be inferred as a measure of the scattering unique to each individual path i.e., energy unaccounted for by either site or source factors, and thus missing in the reconstructions.

This multichannel deconvolution approach for estimating source and site region characteristics has several advantages. First, the method utilizes both amplitude and phase information in the frequency domain calculations. Furthermore, no *a priori* assumptions need to be made about the complexity of either the source or the site spike series, e.g. the presence of pP does not need to be presupposed by providing an initial guess of the pP delay time and amplitude.

These iterative formulas yield progressively improved estimates of the source and receiver factors and their equivalent time functions as evidenced by the gradually improving quality of

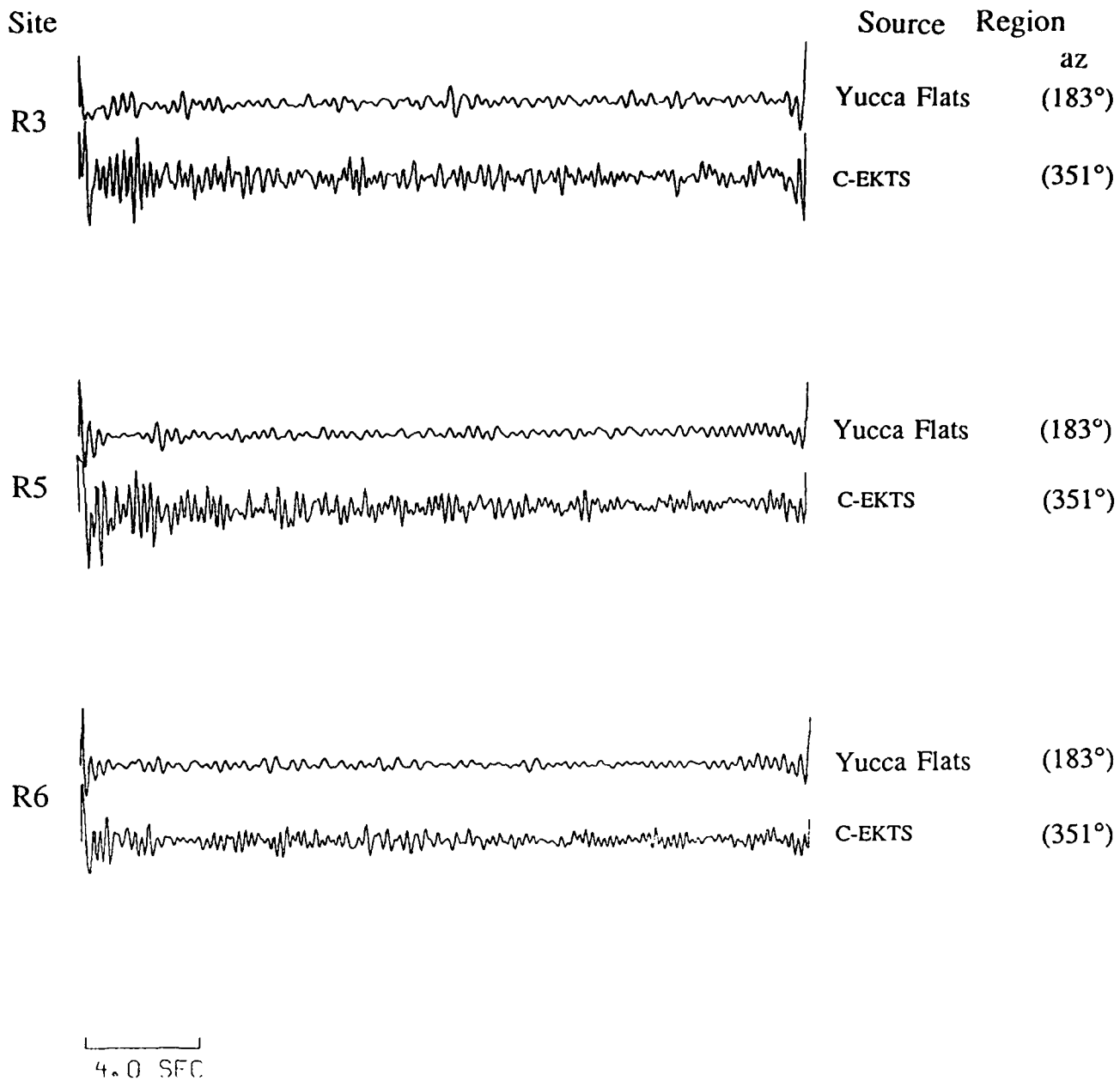

Figure 4. Estimated site time functions (wrapped around time zero) at three sensors of YKA for two test sites.

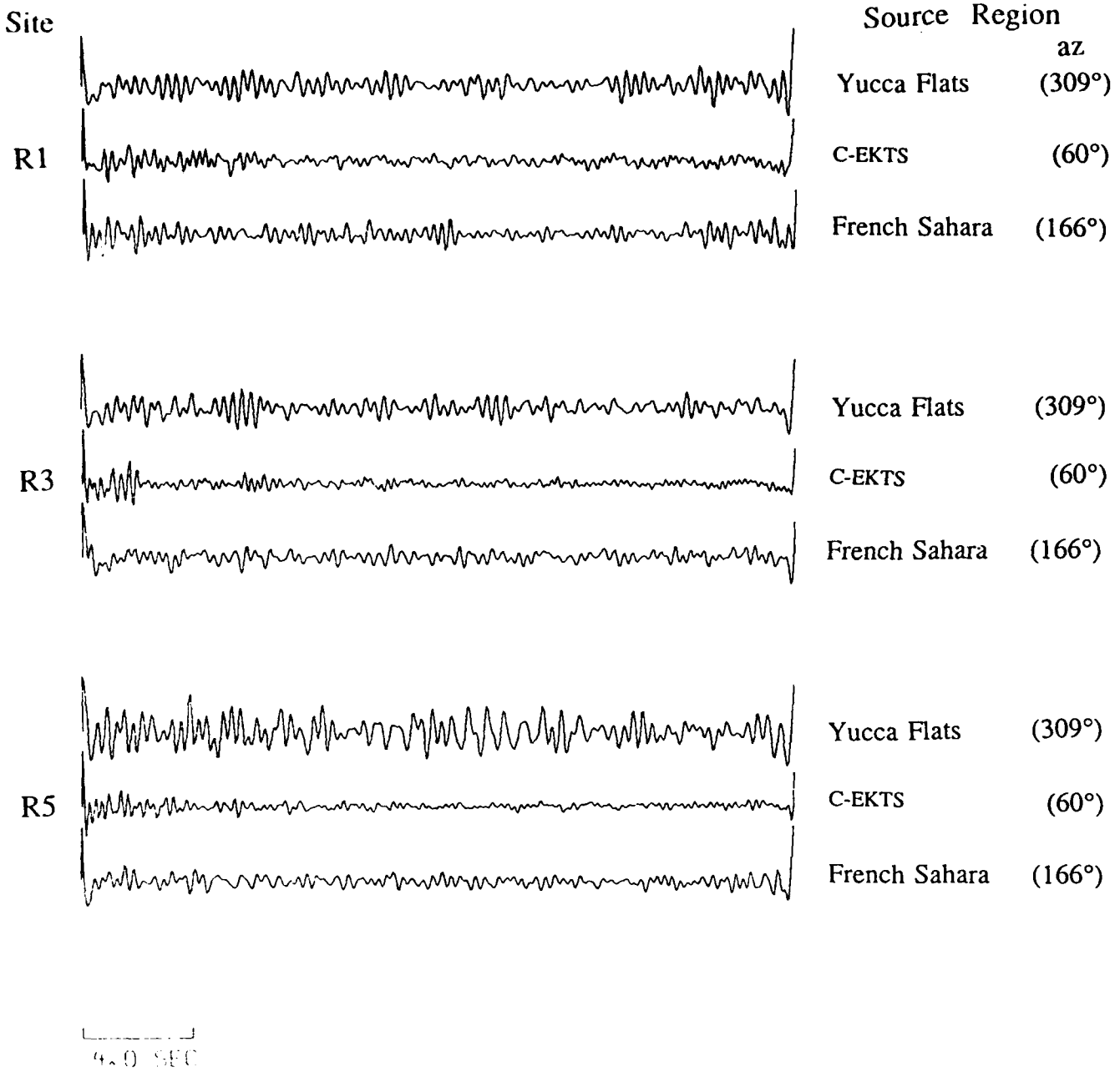

Figure 5. Estimated site time functions at three sensors of EKA for three test sites.

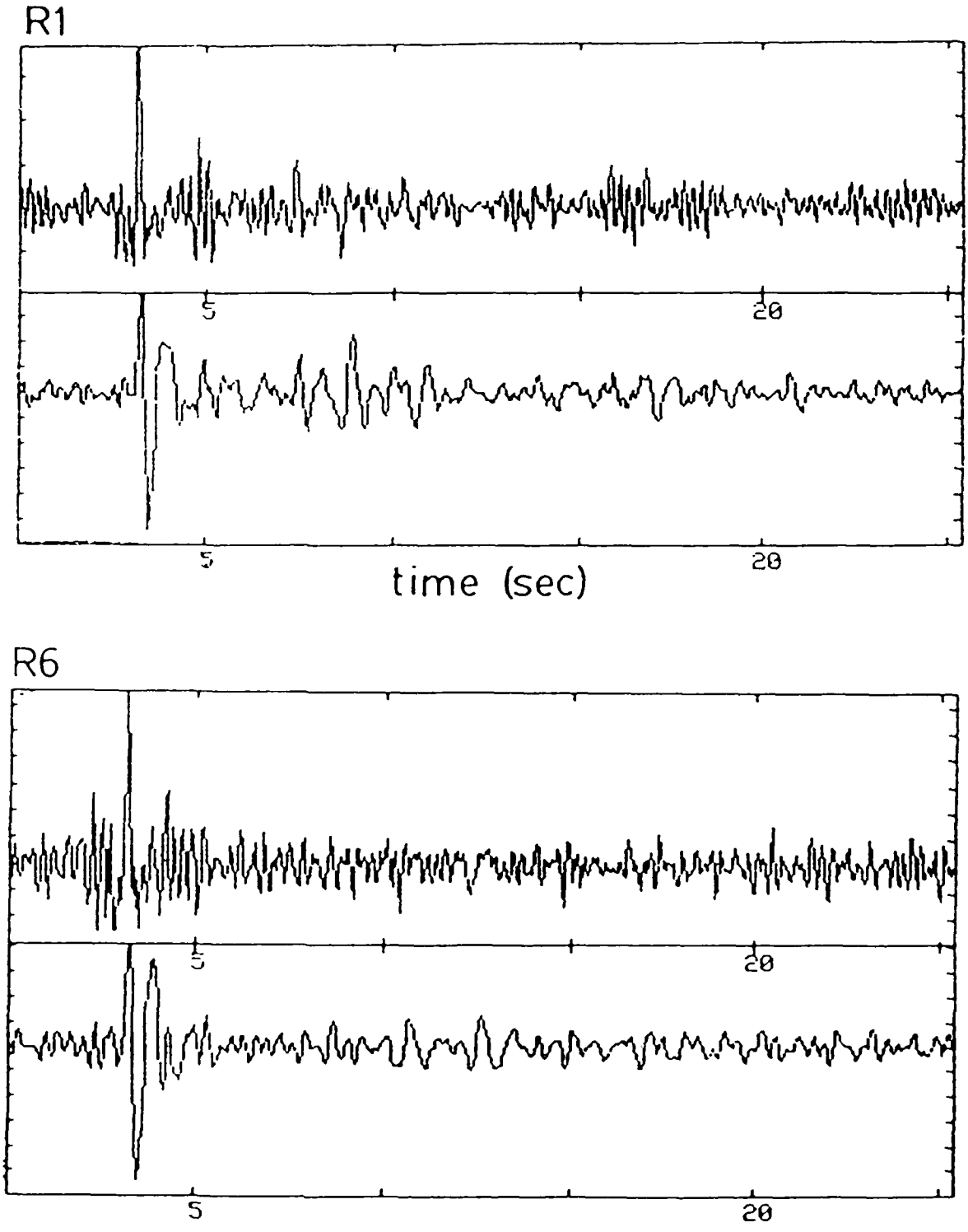

Figure 6. Original (top) and band pass filtered (bottom) site impulse responses at EKA for two sensors obtained by using a von Seggern-Blandford wavelet as a convolution operator to extract the low-to-intermediate frequency contribution to the site response function. The top sensor, R1, has a considerable amount approximately 1 Hz coda due to the site response.

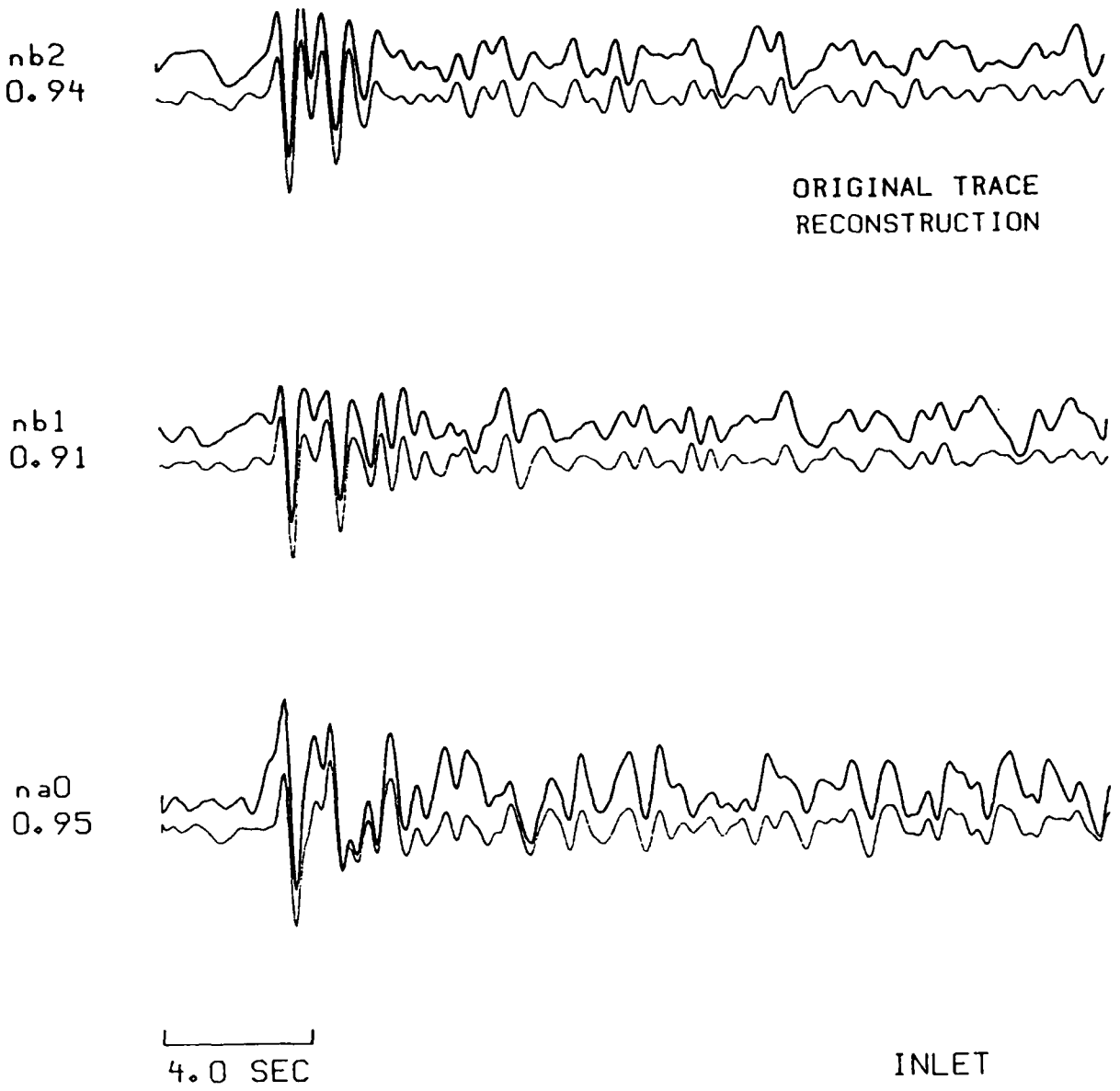

Figure 7a. Examples of trace reconstructions (bottom) and original traces (top) for the NTS event Inlet at NORSAR for three sites. On the left side of each pair of traces is the name of the sensor and the correlation coefficient between the original and reconstructed traces.

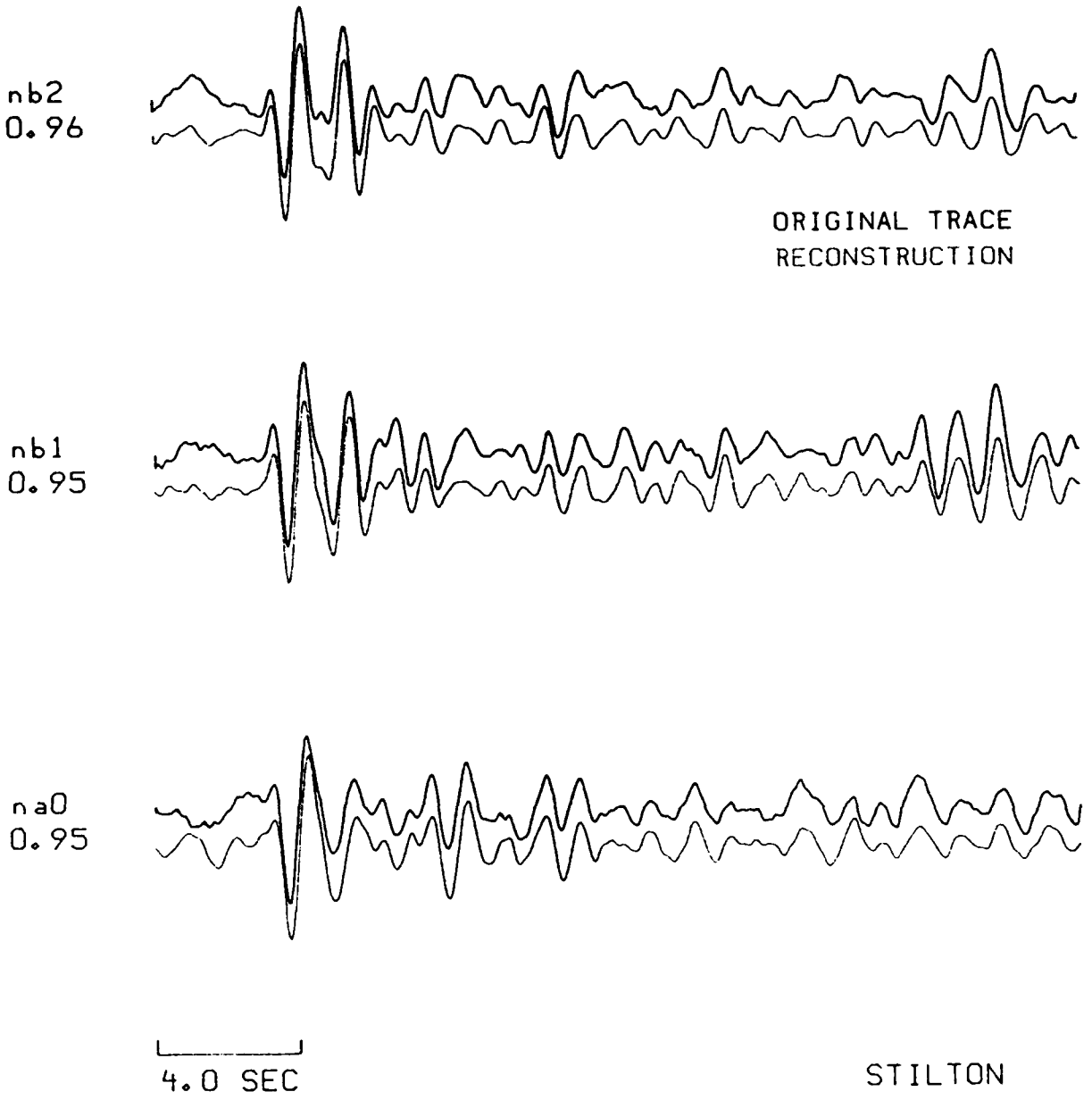

Figure 7b. Examples of trace reconstructions (bottom) and original traces (top) for the NTS event Stilton at NORSAR for three sites. On the left side of each pair of traces is the name of the sensor and the correlation coefficient between the original and reconstructed traces.

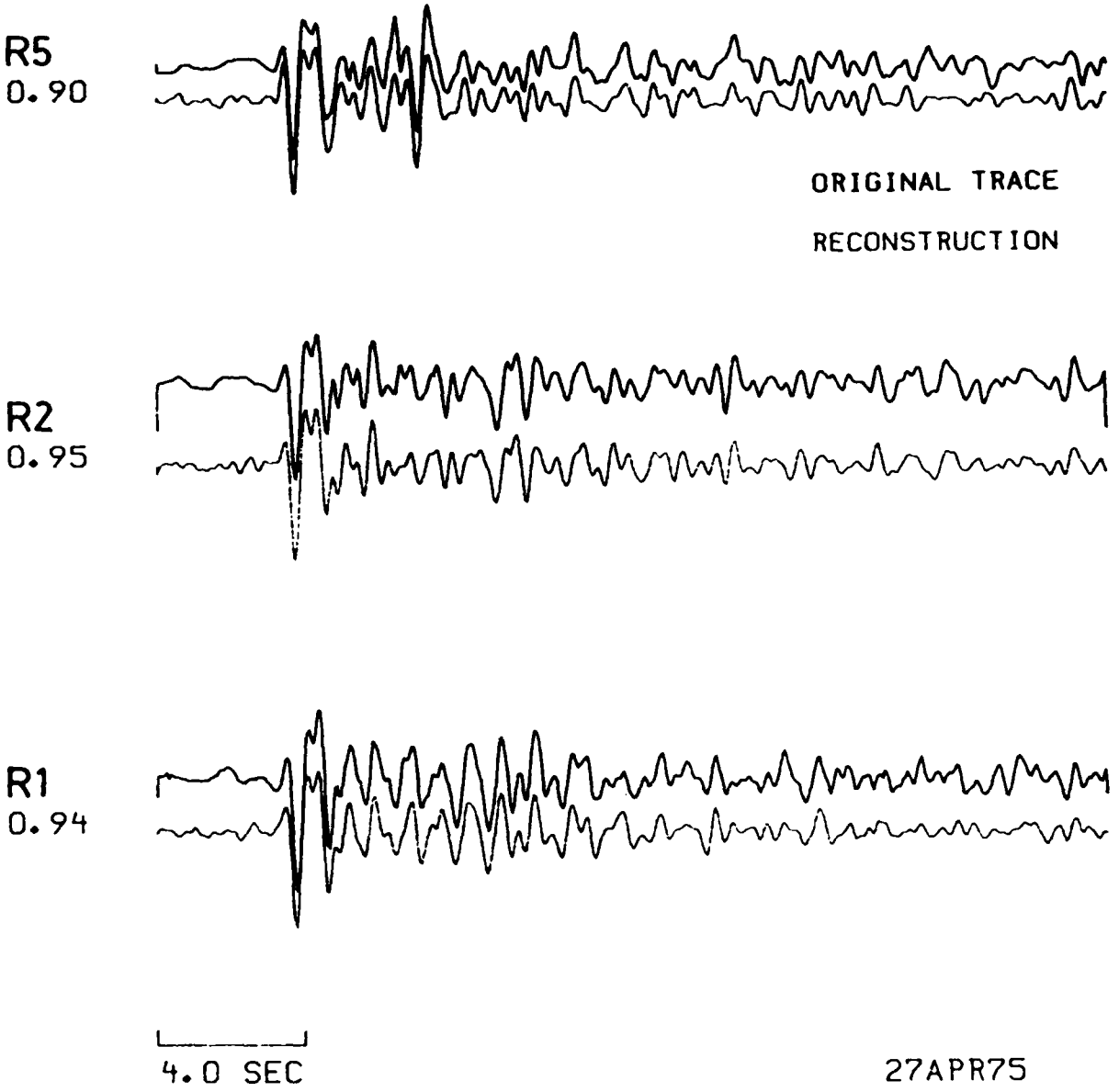

Figure 8a. Examples of trace reconstructions (bottom) and original traces (top) for the 27 April, 1975 E-EKTS event at EKA for three sites. On the left side of each pair of traces is the name of the sensor and the correlation coefficient between the original and reconstructed traces.

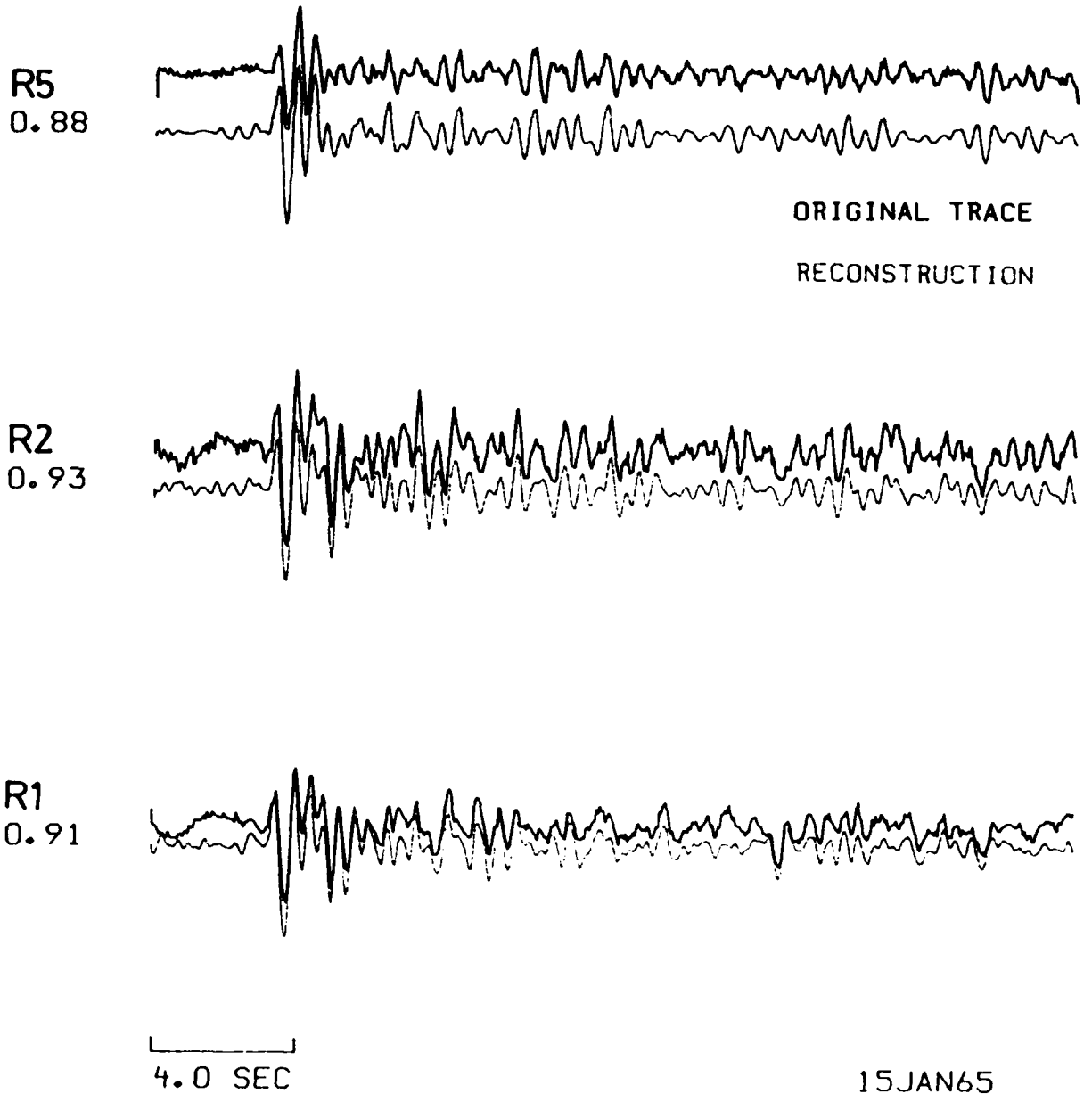

Figure 8b. Examples of trace reconstructions (bottom) and original traces (top) for the 15 January, 1965 cratering E-EKTS event at EKA for three sites. On the left side of each pair of traces is the name of the sensor and the correlation coefficient between the original and reconstructed traces.

trace reconstructions. We have done numerous theoretical simulations with known inputs and the method converged in all cases where the site responses were set to be notably different from the initial impulse at the beginning of the site related pulse sequence. We have found that four iterations were sufficient to stabilize the shapes of the source and site related pulse sequences.

Another approach is to include only the t* and the instrument response, and not the von Seggern and Blandford source wavelet, into the "known" factor to be divided out in each step of the iteration (Douglas 1986). This way the source pulses may directly be seen in the source deconvolutions, together with the pulse width and the "overshoot". This approach thus has some advantages over the one that includes an estimate of the explosion source wavelet, because the source pulse shapes may be directly seen, but it is harder to estimate small closely spaced P and pP delay times from such results. This approach is also not subject to errors due to incorrect *a priori* assumptions about the shapes of the explosion time functions, as the explosion source parameters (k, B) are not very well known in advance (von Seggern and Blandford 1972, Mueller and Murphy 1970, Lay et al 1984b); on the other hand, it appears the we know the shapes of the time domain attenuation and instrument response operators adequately enough to obtain reliable deconvolutions. An additional argument for the omission of the explosion source pulse from the deconvolution process is that inclusion of such a pulse makes sense only for finding the pP reflection (that has supposedly the same shape as the direct P); other arrivals (spall and arrivals in the coda) cannot be expected to have the same shape as the direct P pulse. If the deconvolution is done without removing the explosion time function, we essentially get a time history of teleseismic displacement smoothed by the approximately sin(x)/x shaped resolution kernel. If the results do not resemble the simple waveforms expected by a P+pP model (and they often do not) then the conclusion is inescapable that such models are not valid. In our work we often performed the deconvolutions in both ways, and

we shall identify results obtained by both approaches in this report.

GENERAL DATA PROCESSING PROCEDURES

All traces were lined up in time on the first arrival. Since we are not interested in the absolute amplitudes in the context of estimating relative pP times and amplitudes, and because we want to give roughly equal weight to all the traces to ensure effective factoring, we multiplied each trace with two factors, one appropriate to the event, the other one to the site, which were designed to approximately equalize all peak amplitudes. This approach is consistent with the multiplicative structure of the spectra, and the exact values of the equalizing factors do not matter. After processing, the initial normalization factors can be divided out to estimate the proper relative amplitudes of the deconvolved traces. The equalizing of traces conflicts somewhat with the optimization of the S/N ratios in the output, but in deconvolving the data improving the S/N ratio is subordinated to the goal of improving the time resolution.

As mentioned above, the iteration is started with the initialization of the time domain representations of the source and site factors to delta functions and the source factors are estimated first by summing the deconvolved results over the sites. During the subsequent iterations both the source and site factors will be progressively refined by factoring the spectral matrix. The first estimates of source functions are similar to the stacked deconvolutions obtained by Marshall (1972) and Douglas et al (1986). Instead of the frequency domain approach used here they used Wiener filters designed in the time domain for removing t* effects and the instrument response. Despite these differences in the procedures their results usually resemble ours closely.

In order to ensure the desired deconvolution effect we do not divide by the noise spectra, which would have resulted, especially for events which have the maxima in S/N ratio below 1 Hz, in no visible deconvolution at all. Instead, we have assigned a unit weight to all frequencies which had S/N ratios above 1 and excluded the frequency ranges with poor S/N ratios

from the iterations. Again, this degrades the S/N in the output, but as we stated above, our main goal is increased resolution.

The results require some interpretation: one must keep in mind that the deconvolution of the "known" source pulses (consisting of t*, instrument, and explosion scaling effects) will produce a one sided pulse, ideally symmetric in time and having some side lobes because of the limitations in the bandwidth of the deconvolution and the noncausal nature of the process. In any case, the results are easier to interpret than the original seismograms which are complex superpositions of complex wavelets. The resolution is typically more than 0.15 sec which is the width at half maximum of the resolution kernels. The deconvolved site terms are byproducts of the deconvolution process in the sense that we are mostly interested in the source time functions in this study. As we pointed out above, since the optimized deconvolutions for source terms cannot have white spectra because of noise constraints, the "site" factors contain a lot of high frequency, much of which is just noise, and only the low frequency part of which is physically meaningful. The site time functions also appear "wrapped around" around time=0 sec because of the way the factoring was set up. Some precursors are visible because the process does not have a causality constraint, and partly because of the wraparound effect. The subsequent reconstructions of the original traces demonstrate, however, that noncausality is not a major problem since most reconstructed traces do not have major precursors.

In all our deconvolution work we have used only complete matrices of event by site of P wave data. For a given array often several such data sets can be found that have only a limited subset of common events and sensors sites. It is reassuring, however, that for the common events the source time function estimates are commonly quite similar regardless of the particular data set. This indicates the robustness of the method.

The deconvolutions presented in the following sections have all utilized the best constant t* operator for a given path as opposed to a frequency dependent t* operator, t*(f). This has been shown previously (i.e. Der and Lees 1985) to be a reasonable way to treat narrow band data when t*(f) is slowly varying. For t* and t*(f) models that are appropriate for the given path, the deconvolved source time functions show only minor differences in waveform shape. The absolute amplitudes of the source functions do change, and this may be important in yield estimation (to be discussed later).

The quality of the reconstructions (and the validity of the spectral factorization assumption) is evaluated in each case by computing the correlation coefficients between the reconstructed and original waveforms. In the rest of this report we shall only show a small fraction of such results and only when it can be justified in making an important point. The work has produced massive amounts of output that cannot be shown in a report of this size. All results are available at request.

RESULTS OF THE DATA ANALYSES

Thus far in this project we have processed the following data sets: C-EKTS explosions plus one earthquake as recorded at the AWRE arrays EKA, GBA, WRA, and YKA, E-EKTS explosions recorded at EKA, GBA, WRA, and YKA, Novaya Zemlya events recorded at EKA, GBA, and YKA, Yucca Flats events plus Piledriver recorded at EKA, GBA, and YKA, Pahute Mesa events including Faultless recorded at EKA, GBA, and WRA, and French Sahara explosions recorded at EKA and YKA. We also present preliminary results for E-EKTS explosions deconvolved at the 3-component RSTN stations. The events in each data set are described in Tables 1a to 1f.

For describing the test sites within the Soviet East Kazakhstan test site, we are using the descriptors E-EKTS, C-EKTS, and NW-EKTS as defined in Figure 9 for the eastern, central, and northwestern test sites within East Kazakhstan. These test sites are described and named on pages 182 and 183 of Dahlman and Israelson (1977) and in Rodean (1979). Dahlman and Israelson describe the E-EKTS, C-EKTS, and NW-EKTS test sites as a marshy lowlands, a mountainous region, and a plain, respectively.

For nearly all of the deconvolutions we have used data recorded at the AWRE arrays EKA, GBA, WRA, and YKA. These arrays are described by Mowat and Burch (1977). Table 2 lists some of the parameters of the arrays and layouts of the arrays are shown in Figures 10 a-d.

Results for C-EKTS Explosions

A map of the locations of the C-EKTS explosions is shown in Figure 11. The data was deconvolved at each array using the options of removing and not removing the estimated von

Table 1a

Central EKTS Events Used in Deconvolutions

Event	Array					Location		
	EKA	YKA	WRA	GBA	Origin Time	Lat(°N)	Lon(°E)	m_b
670226	X				03:57:57.4	49.750:78.125	6.0	
711230	X				06:20:57.8	49.772	78.093	5.8
770329	X	X		X	03:56:57.6	49.790	78.086	5.4
770730	X	X	X	X	01:56:57.7	49.759	78.097	5.1
780326		X	X	X	03:56:57.6	49.768	78.044	5.6
780422	X	X	X	X	03:06:57.6	49.761	78.186	5.3
781031	X	X	X	X	04:16:57.8	49.806	78.143	5.2
790506	X	X	X	X	03:16:57.7	49.774	78.049	5.2
790531	X	X	X	X	05:54:57.7	49.835	78.127	5.2
791018			X	X	04:16:57.7	49.837	78.148	5.2
800522	X	X		X	03:56:57.7	49.784	78.082	5.5
800731	X	X	X	X	03:32:57.7	49.807	78.148	5.3

Location information from Marshall et al (1984).

Table 1b

Eastern EKTS Events Used in Deconvolutions

Event	Array				Location			
	EKA	YKA	WRA	GBA	Origin Time	Lat(°N)	Lon(°E)	m_b
650115	X				05:59:58.4	49.940	79.010	5.8
720210	X				05:02:57.5	50.014	78.878	5.4
721210	X				04:27:07.3	50.001	78.973	6.0
731214		X			07:46:57.2	50.044	78.987	5.8
741016	X	X		X	06:32:57.6	49.979	78.898	5.5
750630		X			03:26:57.6	50.004	78.957	4.6
751029	X			X	04:46:57.3	49.946	78.878	5.7
751225	X		X	X	05:16:57.2	50.044	78.814	5.7
760421	X	X		X	05:02:57.2	49.890	78.827	5.3
760609		X		X	03:02:57.2	49.989	79.022	5.1
760704	X				02:56:57.5	49.909	78.911	5.8
761123				X	05:02:57.3	50.008	78.963	5.9
761207	X				04:56:57.4	49.922	78.846	5.9
770629	X	X		X	03:06:57.8	50.006	78.869	5.2
770905	X		X	X	03:02:57.3	50.035	78.921	5.7
771130	X				04:06:57.4	49.958	78.885	6.0
780611	X		X	X	02:56:57.6	49.898	78.797	5.9
780705	X			X	02:46:57.5	49.887	78.871	5.8
780829	X		X	X	02:37:06.3	50.000	78.978	5.9
780915	X		X		02:36:57.4	49.916	78.879	6.0
781104	X		X	X	05:05:57.3	50.034	78.943	5.6
781129	X				04:33:02.5	49.949	78.798	6.0
790623	X				02:56:57.5	49.903	78.855	6.2
790707	X				03:46:57.3	50.026	78.991	5.8
790804	X				03:56:57.1	49.894	78.904	6.2
791028	X				03:16:56.9	49.973	78.997	6.0
791202	X				04:36:57.5	49.891	78.796	6.0
791223	X				04:56:57.4	49.916	78.755	6.2
800629	X				02:32:57.7	49.939	78.815	5.7
801227	X				04:09:08.1	50.057	78.981	5.9
810422	X				01:17:11.3	49.885	78.810	6.1
811018	X				03:57:02.6	49.923	78.859	6.1
811129	X				03:35:08.6	49.887	78.860	5.7
820831	X				01:31:00.7	49.924	78.761	5.4
821226	X				03:35:14.2	50.071	78.988	5.7

Location information from Marshall et al (1984).

Table 1c

Novaya Zemlya Events Used in Deconvolutions

Event	Array				Location			
	EKA	YKA	WRA	GBA	Origin Time	Lat(°N)	Lon(°E)	m_b
730927	X	X			06:59:58.5	70.756	53.754	5.84
760927		X			02:59:57.7	73.360	54.880	5.77
761020	X			X	07:59:58.1	73.399	54.835	4.89
770901	X	X			02:59:58.0	73.339	54.626	5.71
780810		X			07:59:58.0	73.293	54.885	6.04
780927	X	X			02:04:58.6	73.350	54.677	5.68
790924	X	X			03:29:58.8	73.346	54.679	5.80
791018	X	X			07:09:58.8	73.318	54.821	5.85
801011	X	X		X	07:09:57.5	73.335	54.938	5.80
811001		X		X	12:14:57.3	73.308	54.817	5.91
821011	X	X		X	07:14:58.7	73.348	54.601	5.52
830818		X		X	16:09:58.9	73.358	55.974	5.84
830925	X	X			13:09:58.2	73.326	54.564	5.71

Location information from Marshall et al (1986).

Table 1d

French Sahara Events Used in Deconvolutions

Event	Array			
	EKA	YKA	WRA	GBA
Emeraude	X	X		
Grenat	X	X		
Rubis	X			
Saphir	X	X		

Table 1e

Pahute Mesa Events Used in Deconvolutions

Event	Array				Location			
	EKA	YKA	WRA	GBA	Date	Origin Time	Lat(°N)	Lon(°W)
BOXCAR	X				680426	15:00:00.0	37.295	116.456
CAMEMBERT	X			X	750626	12:30:00.2	37.279	116.369
CHESHIRE	X				760214	11:30:00.2	37.243	116.420
ESTUARY	X			X	760309	14:00:00.1	37.310	116.364
FAULTLESS	X				680119	18:15:00.1	38.63	116.22
FONTINA	X				760212	14:45:00.2	37.271	116.488
HANDLEY	X				700326	19:00:00.2	37.300	116.534
INLET	X				751120	15:00:00.1	37.225	116.368
KASSERI	X		X	X	751028	14:30:00.2	37.290	116.412
MAST	X				750619	13:00:00.1	37.350	116.320
MUENSTER	X		X	X	760103	19:15:00.2	37.297	116.333
PURSE	X				690507	13:45:00.0	37.283	116.501
TYBO	X			X	750514	14:00:00.2	37.221	116.474

Locations were announced except for FAULTLESS, for which the location is from the ISC.

Table 1f

Yucca Flats Events Used in Deconvolutions

Event	Array				Location			
	EKA	YKA	WRA	GBA	Date	Origin Time	Lat(°N)	Lon(°W)
BULKHEAD		X		X	770427	15:00:00.1	37.095	116.028
CABRILLO		X			750307	15:00:00.2	37.134	116.084
CHIBERTA	X				751220	20:00:00.2	37.128	116.062
CREWLINE		X		X	770525	17:00:00.1	37.094	116.045
FARALLONES	X			X	771214	15:00:00.1	37.136	116.086
HEARTS	X				790906	15:00:00.1	37.088	116.053
LOWBALL	X	X			780712	17:00:00.1	37.079	116.044
QUARGEL		X		X	781118	19:00:00.2	37.127	116.084
SCANTLING		X			770819	17:55:00.1	37.110	116.055
STRAIT	X			X	760317	14:45:00.1	37.107	116.052
TOPGALLANT	X	X			750228	15:15:00.1	37.106	116.056
PILEDRIVER	X				660602	15:30:00.1	37.227	116.056

Locations were announced.

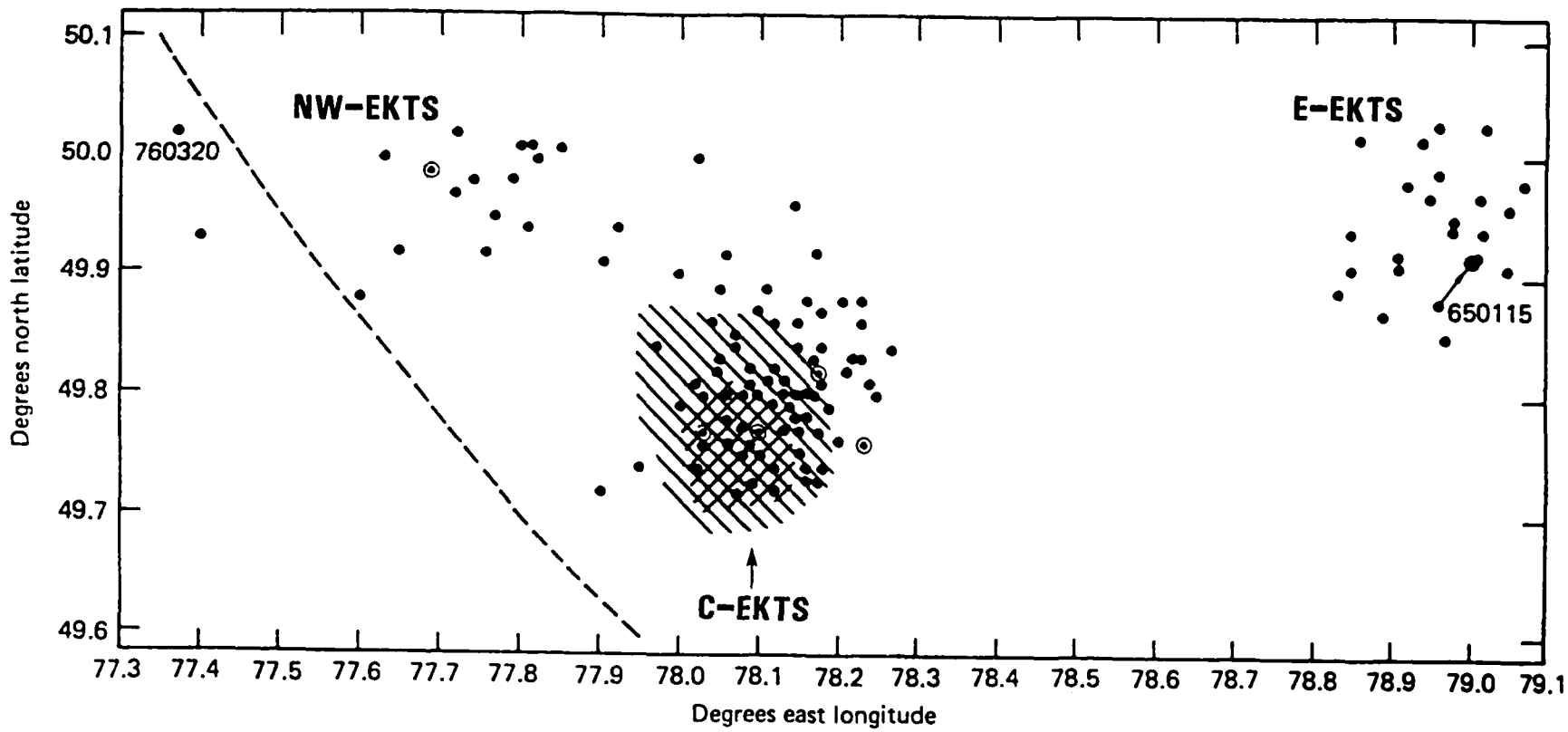

Figure 9. ISC locations of events at the three Eastern Kazakh test areas (after Rodean 1979). Circles denote multiple events at the same coordinates, double hatching indicates mountainous terrain and higher elevations, arrow points to the location of the cratering event, dashed line is a known fault. There are three main testing areas within the Eastern Kazakh Tesat Site (EKTS); a northwestern diffuse area, a central area covering a rugged, mountainous region and an eastern area clearly separated from the rest. These will be referred to by the abbreviations NW-EKTS, C-EKTS and E-EKTS in the rest of this report.

Table 2

United Kingdom Sponsored Arrays

Station	Code	Location	Element Spacing (km)	Maximum Element Spacing (km)	Date Operational	Date of Digital Recording
Eskdalemuir Scotland	EKA	55°19'59"N 3°09'33"W	0.9	9.8	17 May 1962	14 Nov 1983
Yellowknife Canada	YKA	62°29'34"N 114°36'17"W	2.5	22.5	26 Nov 1962	-
Gauribidanur India	GBA	13°36'15"N 77°26'10"E	2.5	32.0	1 Feb 1966	4 Mar 1979
Warramunga Australia	WRA	19°56'39"S 134°20'27"E	2.5	26.3	1 Mar 1966	7 Jun 1977

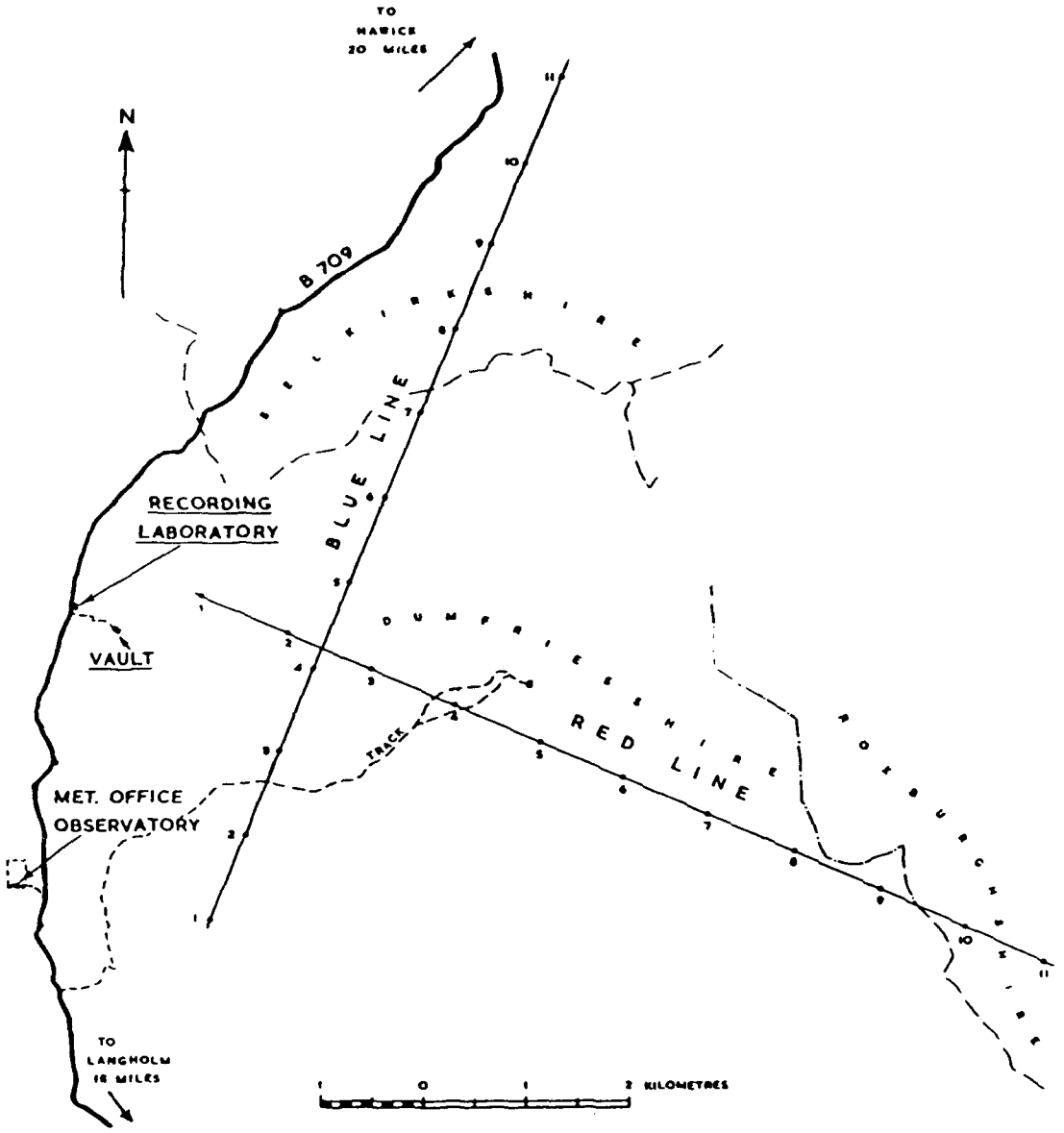

Figure 10a. Layout of the AWRE array EKA.

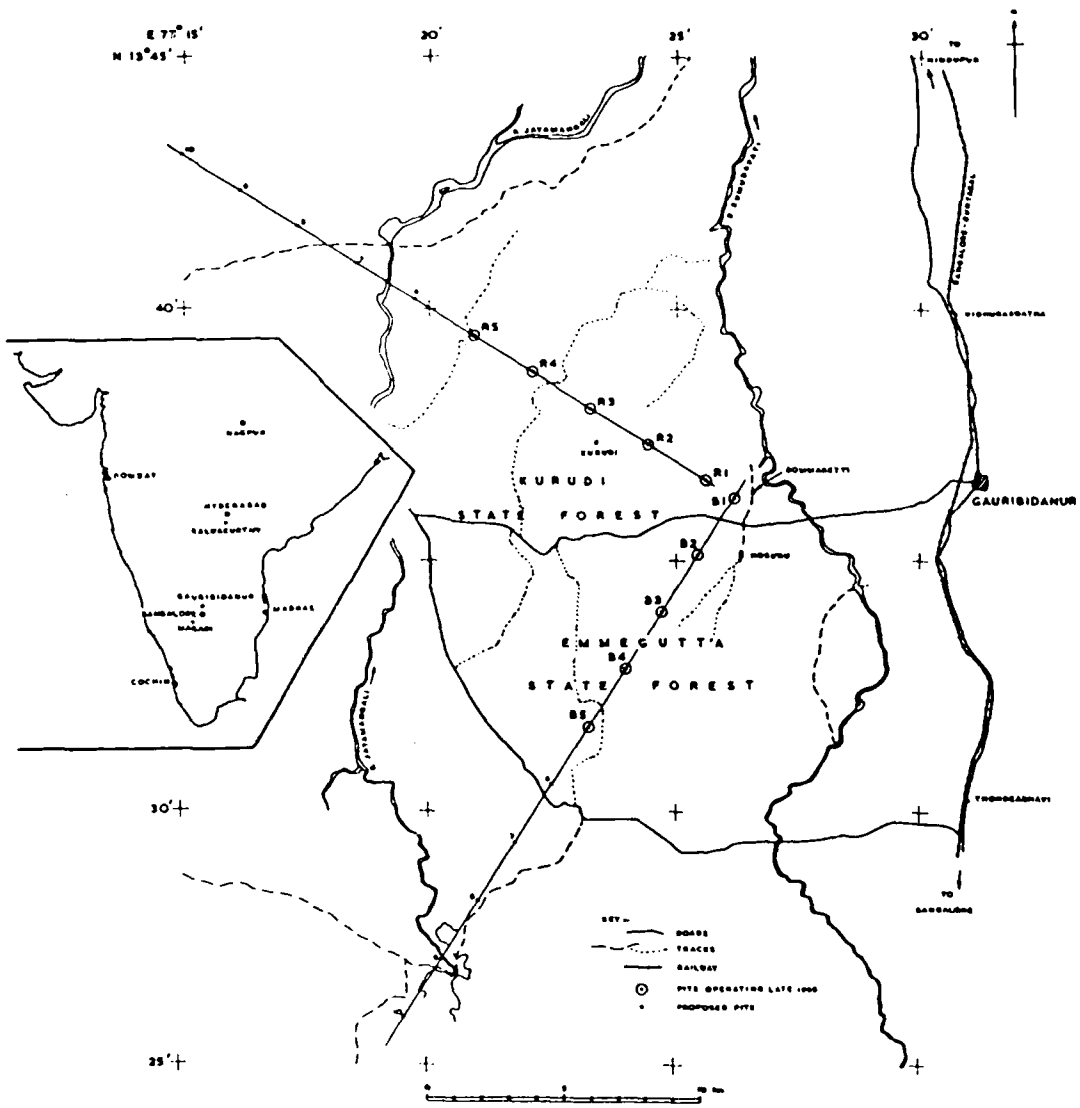

Figure 10b. Layout of the AWRE array GBA.

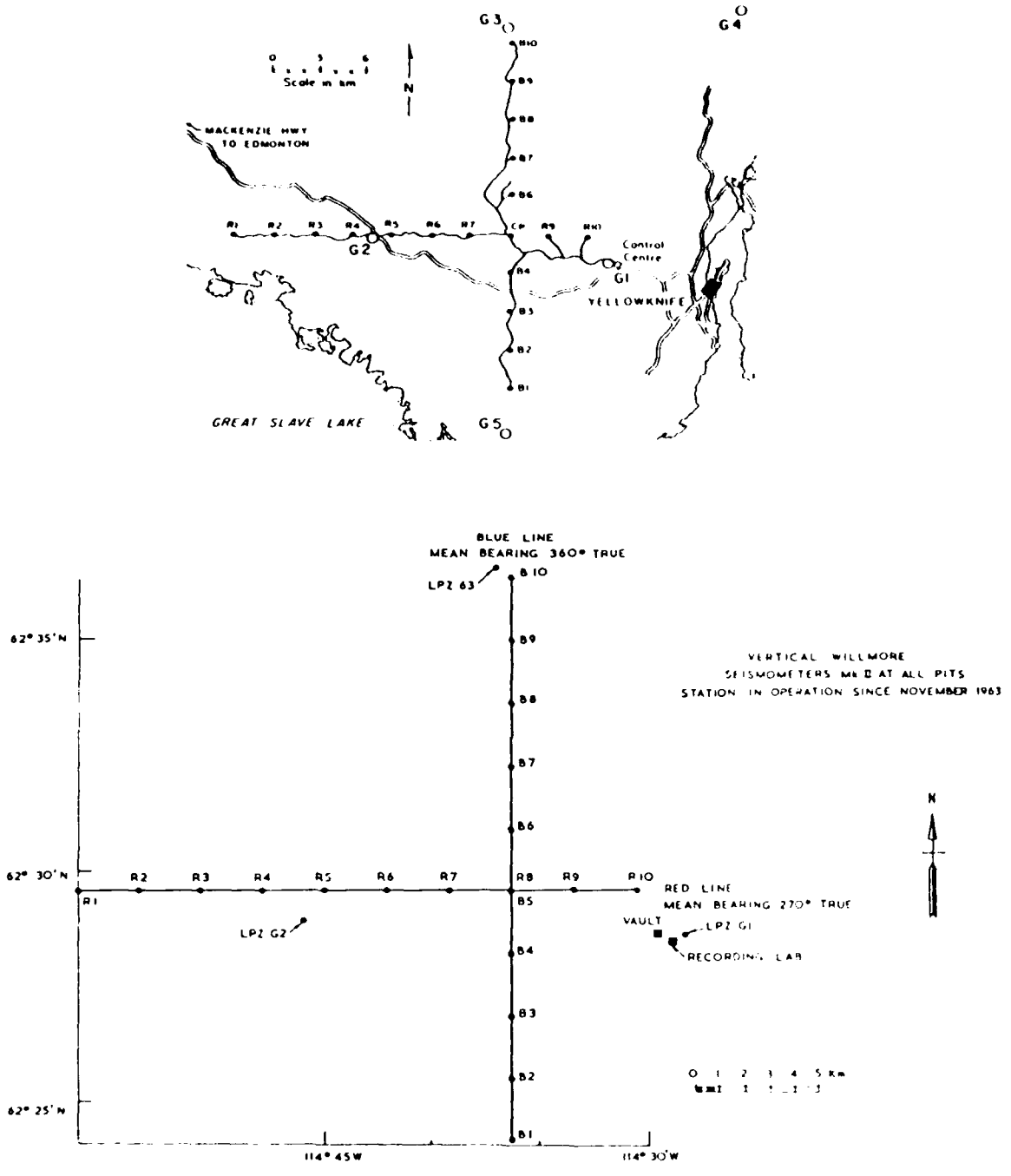

Figure 10c. Layout of the AWRE array YKA.

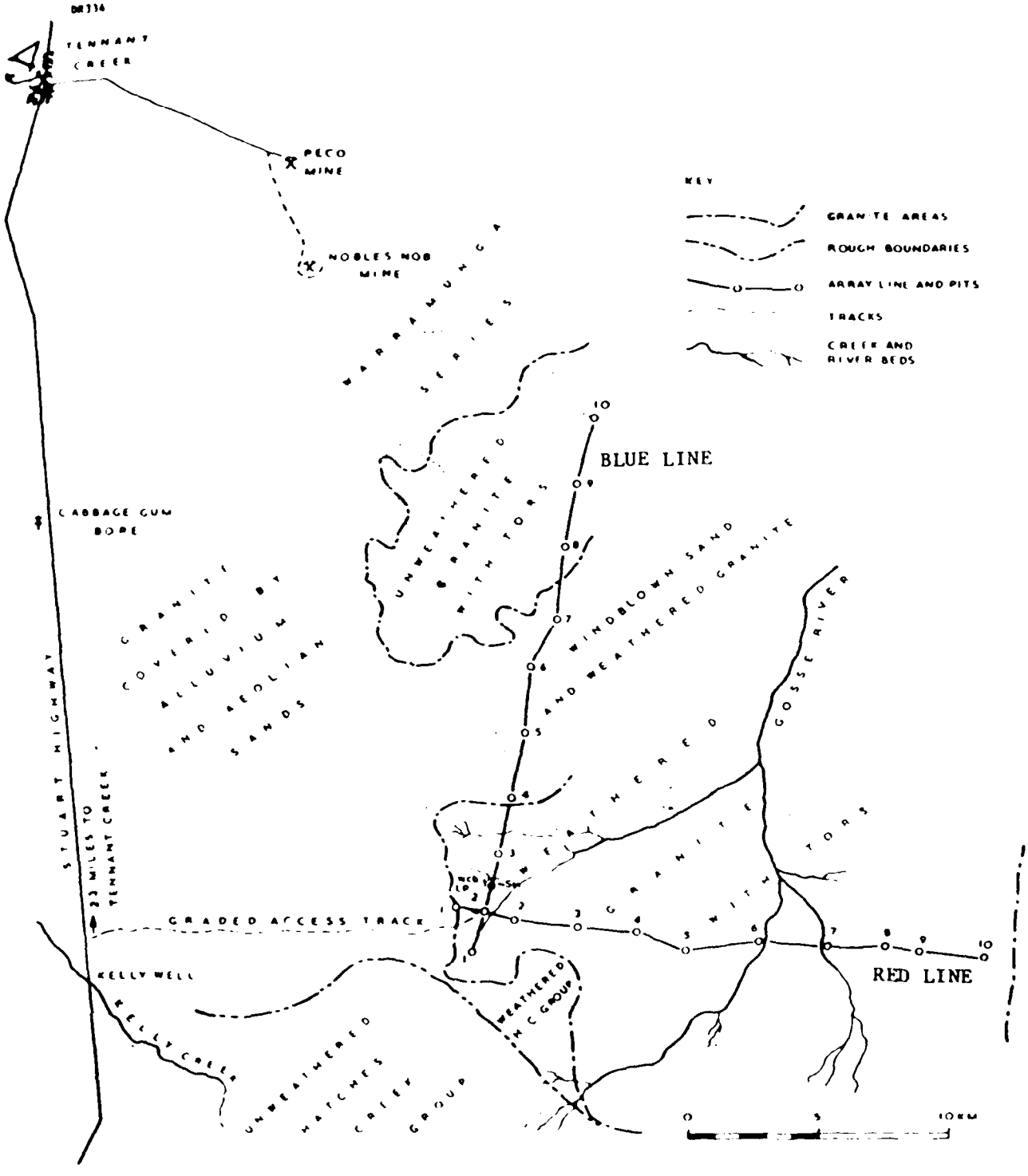

Figure 10d. Layout of the AWRE array WRA.

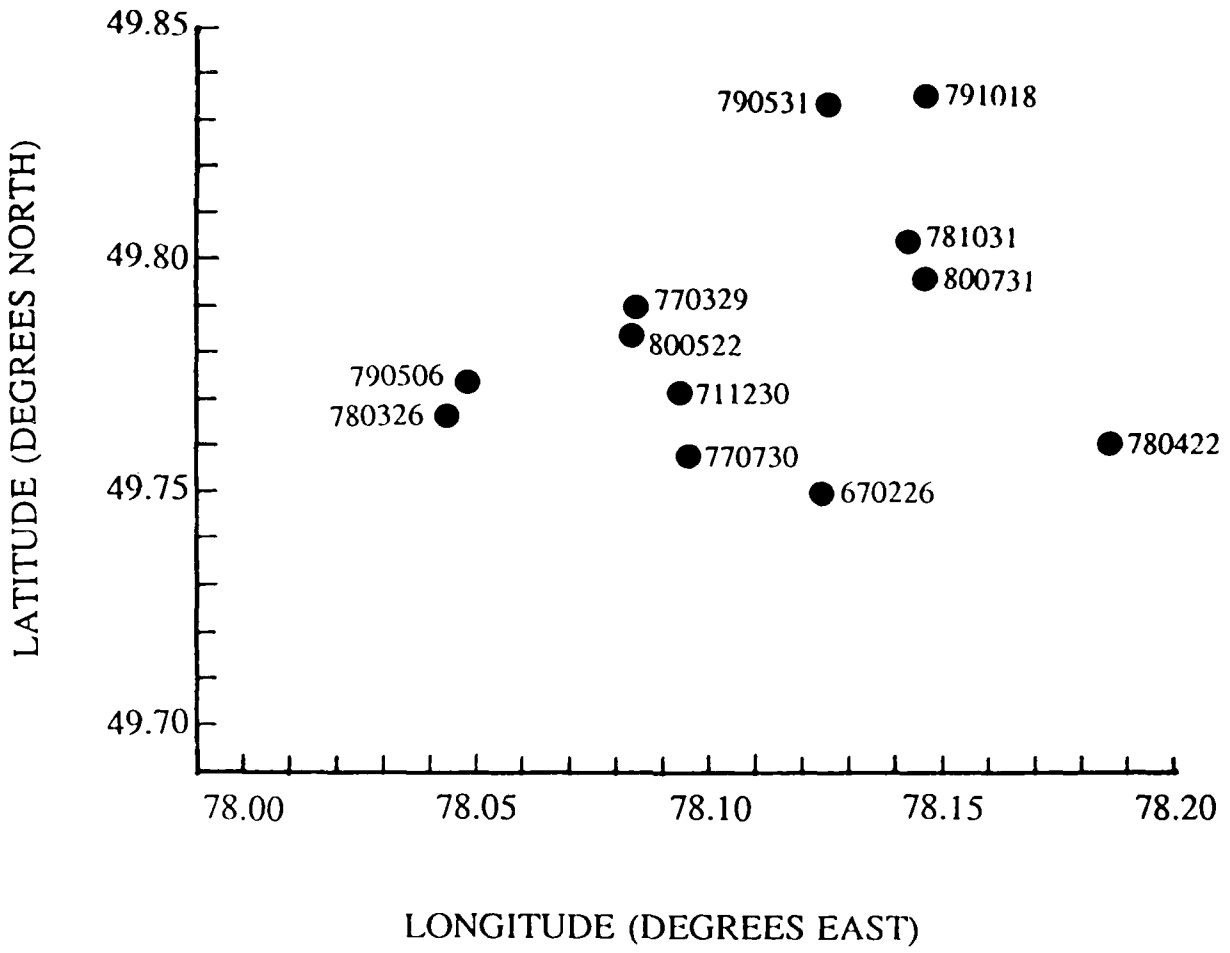

Figure 11. Locations of the C-EKTS events analyzed in this study.

Seggern Blandford (VSB) explosion source wavelet. Figures 12 through 15 show the source functions at the various arrays with the estimated VSB removed in the deconvolution process. The P and pP phases are marked on each trace. It is apparent that only a few of the events show secondary arrivals, interpretable as pP, with negative amplitudes similar in size to the initial P wave pulse. Most events do not show a clear pP. It may be argued that many C-EKTS events were shallow enough for preventing the development of pP pulses, possibly by non-linearity of deformation near the surface. An alternative explanation may be the complex topography above the explosions.

Another interesting feature is the differences in the deconvolved waveforms at the different arrays. In Figure 16 we show the results obtained for common events at the four AWRE arrays, this time without removing the VSB source pulse. The events are loosely arranged by the locations in Figure 11. For events recorded at a given array, there often appear to be more similarities between the source functions of events that were spacially close to each other, though we have not studied this in a quantitative manner. The event of March 20, 1976 (760320) is an earthquake (see, for example, Rodean 1979). Variations in pP and sP amplitude and polarity are clearly seen at the different azimuths for this event. Another interesting event (770329) has been identified as a double event (McLaughlin et al 1986c) with time shifts appropriate to different distances relative to the various arrays. For this event, note that the second event has a clear pP arrival, unlike most of the C-EKTS events. The second event is an explosion which occurred at the NW-EKTS test site, which is a relatively flat and simple geologic region.

With these events aside there is still a large difference among the deconvolved waveforms at the different arrays, WRA and GBA show more of a high frequency coda than the other two arrays. (Some of the complexity at WRA may be due to its distance of ~85° from C-EKTS.

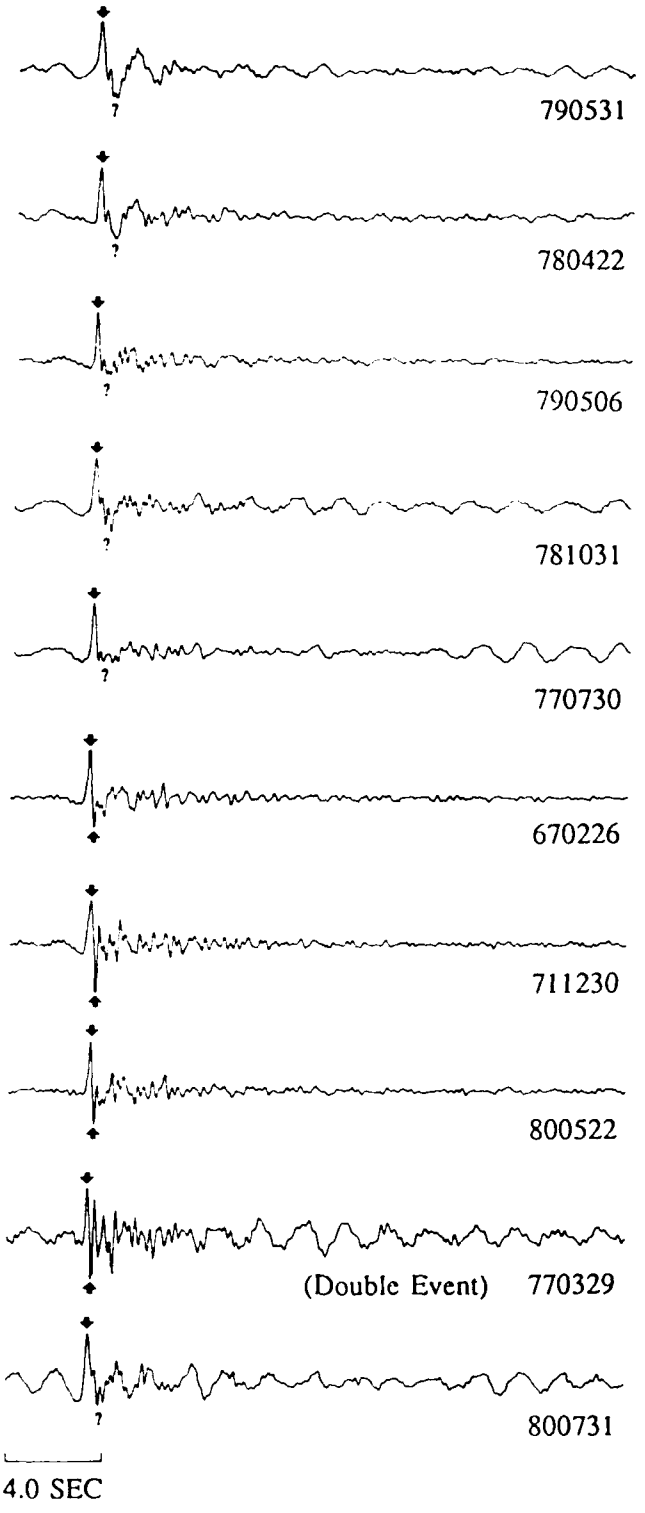

Figure 12. Deconvolved source functions for C-EKTS events at EKA. The estimated von Seggern and Blandford wavelet has been removed in the deconvolutions. The P and pP, if present, arrivals are marked on each trace.

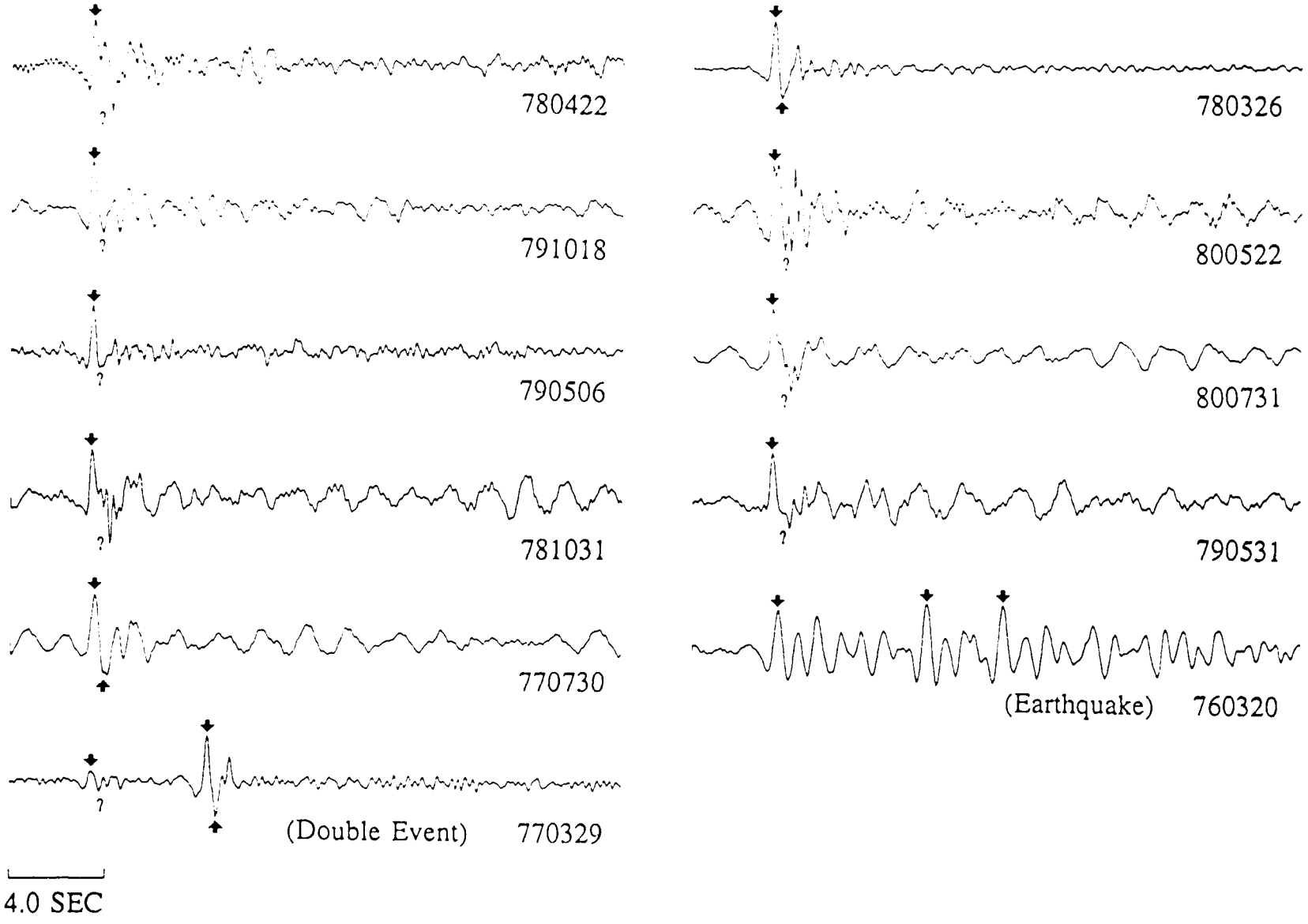

Figure 13. Deconvolved source functions for C-EKTS events at GBA. The estimated von Seggern and Blandford wavelet has been removed in the deconvolutions. The P and pP, if present, arrivals are marked on each trace.

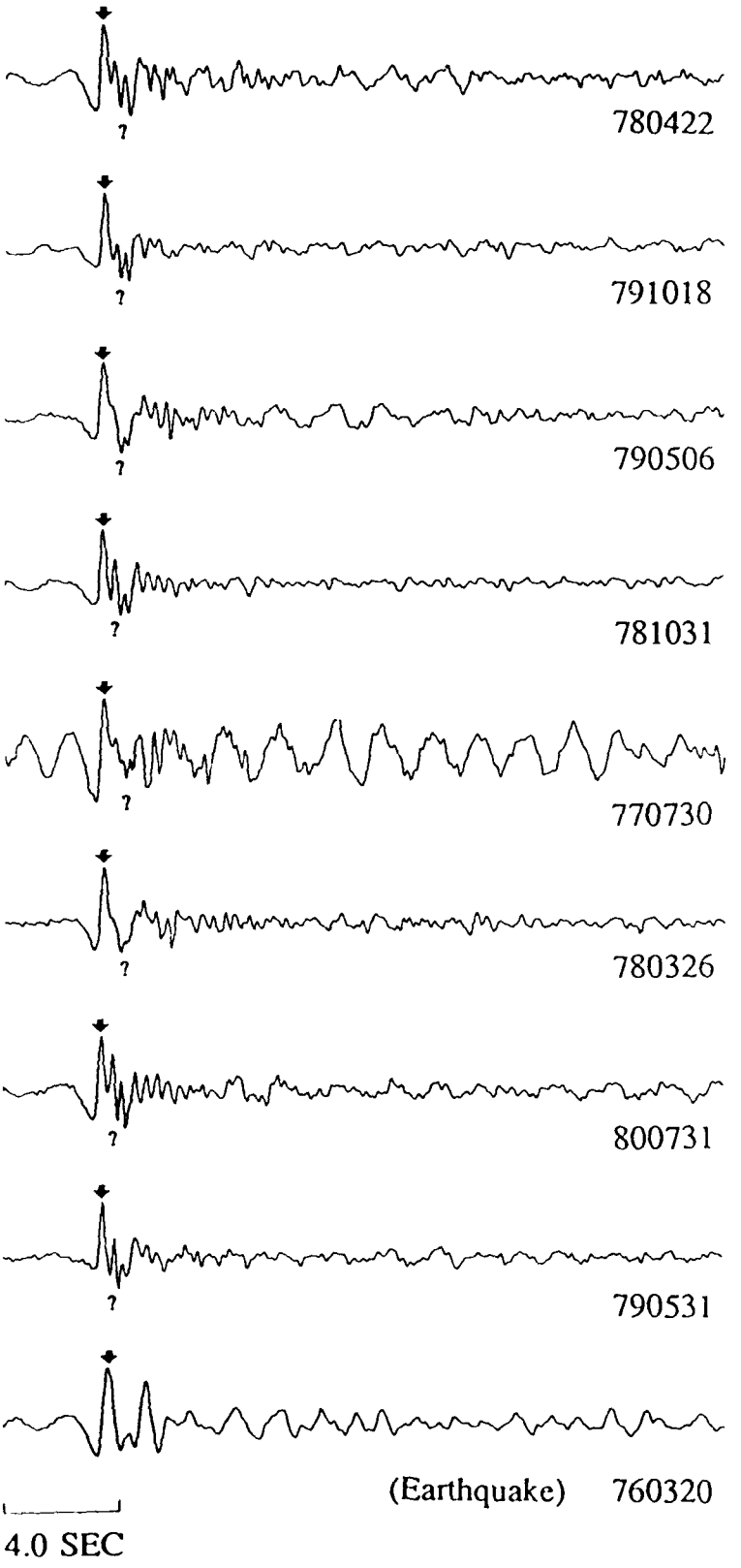

Figure 14. Deconvolved source functions for C-EKTS events at WRA. The estimated von Seggern and Blandford wavelet has been removed in the deconvolutions. The P and pP, if present, arrivals are marked on each trace.

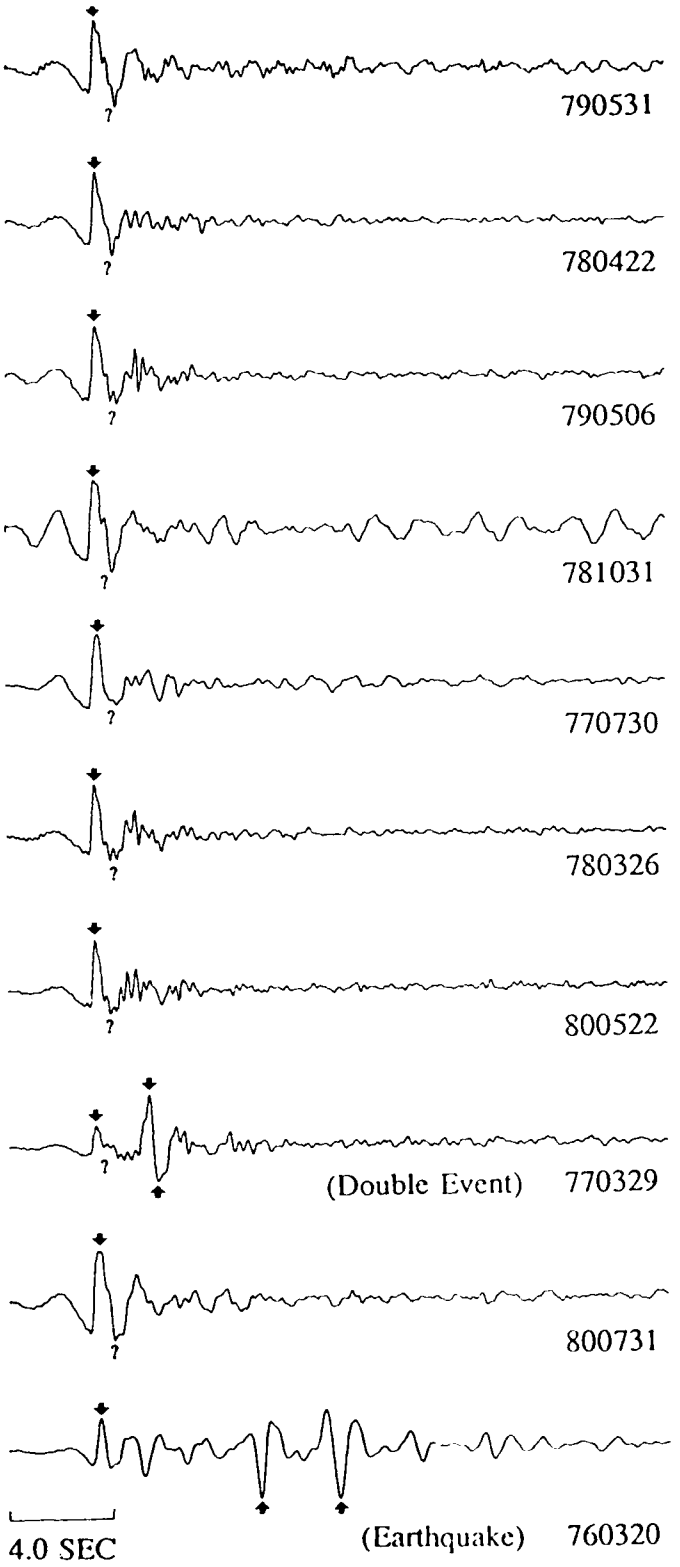

Figure 15. Deconvolved source functions for C-EKTS events at YKA. The estimated von Seggern and Blandford wavelet has been removed in the deconvolutions. The P and pP, if present, arrivals are marked on each trace.

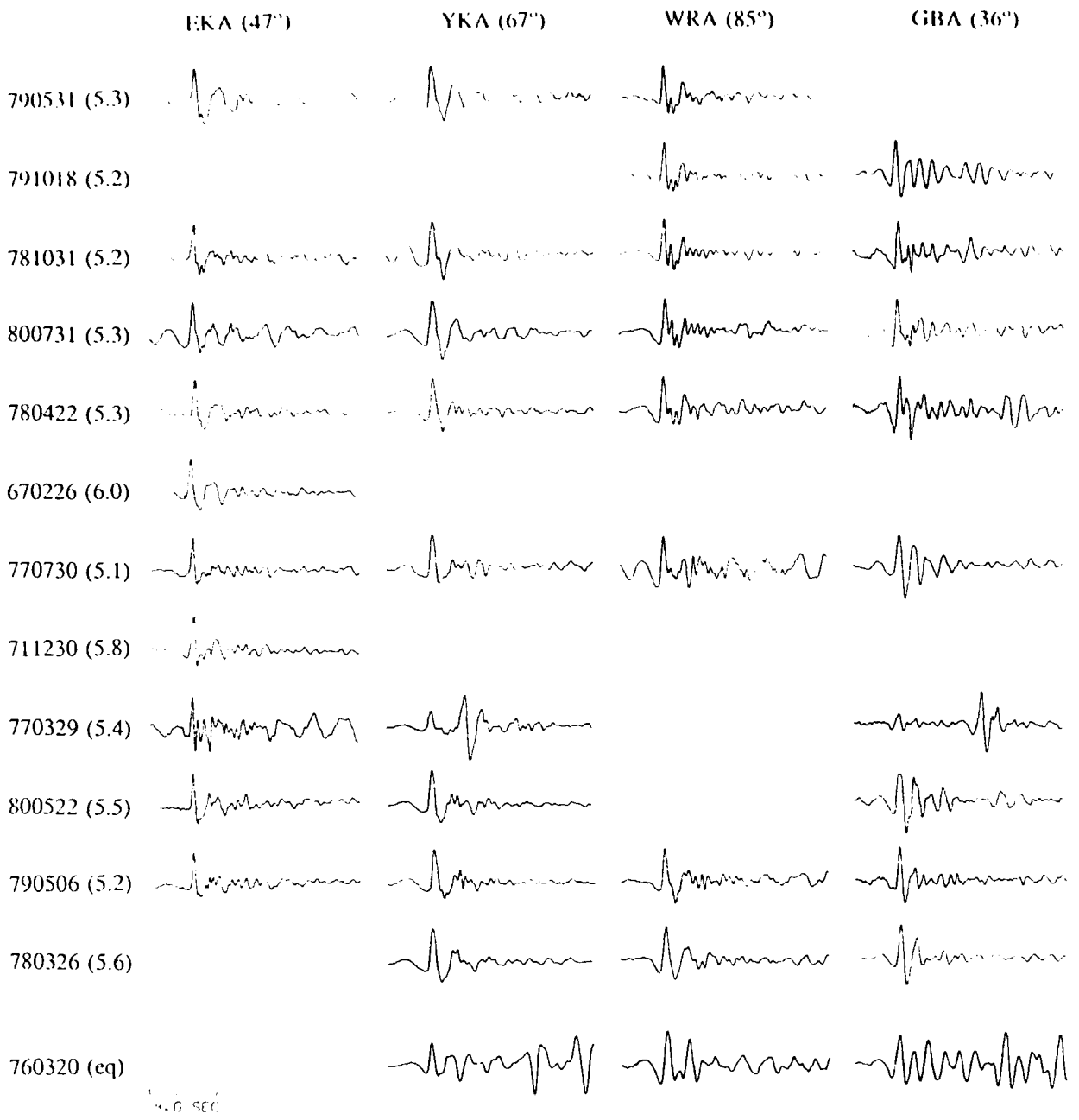

Figure 16. A set of source time functions for the C-EKTS test site and an earthquake (bottom) obtained at AWRE arrays. VSB wavelets have not been removed in these deconvolutions. Most of the traces do not show a clearly identifiable pP. The 770329 event consists of two nearly coincident events at two test sites (C-EKTS and NW-EKTS) and shows variable time delays at the various arrays.

At this distance, the Jeffreys-Bullen travel time curves predict that PcP will arrive ~3.8 sec after the P, and in this case perhaps even sooner since both the source and receiver regions are on shields which tend to have faster than average velocities.) There are two working hypotheses to explain this phenomenon. The first is that there are components in the site responses at each array (multiplicative factors in the frequency domain) that need to be removed in order to equalize the results. The other is that the time functions radiated by the various events are not the same in all directions, i.e. the source radiation is azimuthally asymmetrical. To decide which of these hypotheses is true we have selected a subset of events and a subset of sensors at each array and jointly deconvolved the data. Joint deconvolution of multi-array data implies that the assumptions appropriate to the first hypothesis, i.e. that the sources are azimuthally symmetrical and that the differences in the deconvolution results can be removed by additional, multiplicative site factors applied to each array, are incorrect. Table 3 lists the events and sensors used in the joint deconvolution and Figure 17 shows the source functions from the joint deconvolutions as well as from deconvolution of the same set of events separately at each array. The source functions derived from the joint deconvolutions are much simpler than the source functions from the deconvolutions at the separate arrays. However, the source and site factors obtained from the joint deconvolution result in a noticeable degradation of the reconstructions of the original data indicating that the differences cannot be attributed to differences in the site functions. This is shown in Figure 18 where reconstructions using the source and site factors from the joint deconvolution give correlation coefficients of only 0.4 to 0.8 when compared with the original traces while reconstructions using source and site factors from deconvolution of the same events at a single array give correlation coefficients of greater that 0.9. This leads to the conclusion that for the C-EKTS events, the differences of the deconvolution results at the various arrays must be attributed to azimuthal asymmetries in the source radiation of the individual events.

Table 3

Events and Receivers used in Joint Deconvolution
of Central EKTS Events at AWRE Arrays

	Sensors Used at Each Array			
Events	EKA	GBA	WRA	YKA
770730	R1	R2	R1	R1
781031	R4	R4	R2	R5
790506	R5	B1	R5	R7
780422	R8	B2	R8	R9
790531	B1	B7	B1	B3
800731	B4	B9	B4	B8

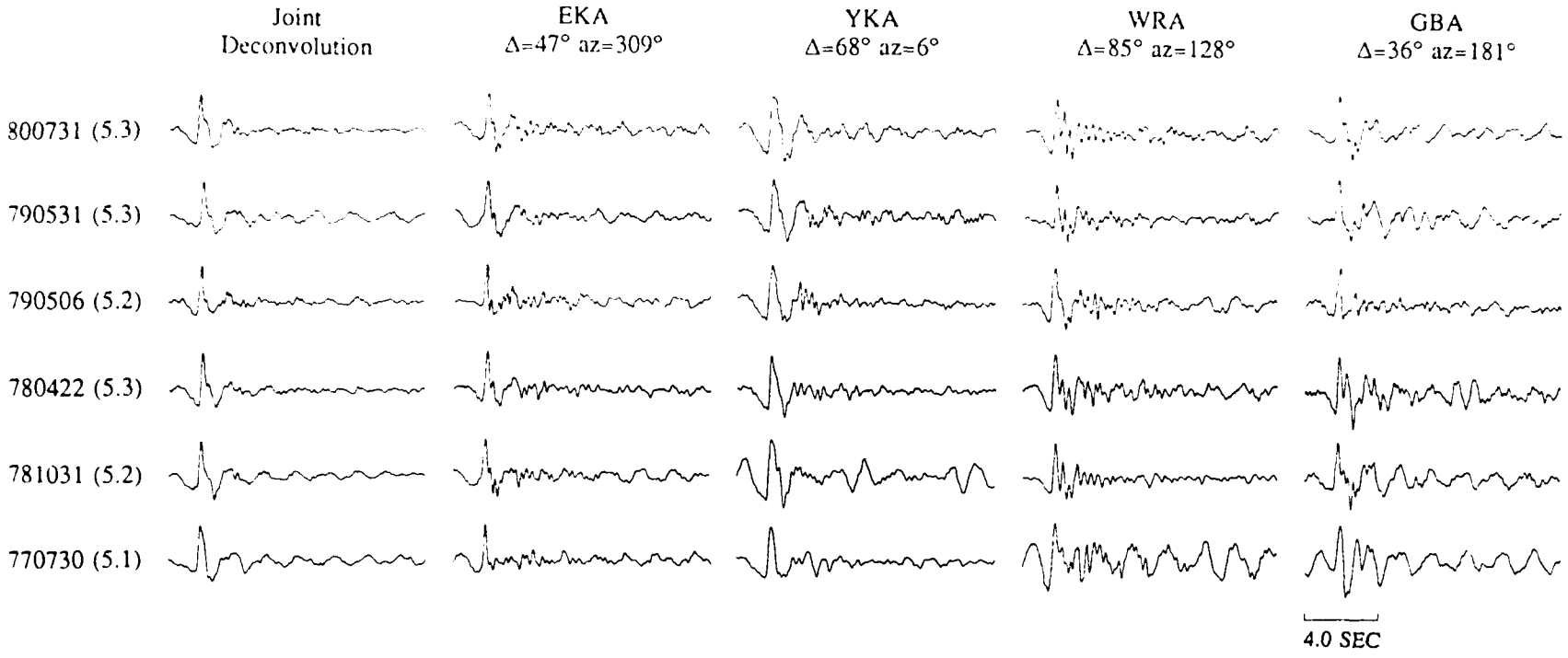

Figure 17. Comparison of source deconvolutions (VSB not removed) for a set of common events at each of the AWRE arrays and a joint deconvolution using six sensors at each array.

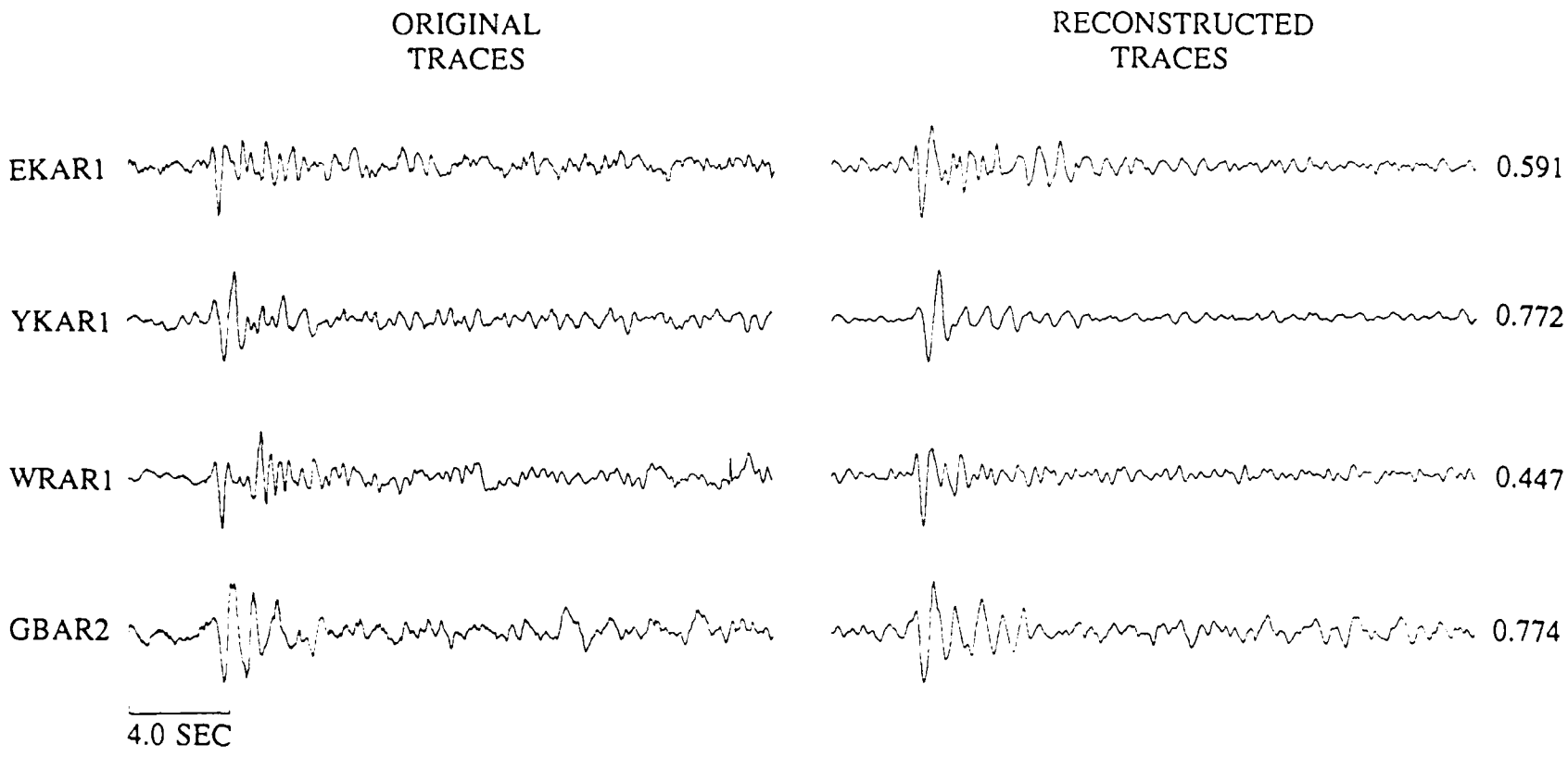

Figure 18. Comparison of some original traces and reconstructions obtained from the joint deconvolution of common events at the four AWRE arrays. The poor quality of reconstructions (unlike those at individual arrays) indicates a considerable asymmetry in the source radiation from C-EKTS.

Results for E-EKTS Explosions

Various subsets of the E-EKTS explosion data were deconvolved at EKA, GBA, WRA, and YKA. Marshall et al (1984) classified the waveforms from E-EKTS events into types 1 (simpler) and 2 (more complex), the origin locations of which are shown on the map in Figure 19. Figure 20 is a map of the locations of the E-EKTS events deconvolved in this study, and Figures 21 to 24 show the source functions from deconvolutions with the VSB source pulse removed. Most events show strong secondary arrivals of negative polarity which may be interpreted as pP following the initial P wave arrival. In this respect, the E-EKTS results are noticeably different from those obtained for the C-EKTS test site. One exception is the cratering explosion (event 650115 at the bottom of Figure 21) which does not have a clear pP arrival. This event was also shown to have a magnitude bias relative to other (E-EKTS) events used for comparison (Der et al 1986a,b). To the right of each trace in Figures 21 to 24 is a "1" or "2" according to the waveform classification of Marshall et al (1984) for of E-EKTS events. Class "1" events show simpler P + pP waveforms than do Class "2" events, and the results of our deconvolutions are generally consistent with the classifications of Marshall et al.

One may ask the question whether the differences between the C-EKTS and E-EKTS source functions may be due to differences between the site responses for the two test sites. Based on past results the answer must be negative. The E-EKTS and C-EKTS test sites are not distant enough to cause appreciable differences in the site responses at common arrays, and it is even less likely that this would happen for three arrays at the same time. Moreover, we have been successful in the past in deconvolving a *mix* of C-EKTS and E-EKTS events recorded at NORSAR using the same site functions for both test sites, and the trace reconstructions were of excellent quality indicating that the site functions were practically the same (Der et al 1986a,b).

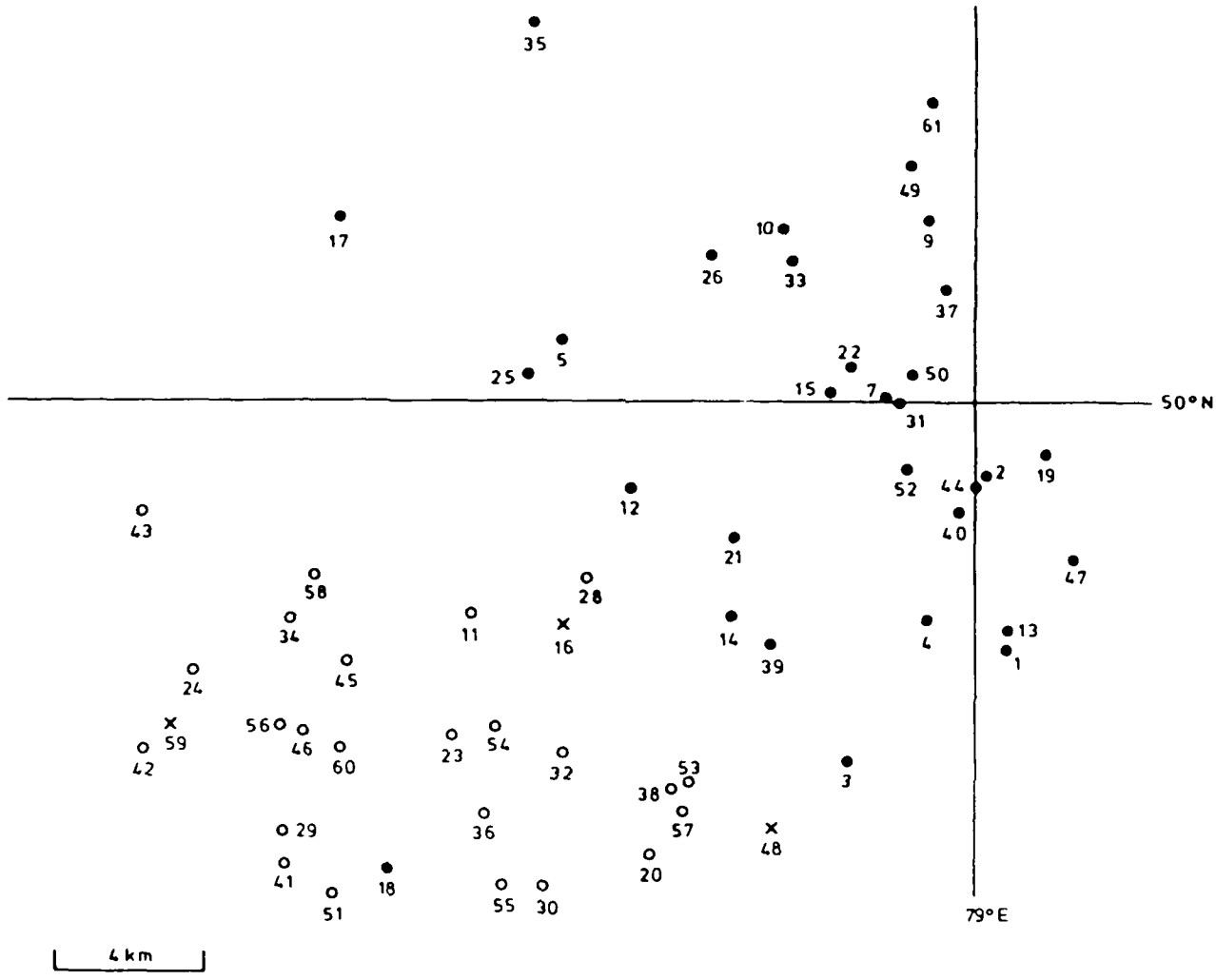

Figure 19. Location of E-EKTS events plotted with symbols representing explosion waveform classification. Open and solid circles represent class 1 and class 2 events, respectively, while an X represents an explosion of ambiguous classification. (from Marshall et al 1984).

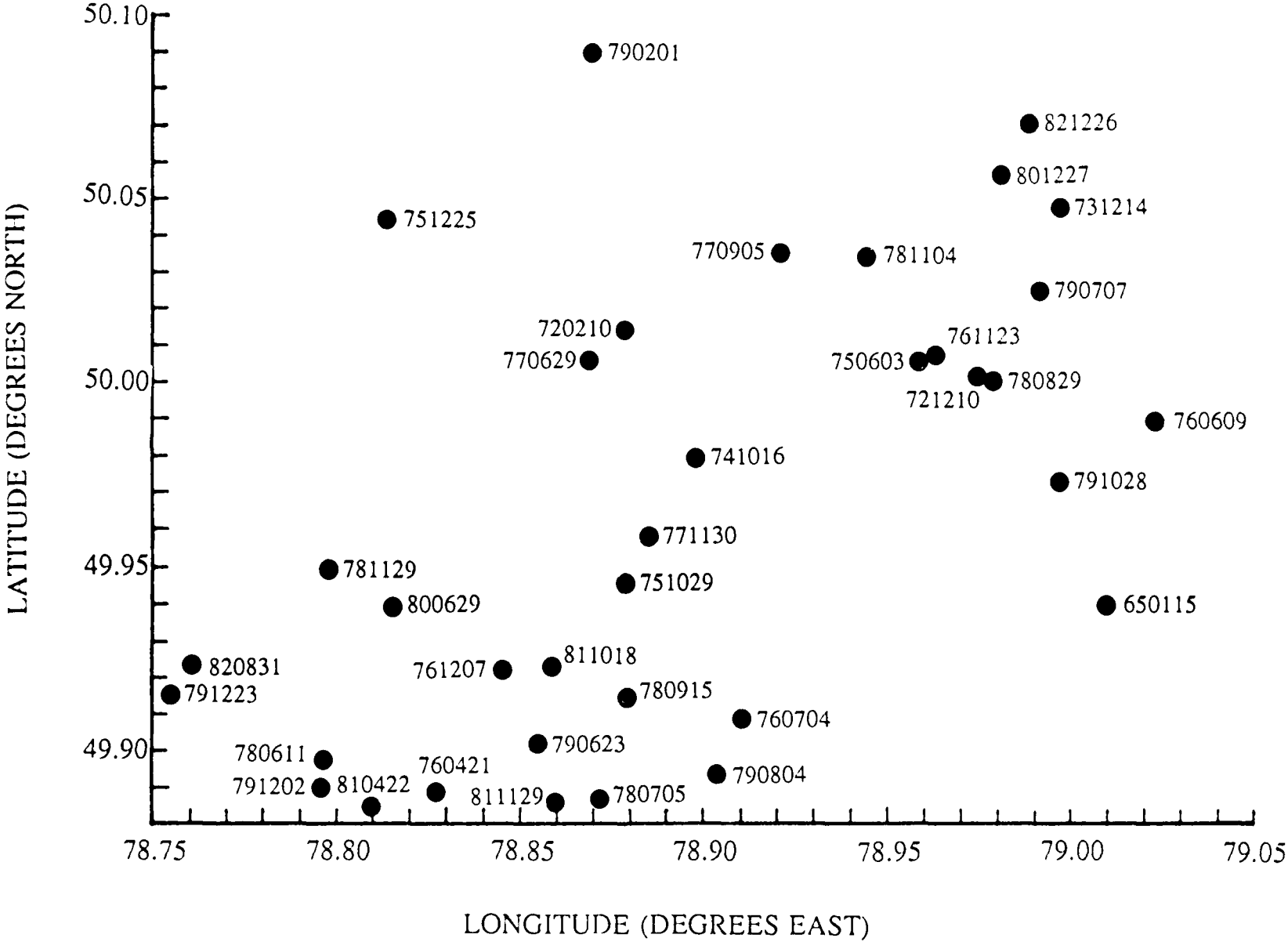

Figure 20. Locations of E-EKTS events analyzed during this study.

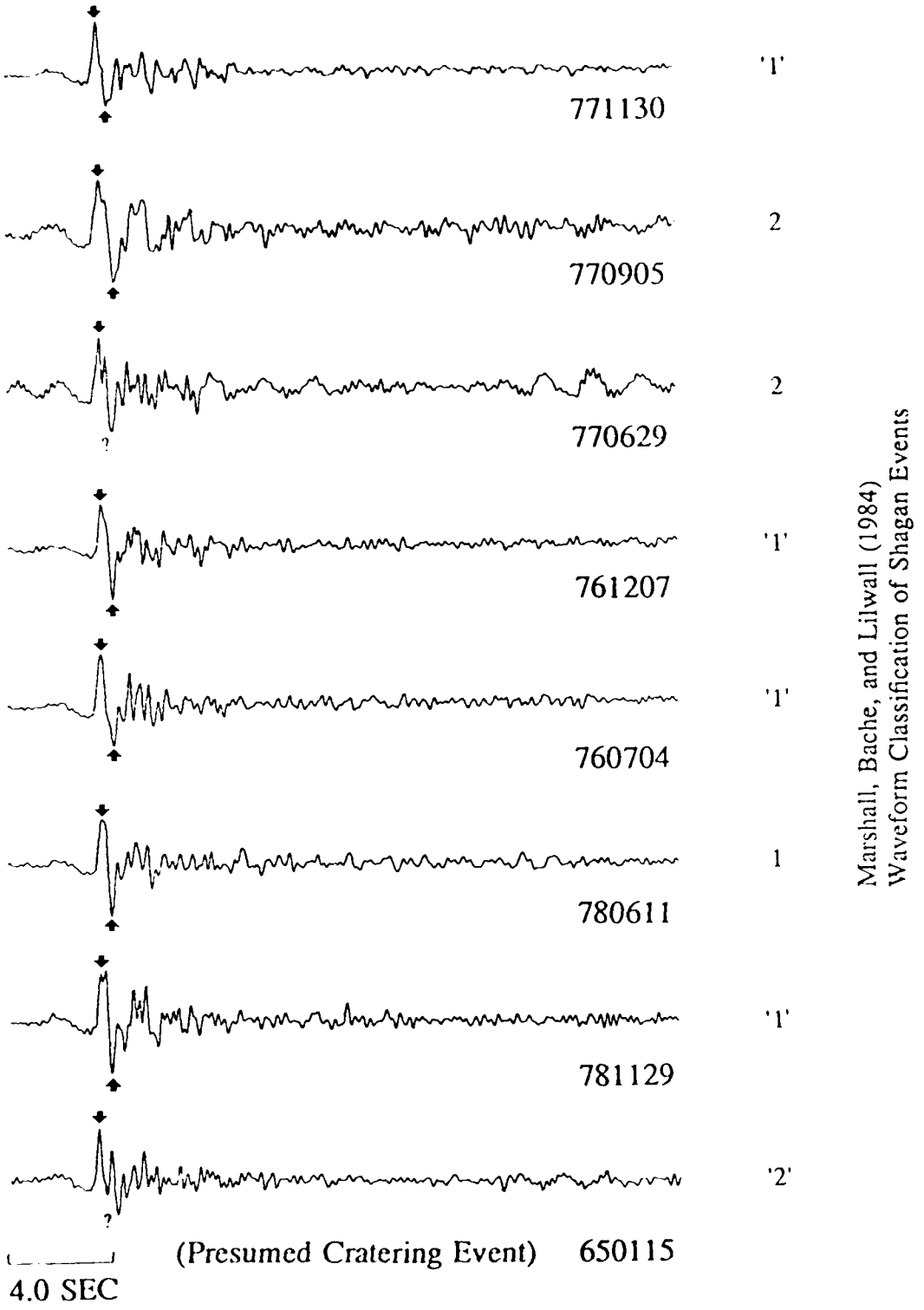

Figure 21 . Source time function estimates obtained for E-EKTS explosions at EKA. A VSB wavelet has been removed in these deconvolutions. The waveform classification assigned by Marshall et al (1984) is noted to the right of each trace. Pulses interpretable as pP are typical of E-EKTS deconvolutions. However, note that the pP is missing for the cratering event (650115).

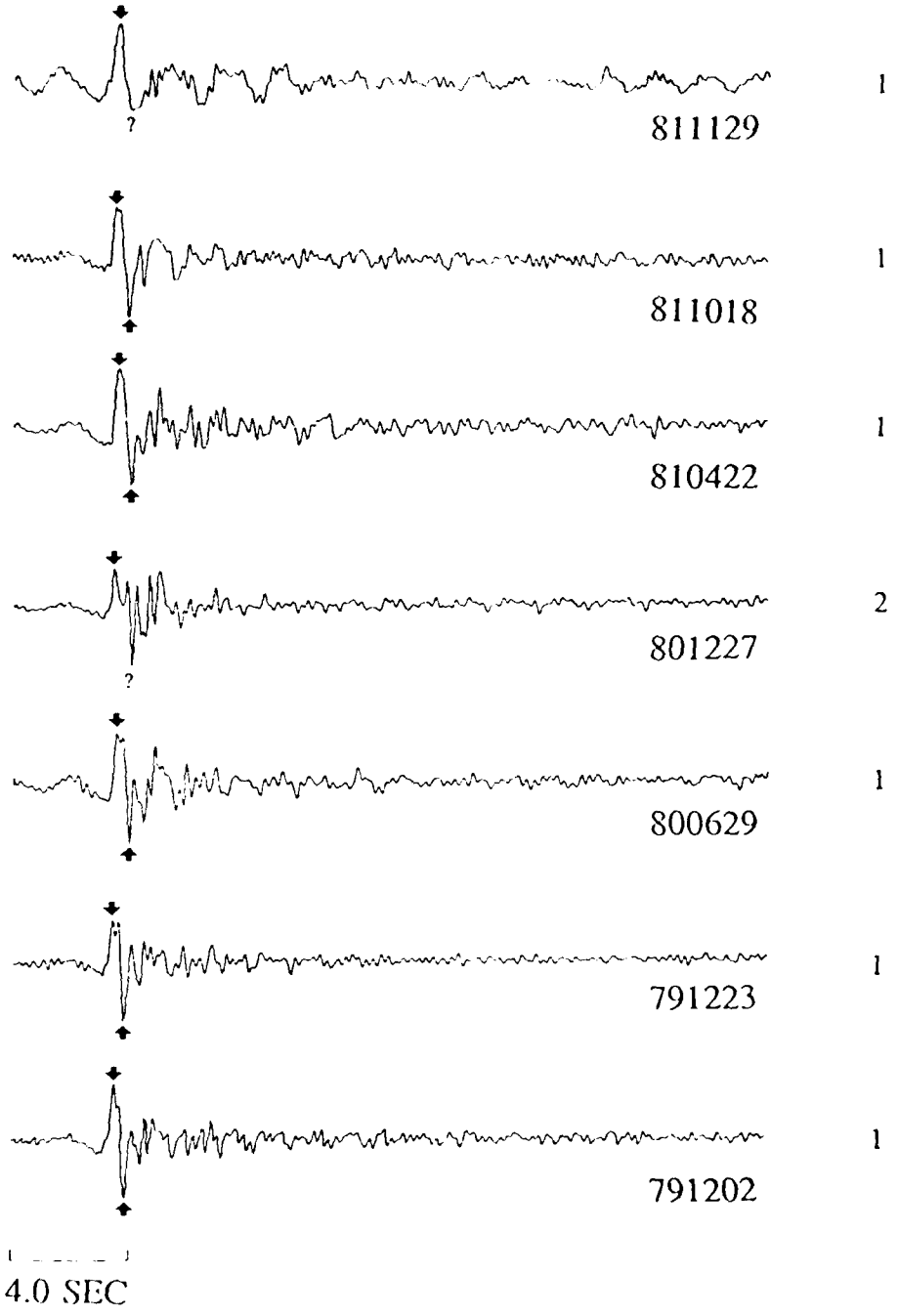

Marshall, Bache, and Lilwall (1984)
Waveform Classification of Shagan Events

Figure 21 Continued.

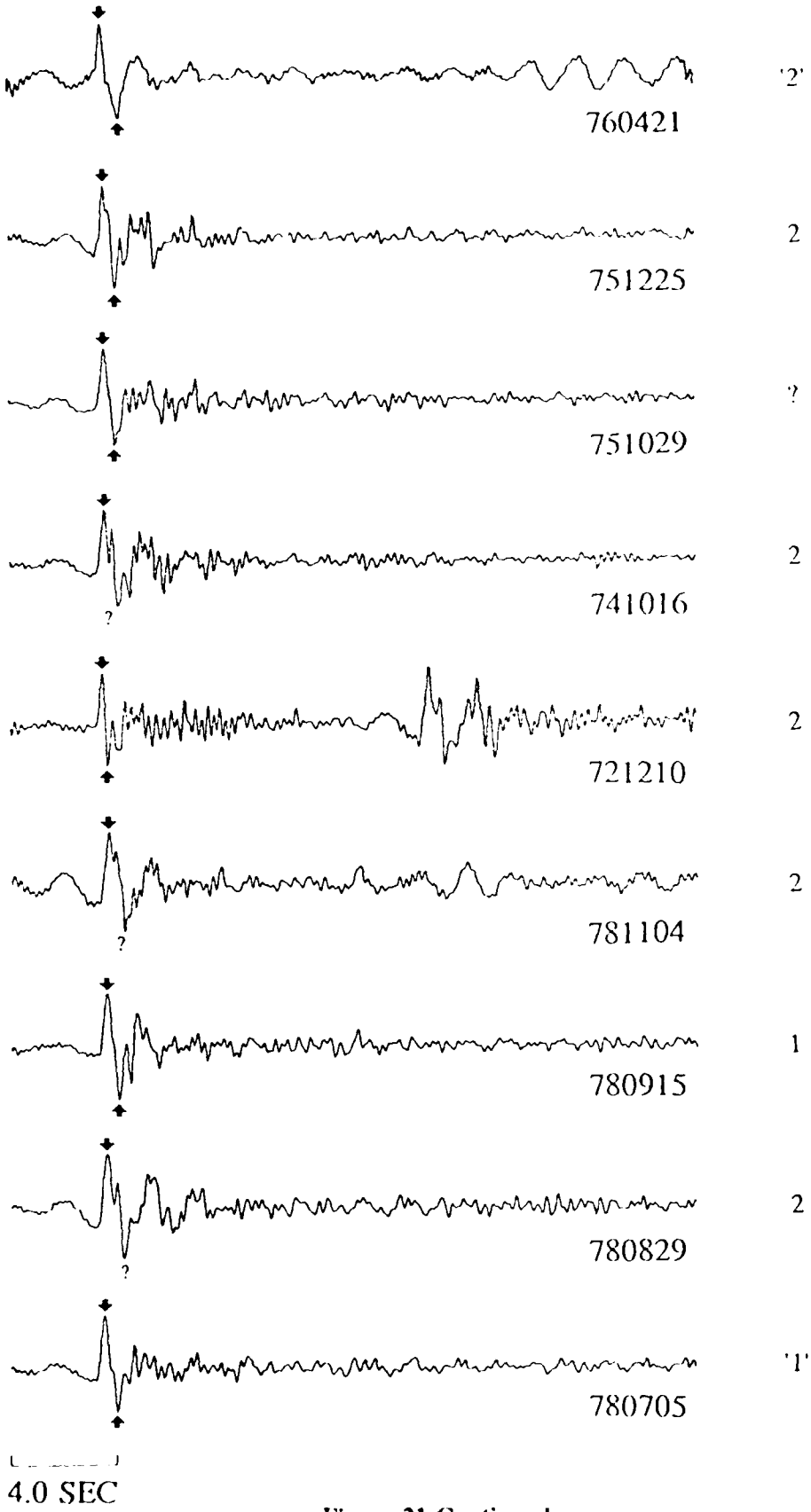

Figure 21 Continued.

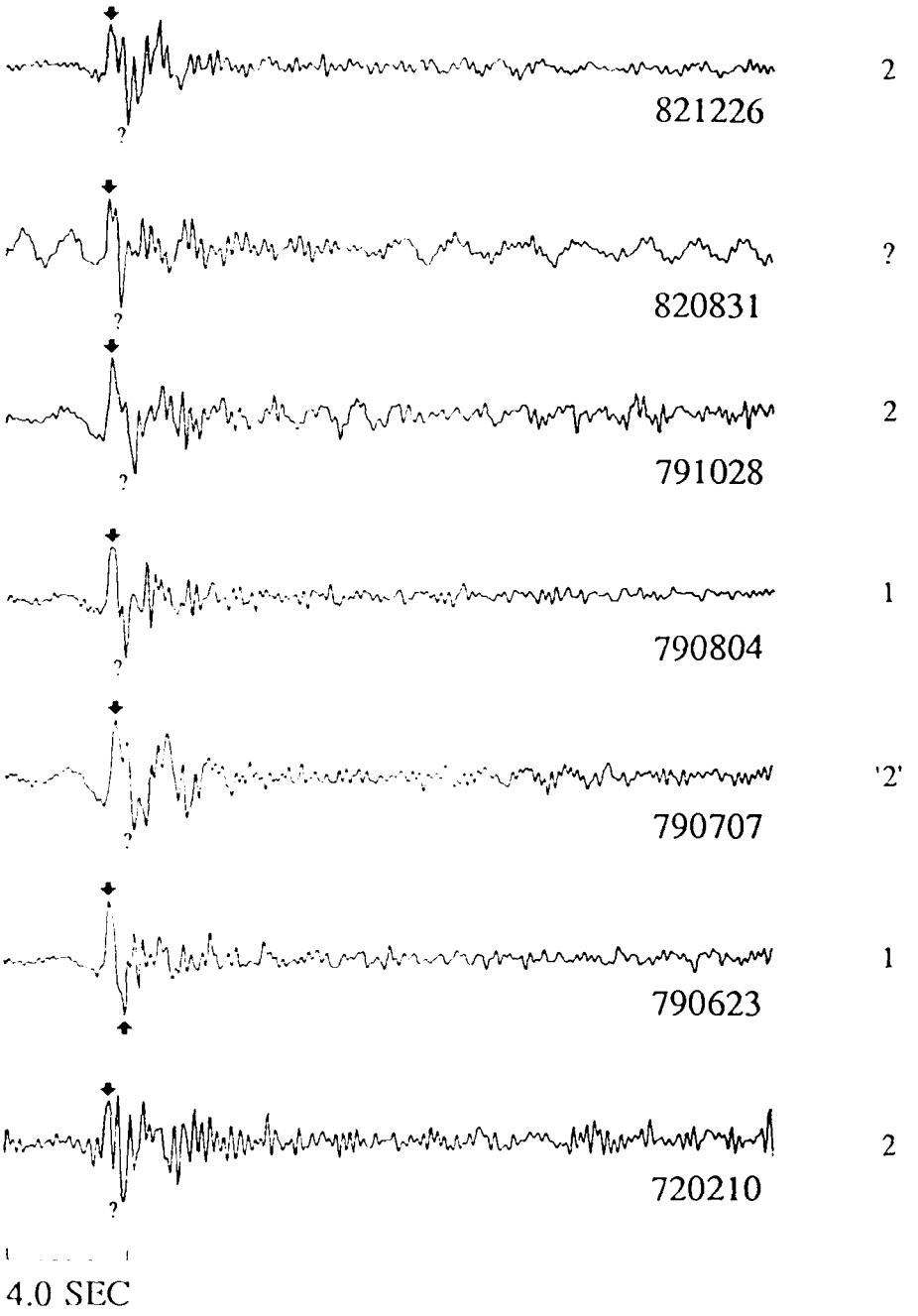

Marshall, Bache, and Lilwall (1984)
Waveform Classification of Shagan Events

Figure 21 Continued.

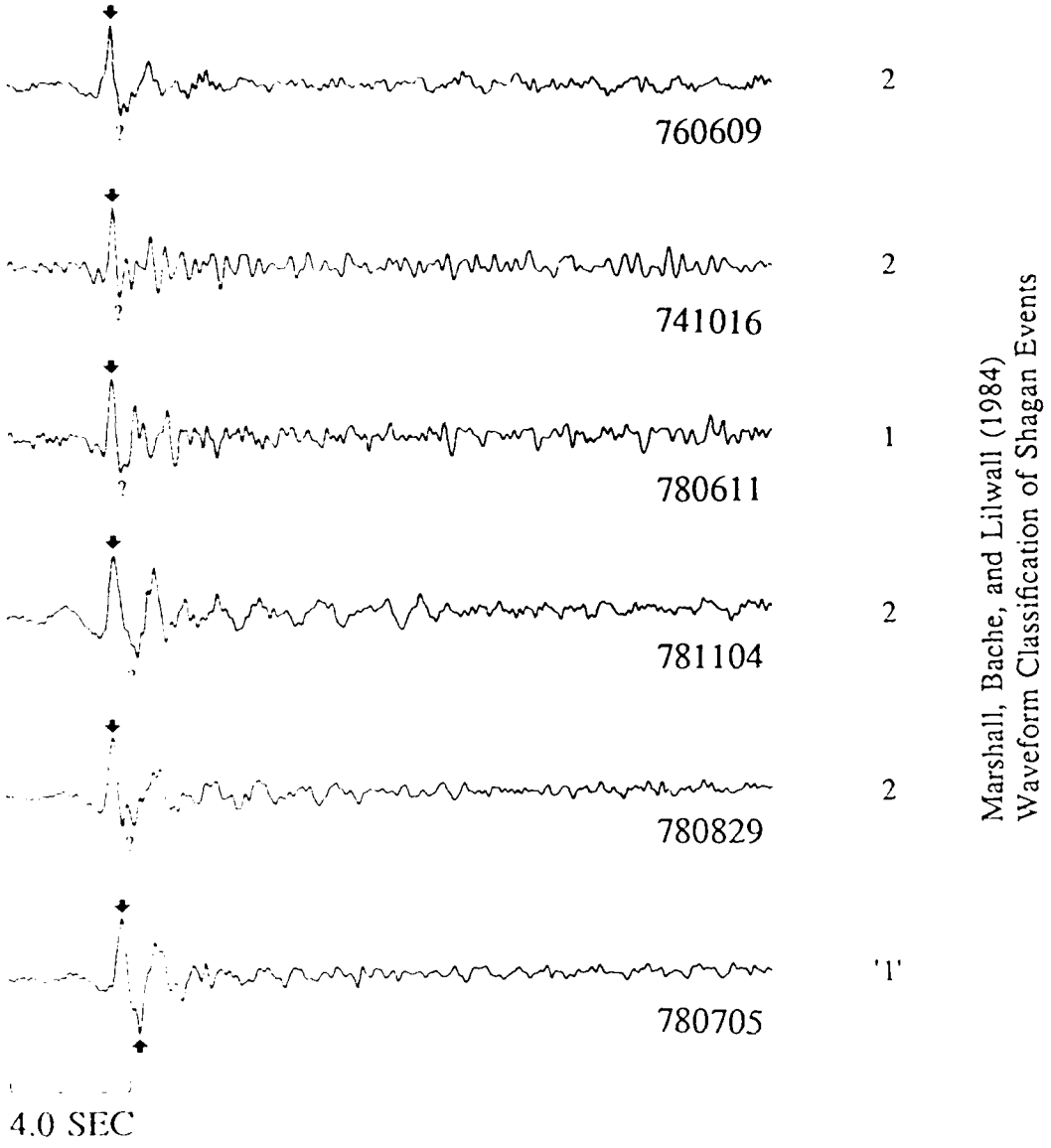

Figure 22. Source time function estimates obtained for E-EKTS explosions at GBA. A VSB wavelet has been removed in these deconvolutions. The waveform classification assigned by Marshall et al (1984) is noted to the right of each trace.

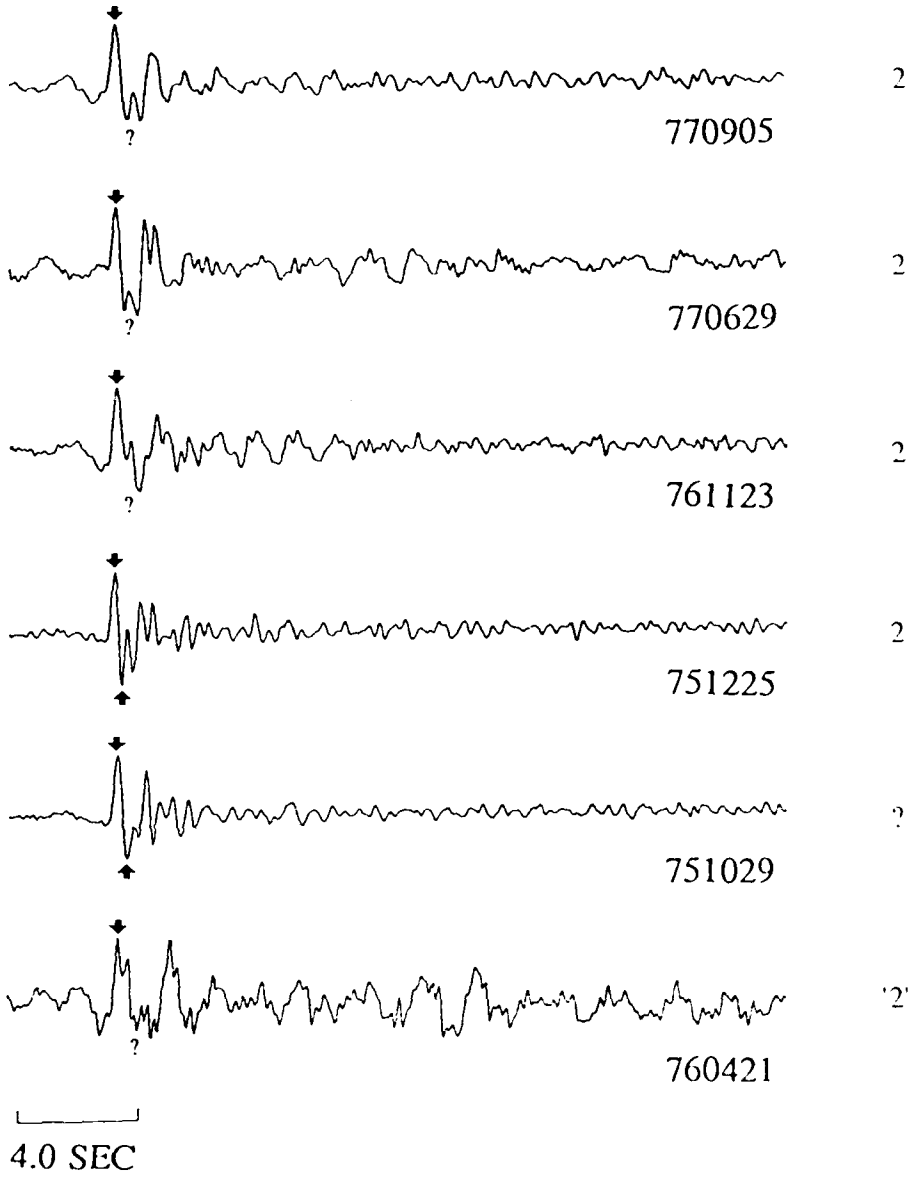

Marshall, Bache, and Lilwall (1984)
Waveform Classification of Shagan Events

Figure 22 Continued.

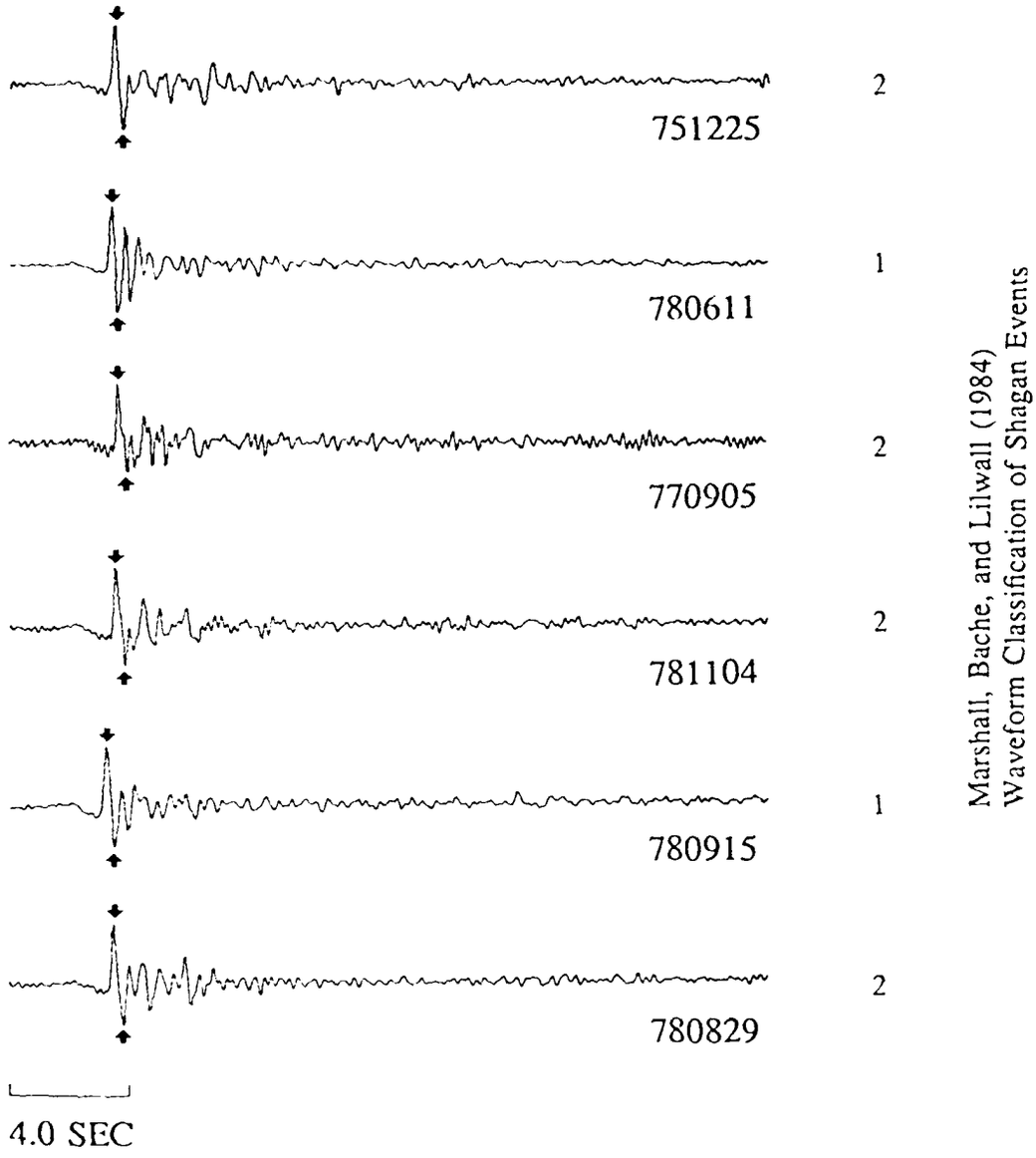

Figure 23. Source time function estimates obtained for E-EKTS explosions at WRA. A VSB wavelet has been removed in these deconvolutions. The waveform classification assigned by Marshall et al (1984) is noted to the right of each trace.

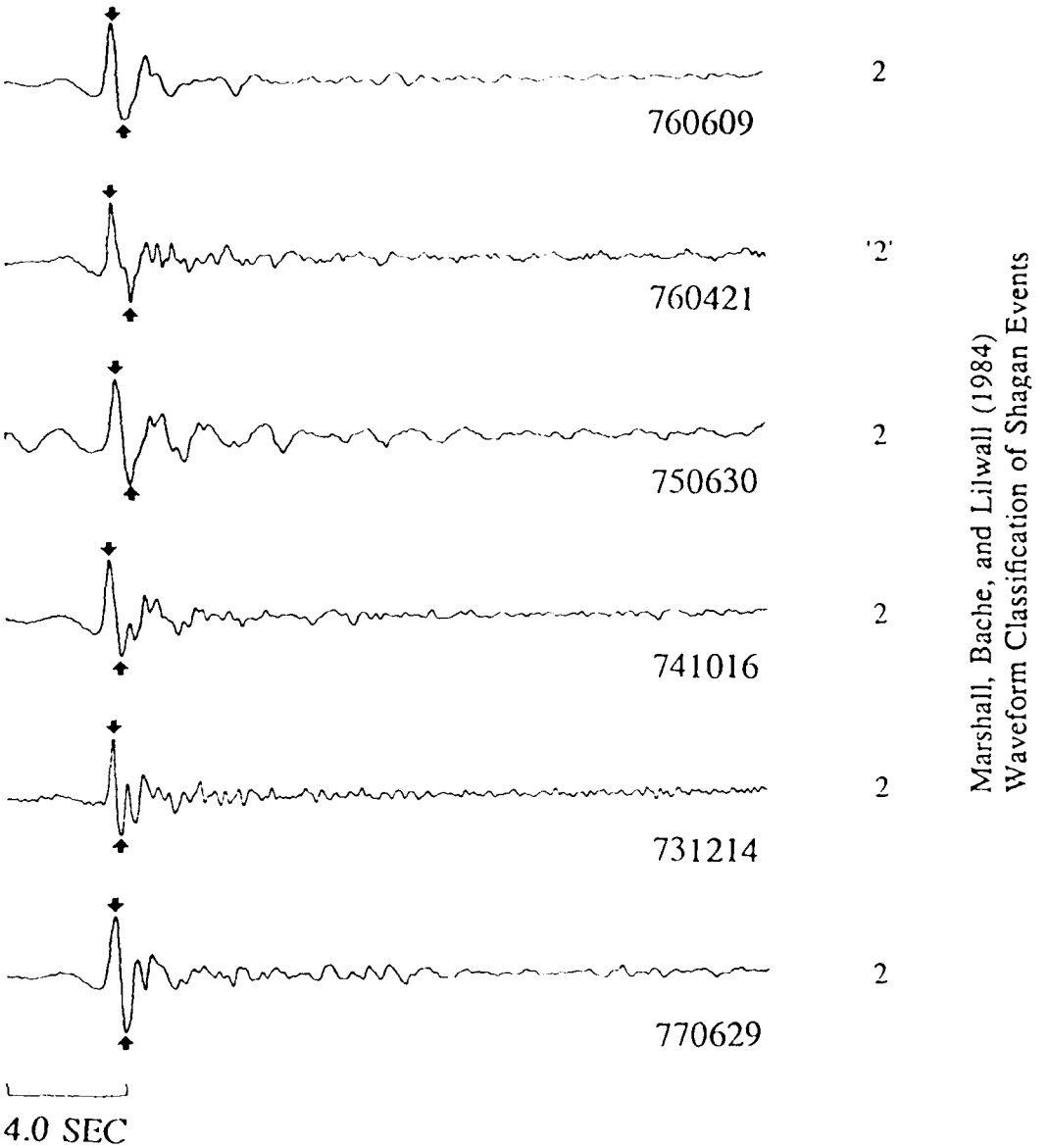

Figure 24. Source time function estimates obtained for E-EKTS explosions at YKA. A VSB wavelet has been removed in these deconvolutions. The waveform classification assigned by Marshall et al (1984) is noted to the right of each trace.

Results for Novaya Zemlya Events

The estimated locations of the 13 Novaya Zemlya events, analyzed at EKA, GBA, and YKA, are shown in Figure 25. We have 12 events from the northern Novaya Zemlya test site and one event from the southern Novaya Zemlya test site. Figures 26 to 28 show source time functions at the three arrays with the VSB source pulse removed and Figure 29 is a composite of deconvolutions at the separate arrays, without the VSB removed. In Figure 29, the events are loosely arranged by location according to the map in Figure 25. Event 801011 has been identified by Marshall et al (1986) as a double event and in our deconvolutions this can best be seen on the source function for 801011 as deconvolved at EKA.

The most striking observation about the waveforms in Figure 29 is how much more complex the P wave and P wave coda are at YKA than at EKA and GBA. However, even though the waveforms at YKA are very complex, they do reconstruct very well as shown in Figure 30. Greenfield (1971) has previously noted the complex coda for Novaya Zemlya events recorded at YKA and McLaughlin et al (1968c) have observed that stations at azimuths of 352 to 111° from Novaya Zemlya have significantly shorter P wave coda than stations at azimuths of 150 to 349°. While the deconvolved sources at YKA are too complex to identify a pP arrival, a pP arrival can be recognized on most of the deconvolutions of recordings at EKA and GBA. Even though the source functions at EKA and GBA are much simpler than those at YKA, they consistently show late arrivals other than pP. Some of the later arrivals at EKA may be due to triplications in the P wave travel time curve which still has two observable branches at a distance of 29° for shield models such as that of King and Calcagnile (1976).

It is also interesting to examine the source functions for the one event from southern Novaya Zemlya (730927). This event has simpler source functions at both EKA and YKA

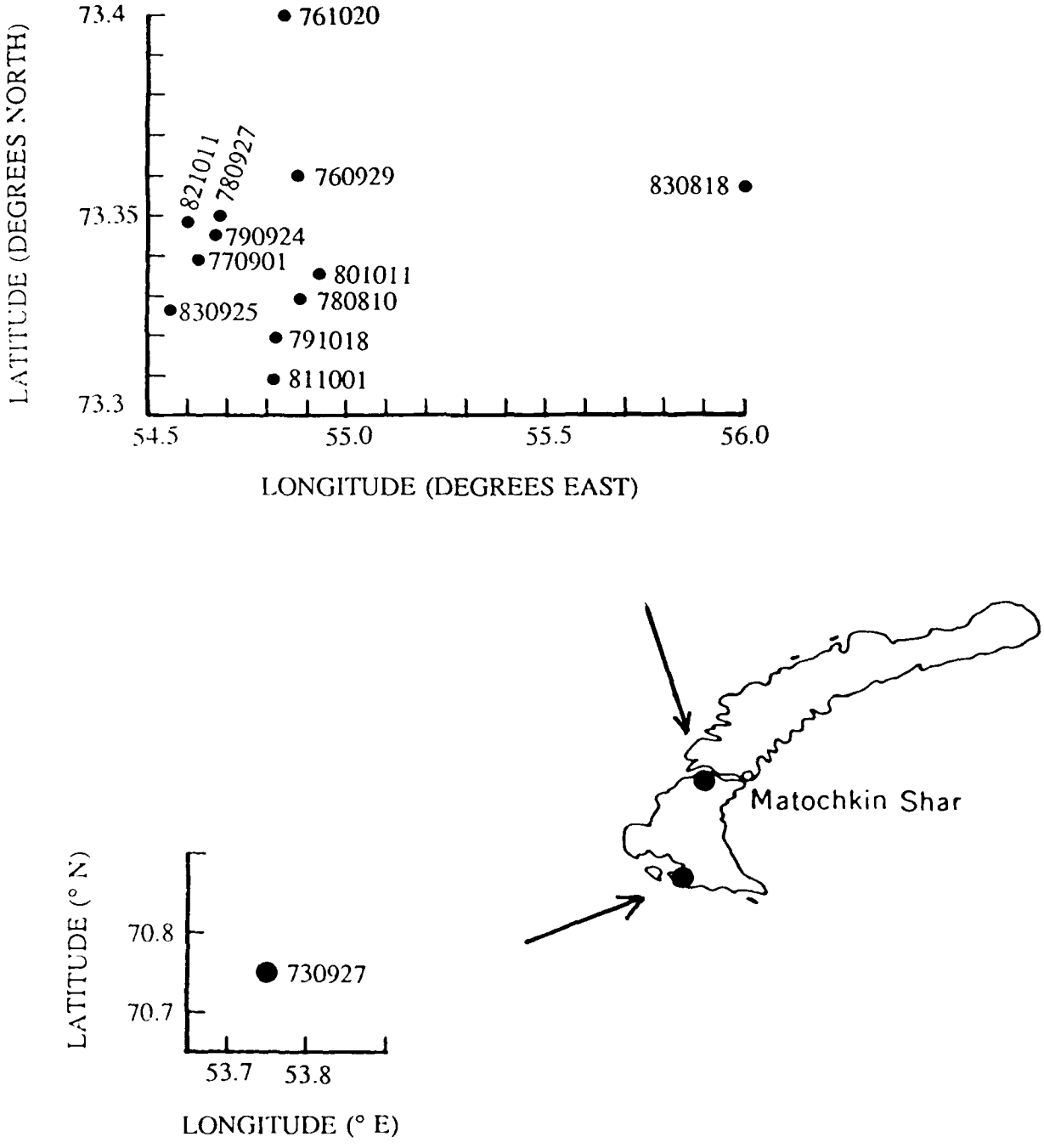

Figure 25. Locations of Novaya Zemlya events analyzed in this report

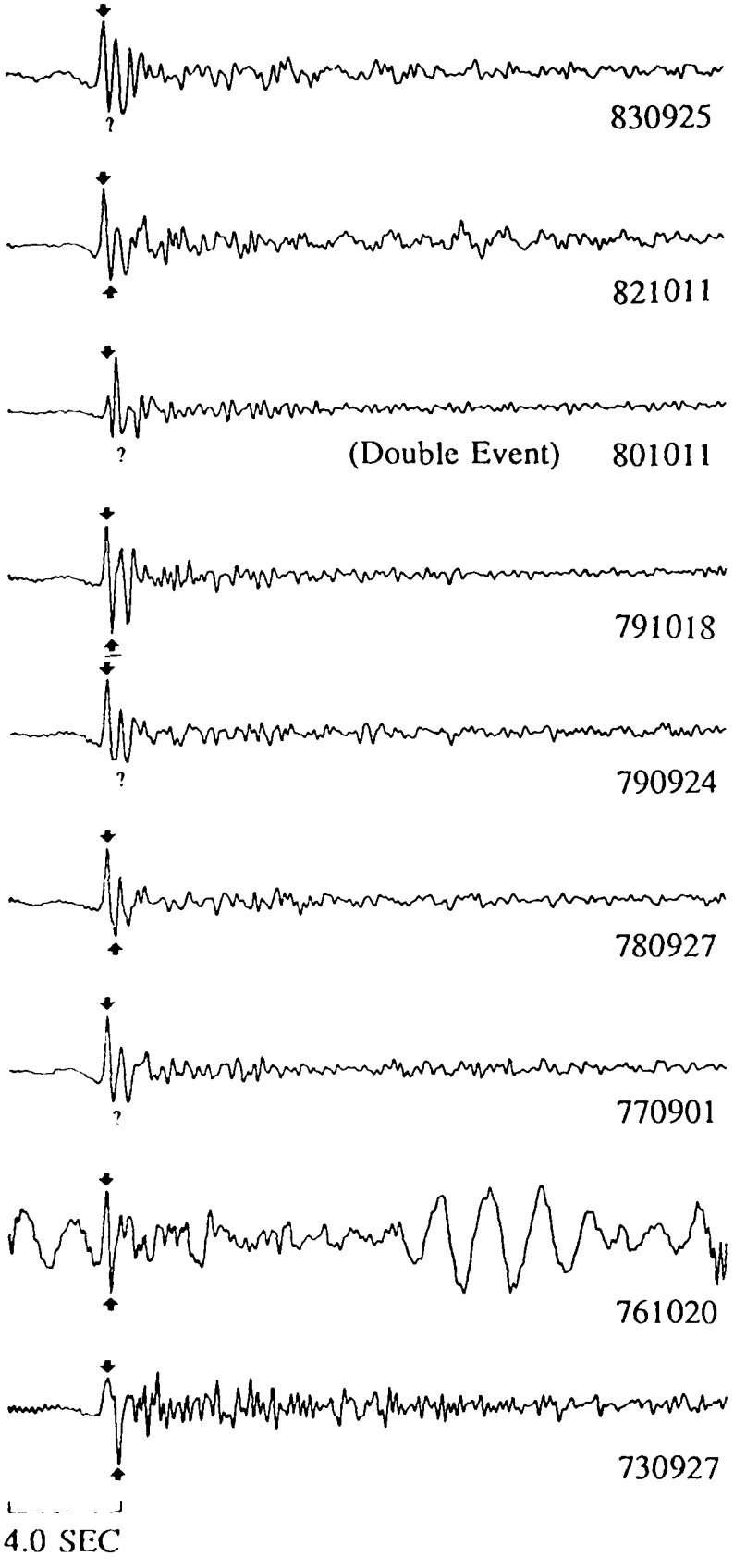

Figure 26. Source time function estimates obtained for Novaya Zemlya events at EKA. A VSB wavelet has been removed in these deconvolutions.

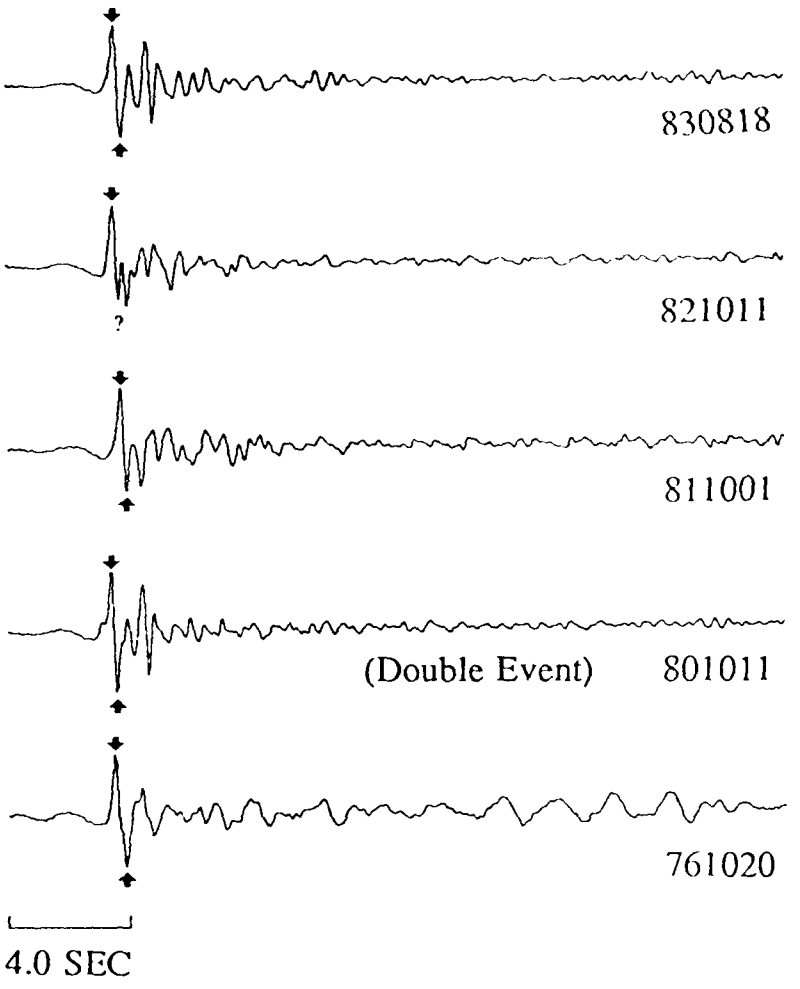

Figure 27. Source time function estimates obtained for Novaya Zemlya events at GBA. A VSB wavelet has been removed in these deconvolutions.

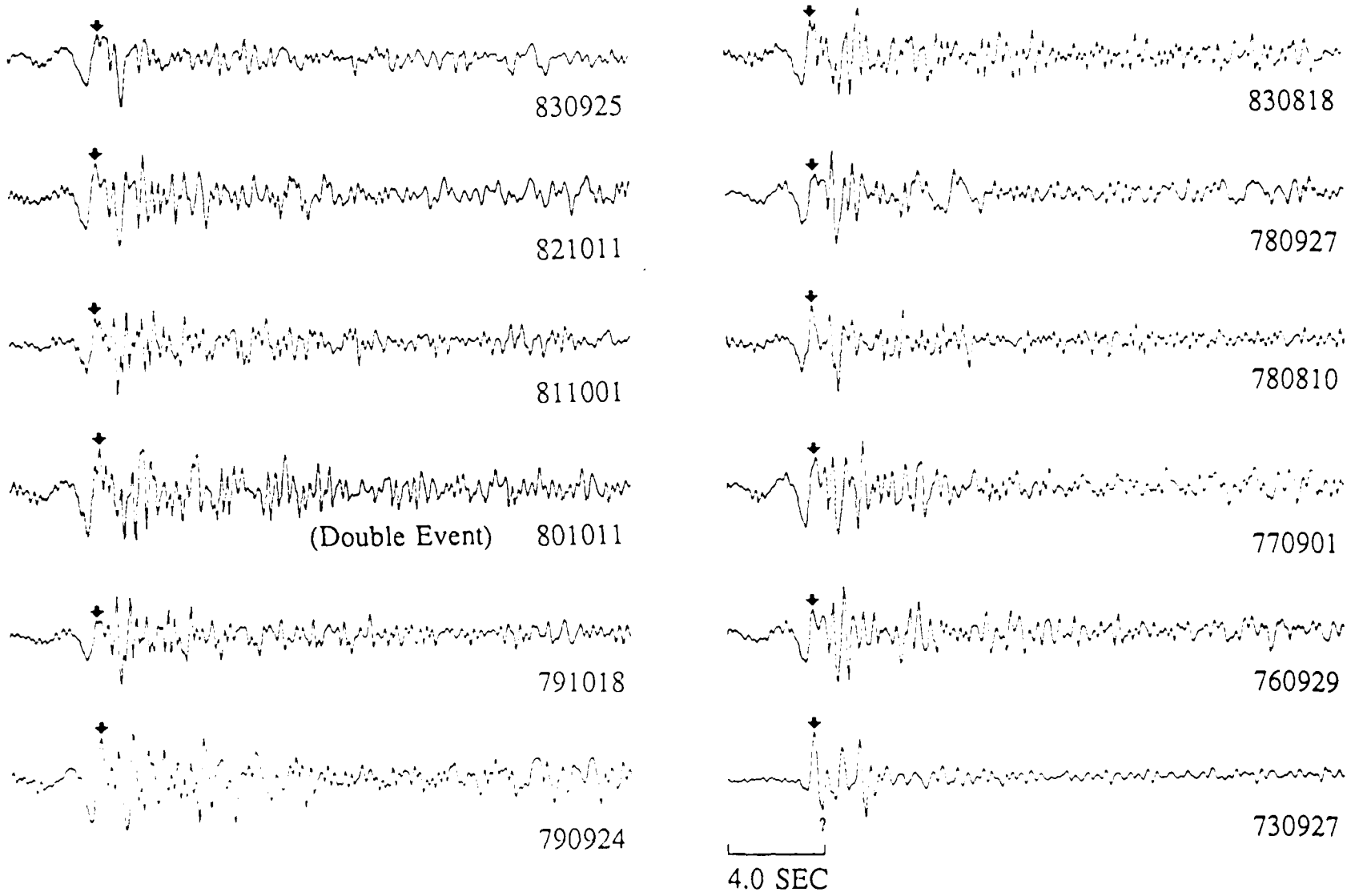

Figure 28. Source time function estimates obtained for Novaya Zemlya events at YKA. A VSB wavelet has been removed in these deconvolutions.

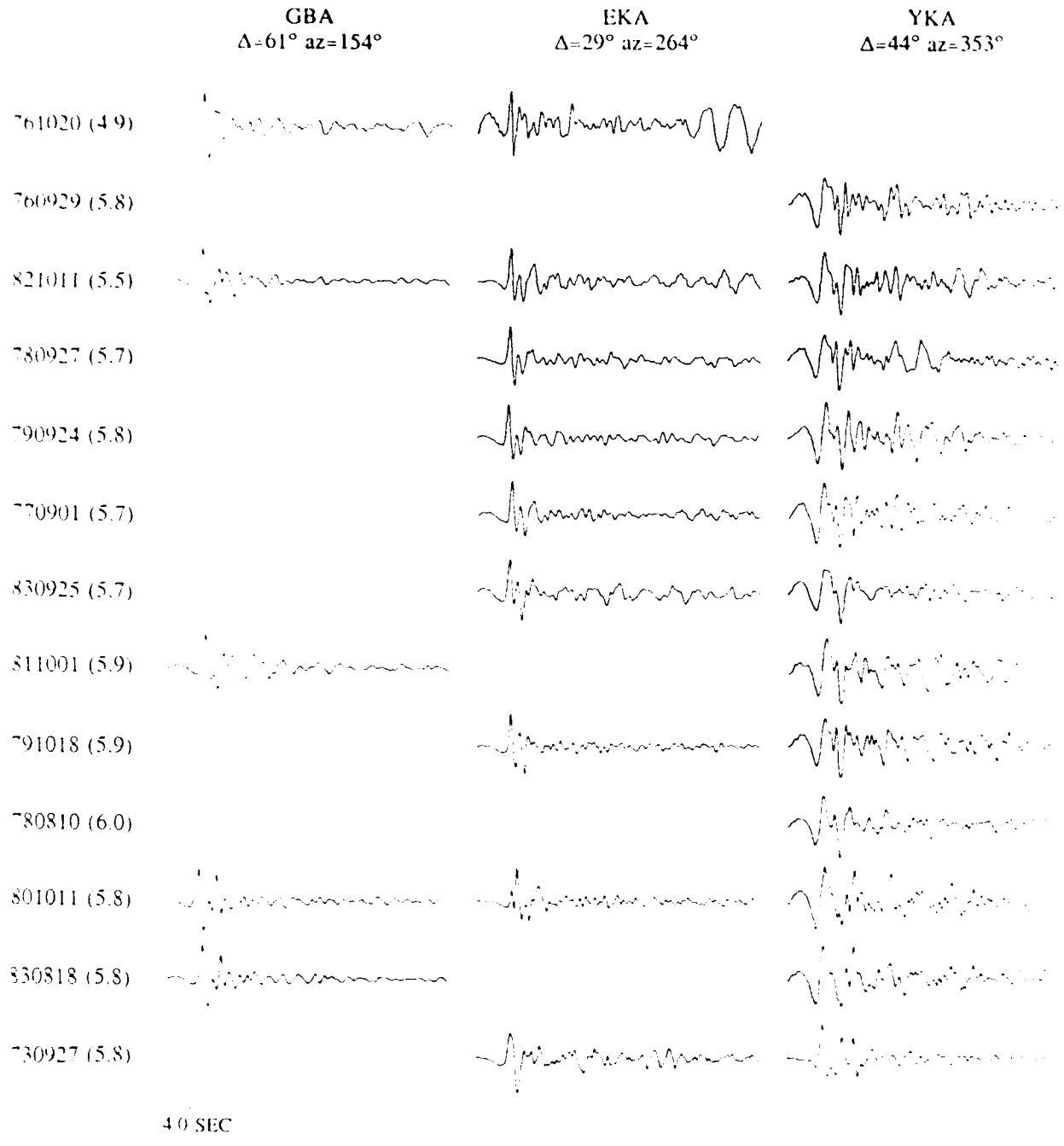

Figure 29. Source time function estimates for Novaya Zemlya events at three AWRE arrays. A VSB wavelet has not been removed in these deconvolutions. The source time functions (as well as the original seismograms) are quite complex at YKA in comparison with the other arrays.

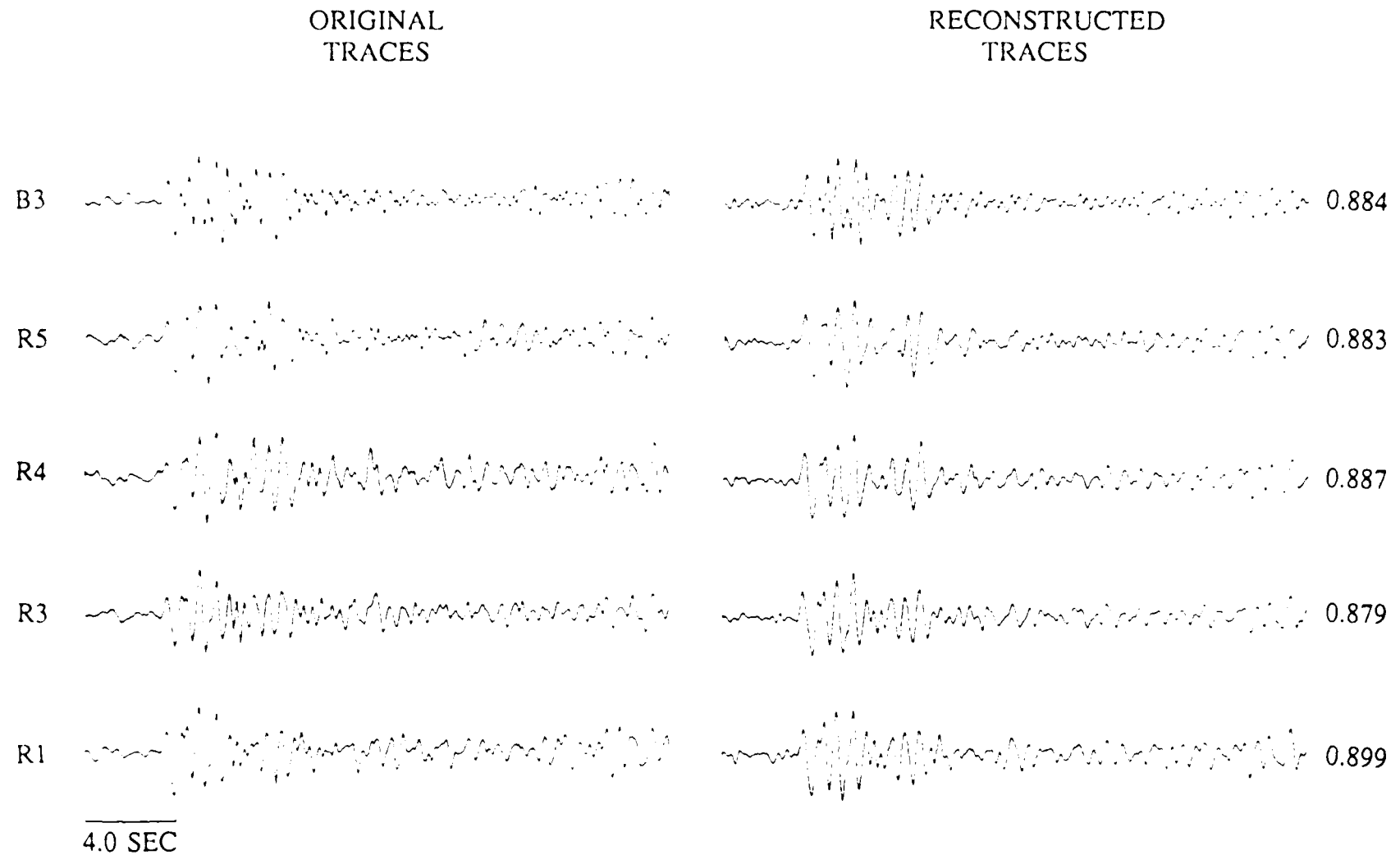

Figure 30. Examples of trace reconstructions compared to original traces at selected sites of YKA. The quality of reconstruction is quite good.

than do the northern Novaya Zemlya events. One possible explanation for this may be the difference in surface topography between the northern and southern test sites; the northern Novaya Zemlya test site is very mountainous while the southern test site is in a much flatter area (per map in Marshall et al, 1986).

Results for French Sahara Nuclear Tests

A map of the locations of the main events at this test site is shown in Figure 31. Only a few nuclear explosions in Sahara were available with acceptable S/N ratios at AWRE arrays. The Sahara test site is another low Q area (Der et al 1985), thus making deconvolutions difficult. The deconvolutions yielded fairly complex time functions for the sources which vary considerably with azimuth (Figure 32) but with good reconstructions in all directions. We interpret this as azimuthal asymmetries in the radiation which, in the view of the complex topography of the test site is to be expected (McLaughlin et al 1986b). Due to the limited bandwidth of the records we did not attempt to factor out the VSB source wavelet.

Results for Pahute Mesa Events

Twelve Pahute Mesa events plus the shot Faultless were deconvolved at EKA, GBA, WRA, and YKA. A map of the relative locations of the events is shown in Figure 33 and deconvolved source functions, with the VSB source pulse removed, are shown in Figures 34 to 36. The deconvolutions of the Pahute Mesa events show a great deal of ringing and a relatively narrow bandwidth due to the high Q in the NTS region. Reliable pP phases cannot be picked for most of the events. The source function of Faultless deconvolved at EKA (on Figure 34) does not appear significantly different from the deconvolved source functions of other large events at Pahute Mesa.

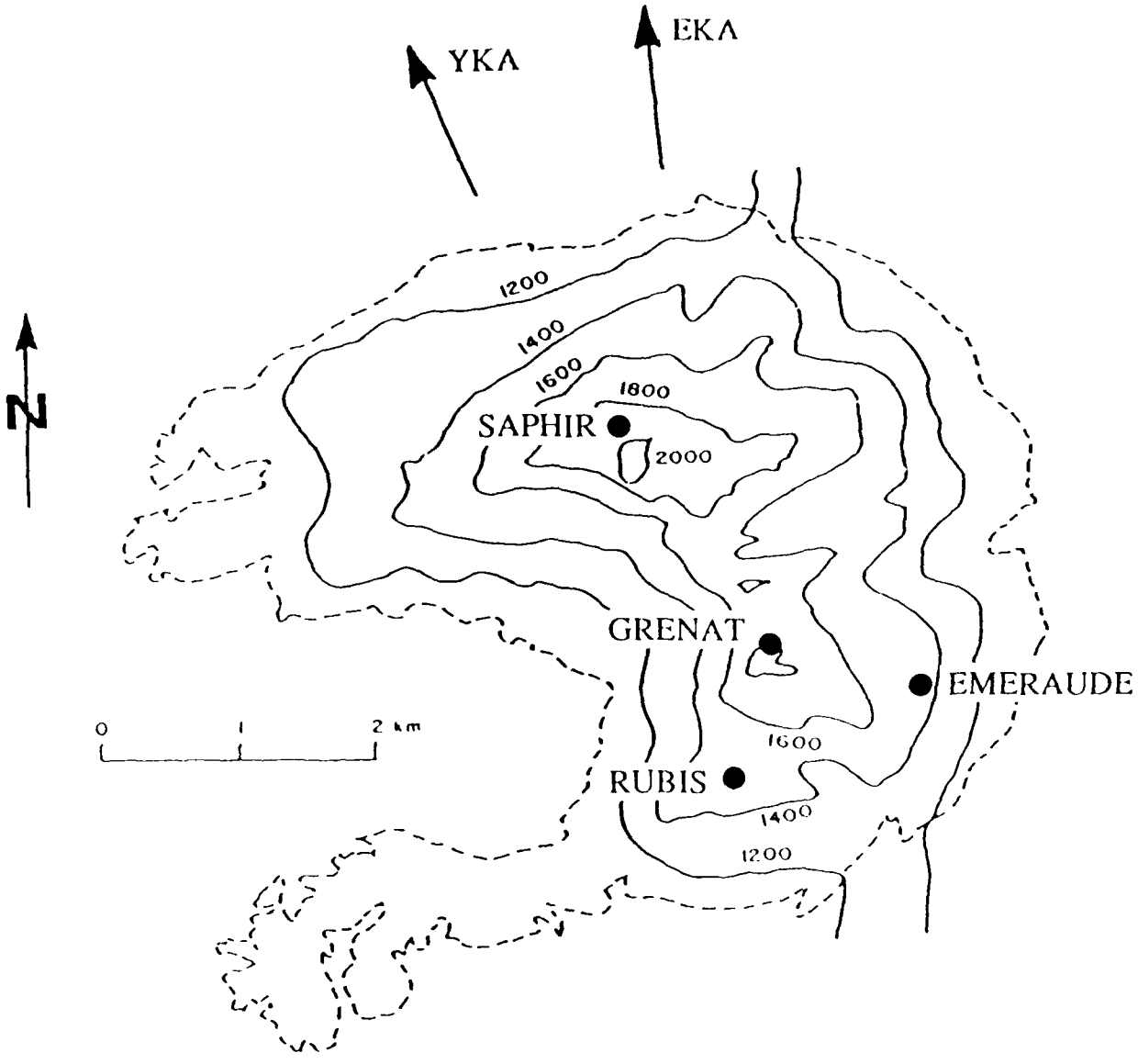

Figure 31. Locations of tests at the French Sahara test area.

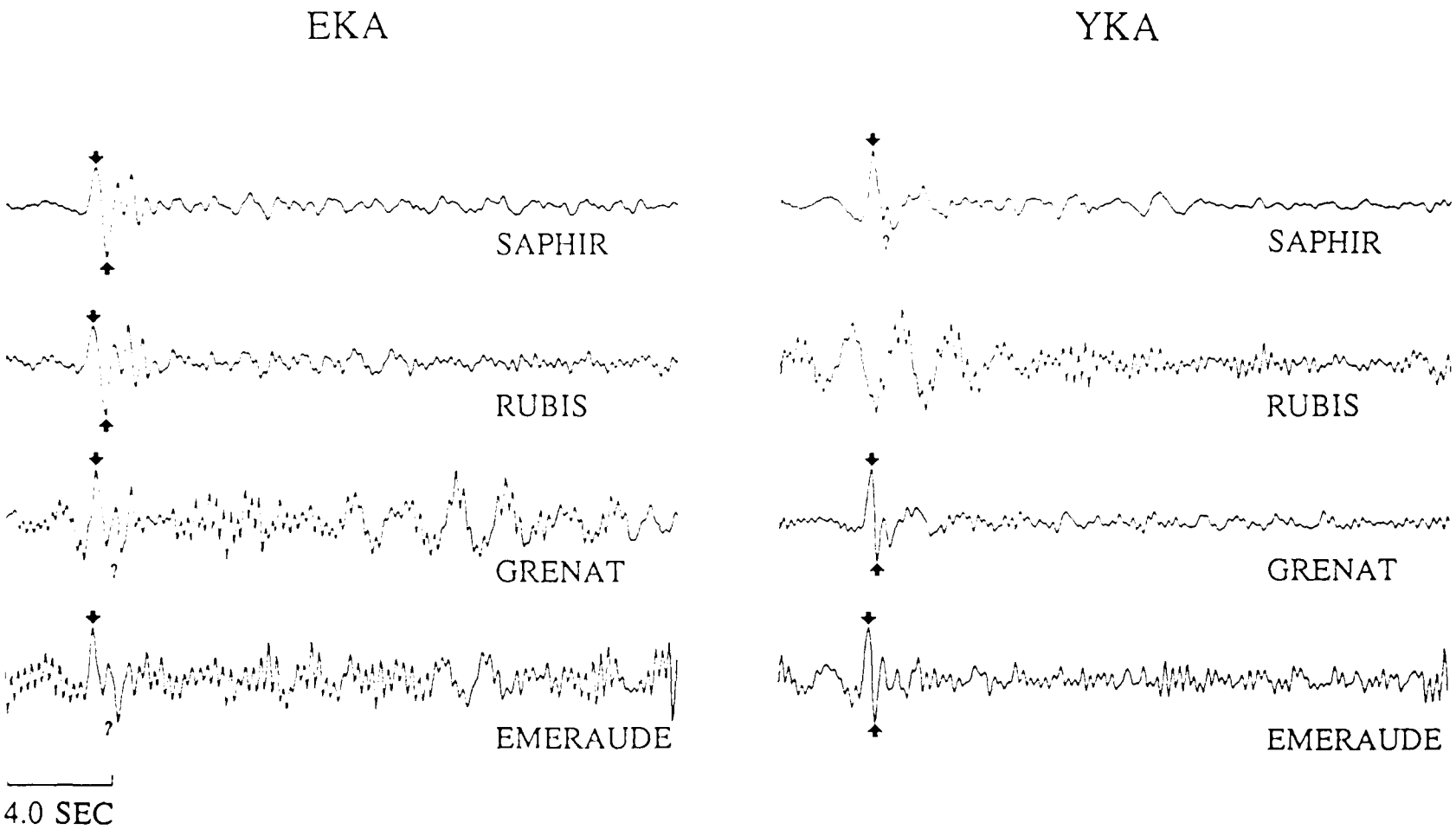

Figure 32. Deconvolution results for source time estimates for all the available data from the French Sahara events at EKA and YKA. VSB wavelets have not been removed in these deconvolutions.

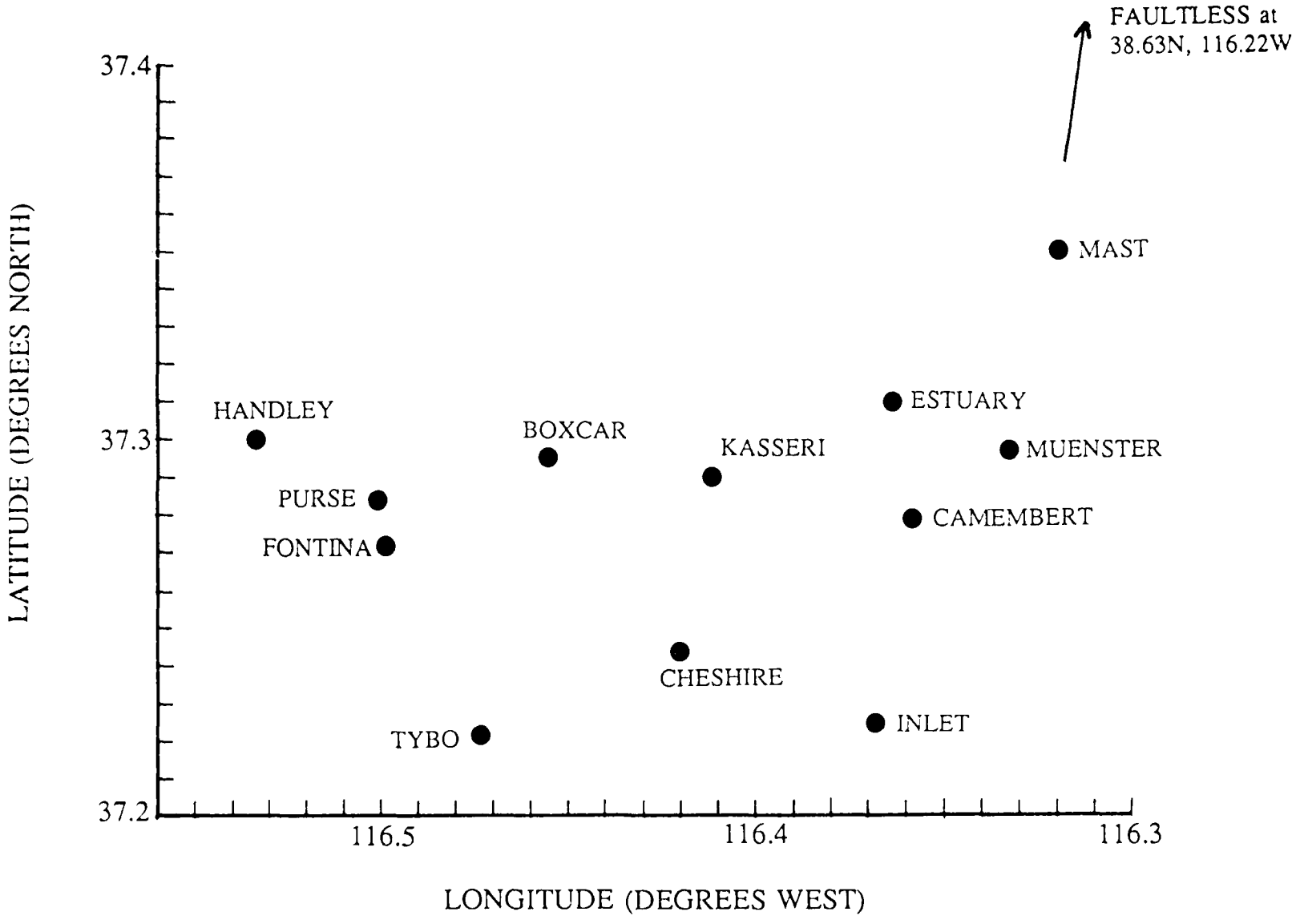

Figure 33. Locations of the Pahute Mesa events analyzed in this report.

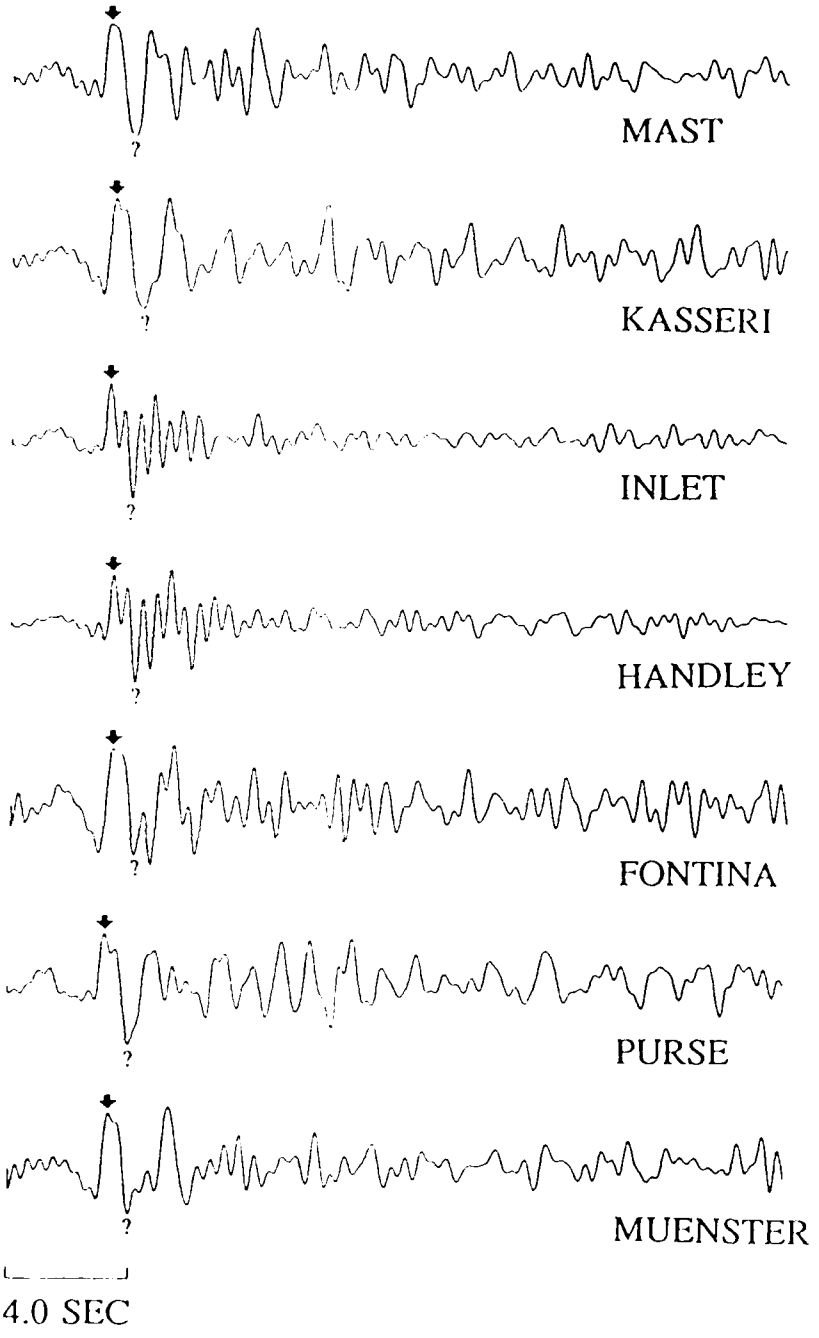

Figure 34. Source time function estimates for thirteen Pahute Mesa explosions at EKA. VSB wavelets have been removed in these deconvolutions.

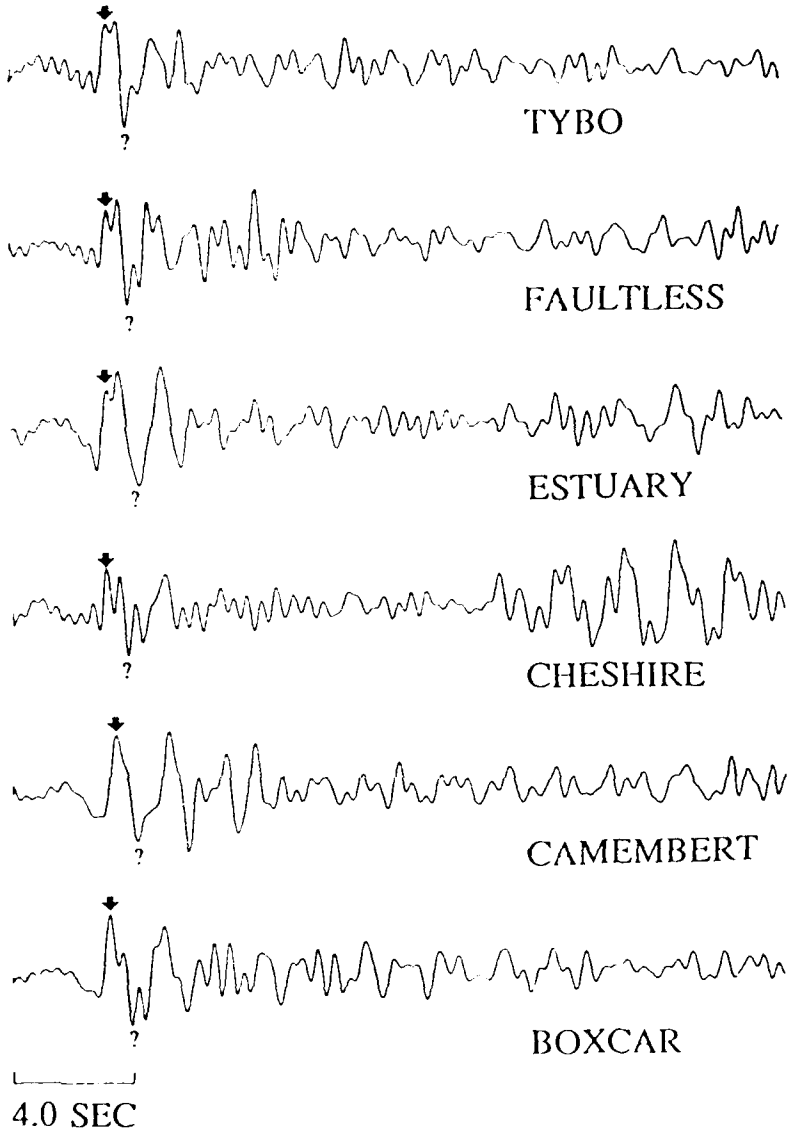

Figure 34 Continued.

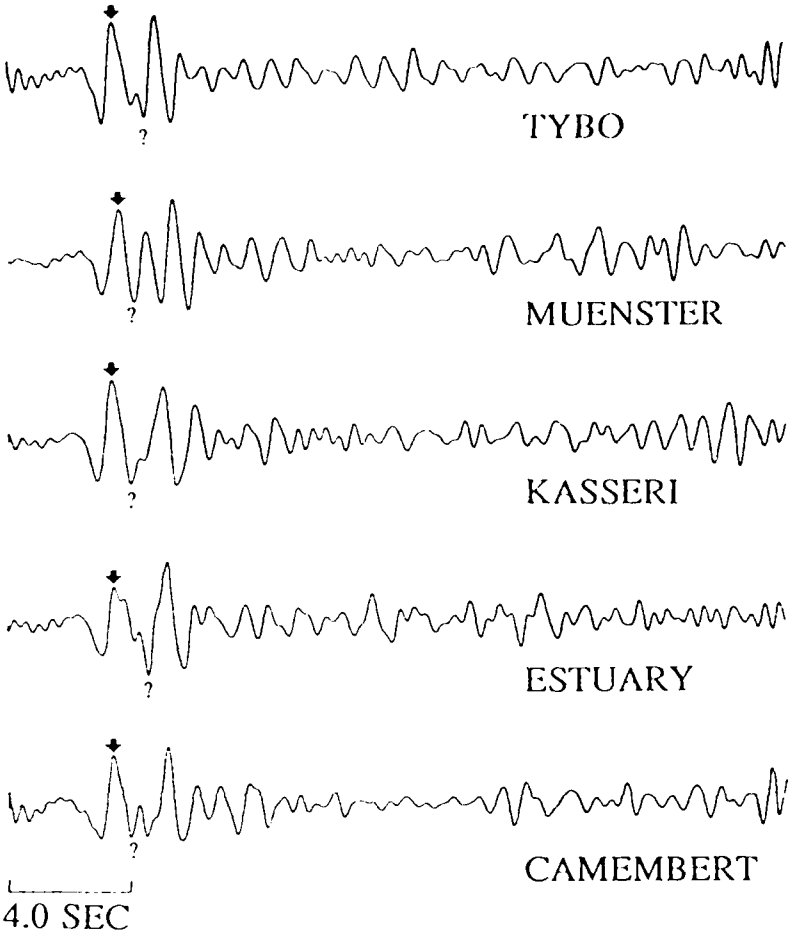

Figure 35. Source time function estimates for five Pahute Mesa explosions at GBA. VSB wavelets have been removed in these deconvolutions.

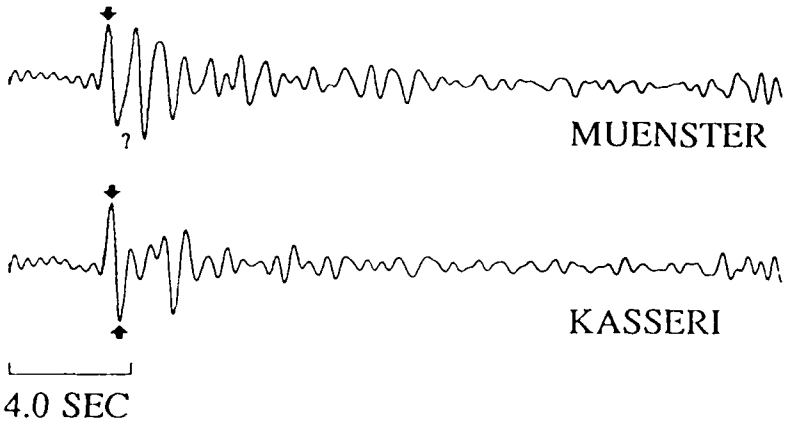

Figure 36. Source time function estimates for two Pahute Mesa explosions at WRA. VSB wavelets have been removed in these deconvolutions.

Results for Yucca Flats events

Data for Yucca Flats events were available at three of the AWRE arrays: EKA, GBA, and YKA. The locations of the events are shown in Figure 37, and deconvolved source time functions with the VSB source pulse removed are shown in Figures 38 to 40. The recordings of Yucca Flats events exhibit complex waveforms and ringing at all arrays. This is commonly attributed to reverberations in the low velocity sediments at Yucca Flats (for finite difference simulations, see McLaughlin et al 1986a). It appears that merely factoring out the instrument and t* operators is not sufficient and some deconvolution of the near source ringing would have to be introduced. At this point, this would have gone beyond the immediate objectives of this project, although we plan to attempt this in the future. The waveforms at YKA are also triplicated by upper mantle discontinuities. The late, ringing wavetrain about 12 seconds after the first arrival in many of the waveforms in Figure 40 is probably due to the forward branch associated with the 600 km discontinuity. Tentative picks for some "pP" arrivals for Yucca Flats show them to be quite late, but the ringing makes such picks doubtful. Since NTS is a low Q site (Der et al 1982, 1985) we have a very limited bandwidth to work with at telesesimic distances. The trace reconstructions for the Yucca Flats events are good reproductions of the original traces (Figure 41). Often the reconstructions seem to have better signal-to-noise ratios than the original traces. This is not surprising since our deconvolution method can be considered as an array processor that uses the redundancy of the data set to enhance the source and site factors. Moreover, by limiting the frequency ranges in the deconvolutions and reconstructions we have reduced the amplitudes of the low and high frequency background noise seen in the original records.

The data set of events recorded at EKA (Figure 38) is particularly interesting in that it includes Piledriver, one of the few granite shots at NTS and an important calibration event in

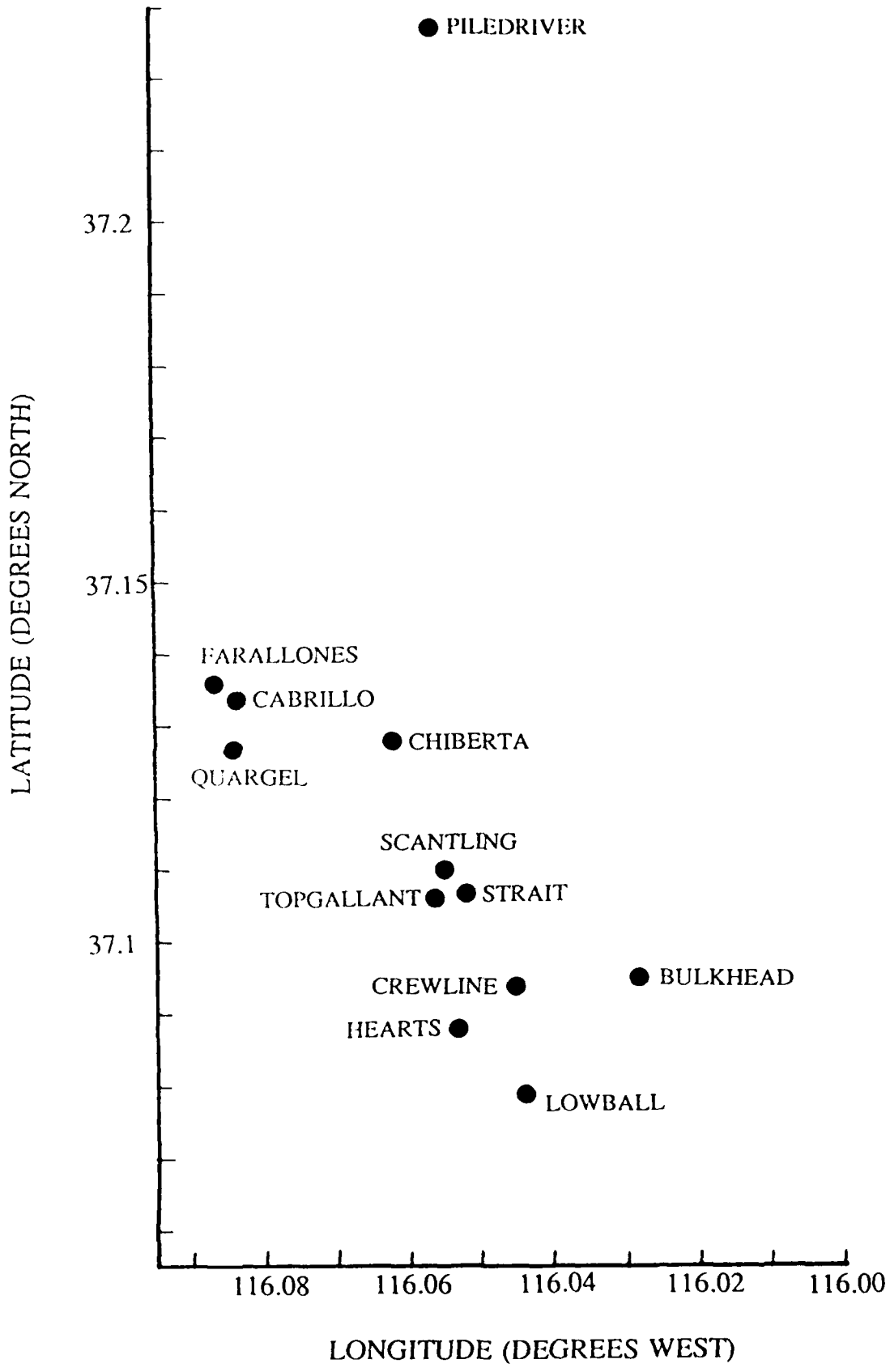

Figure 37. Locations of the Yucca Flats events analyzed in this report.

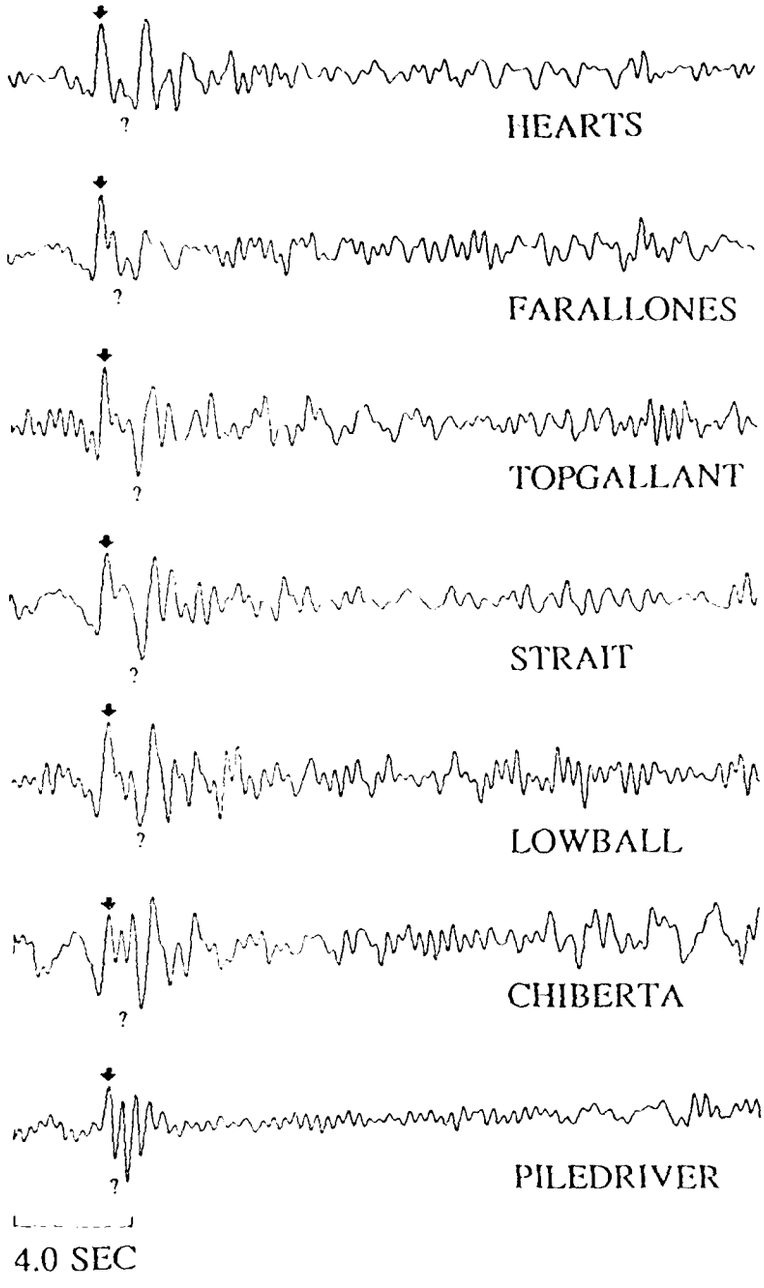

Figure 38. *Source time function estimates for a set of Yucca Flats events at EKA. VSB wavelets have been removed in these deconvolutions. The explosion Piledriver (north of Yucca Flats) shows a simpler waveform without the ringing associated with Yucca Flats events.*

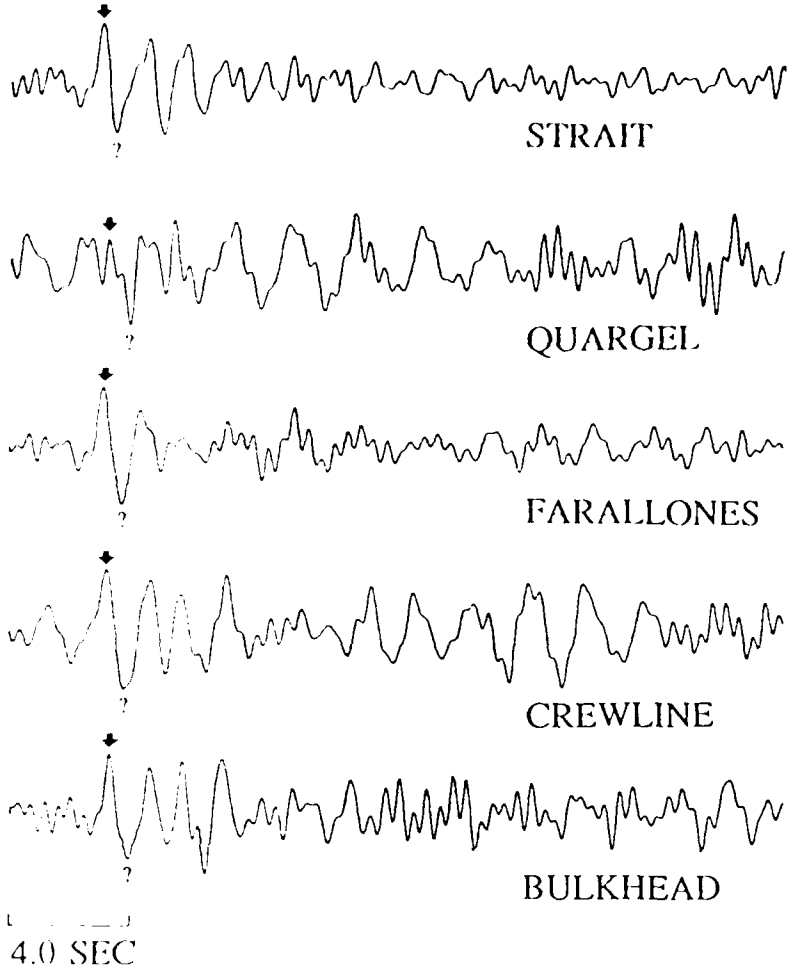

Figure 39. Source time function estimates for a set of Yucca Flats events at GBA. VSB wavelets have been removed in these deconvolutions.

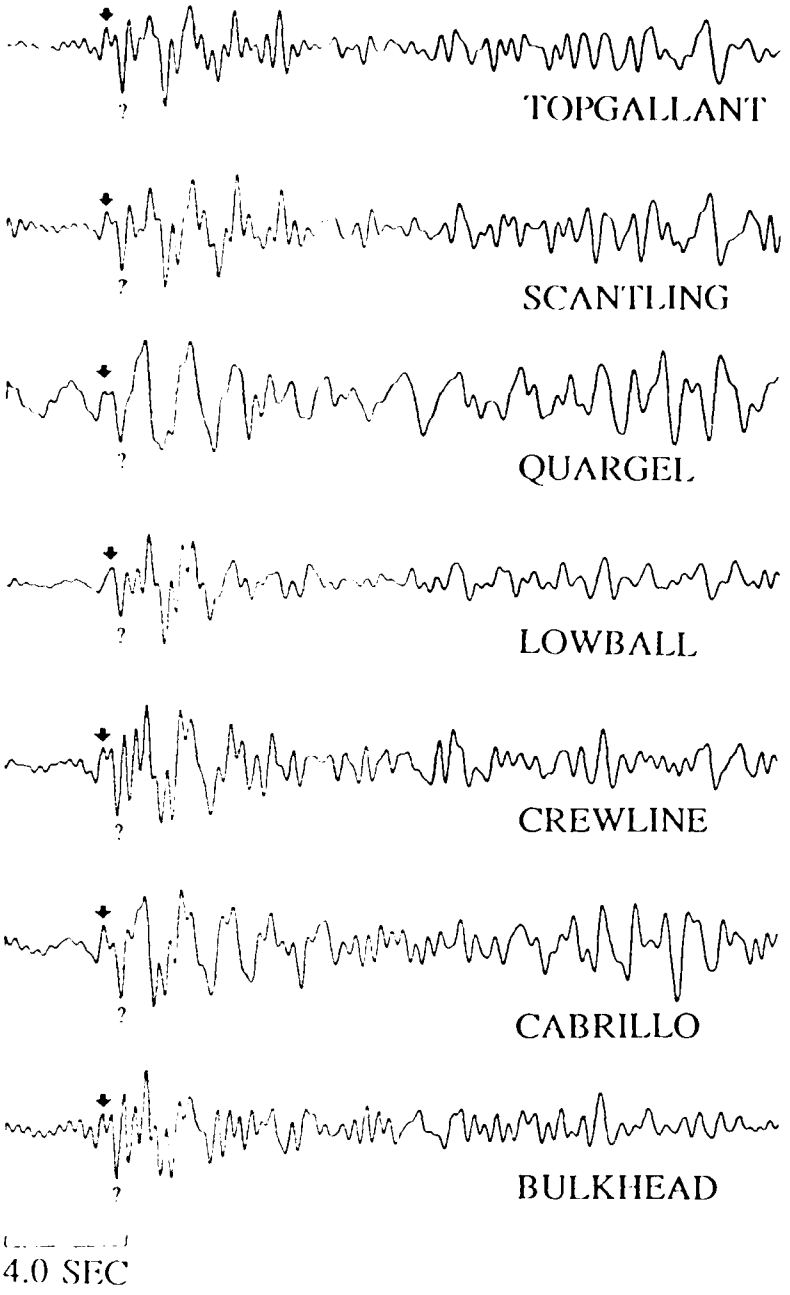

Figure 40. Source time function estimates for Yucca Flats events at YKA. The second set of arrivals is an upper mantle triplication. VSB wavelets have been removed in these deconvolutions.

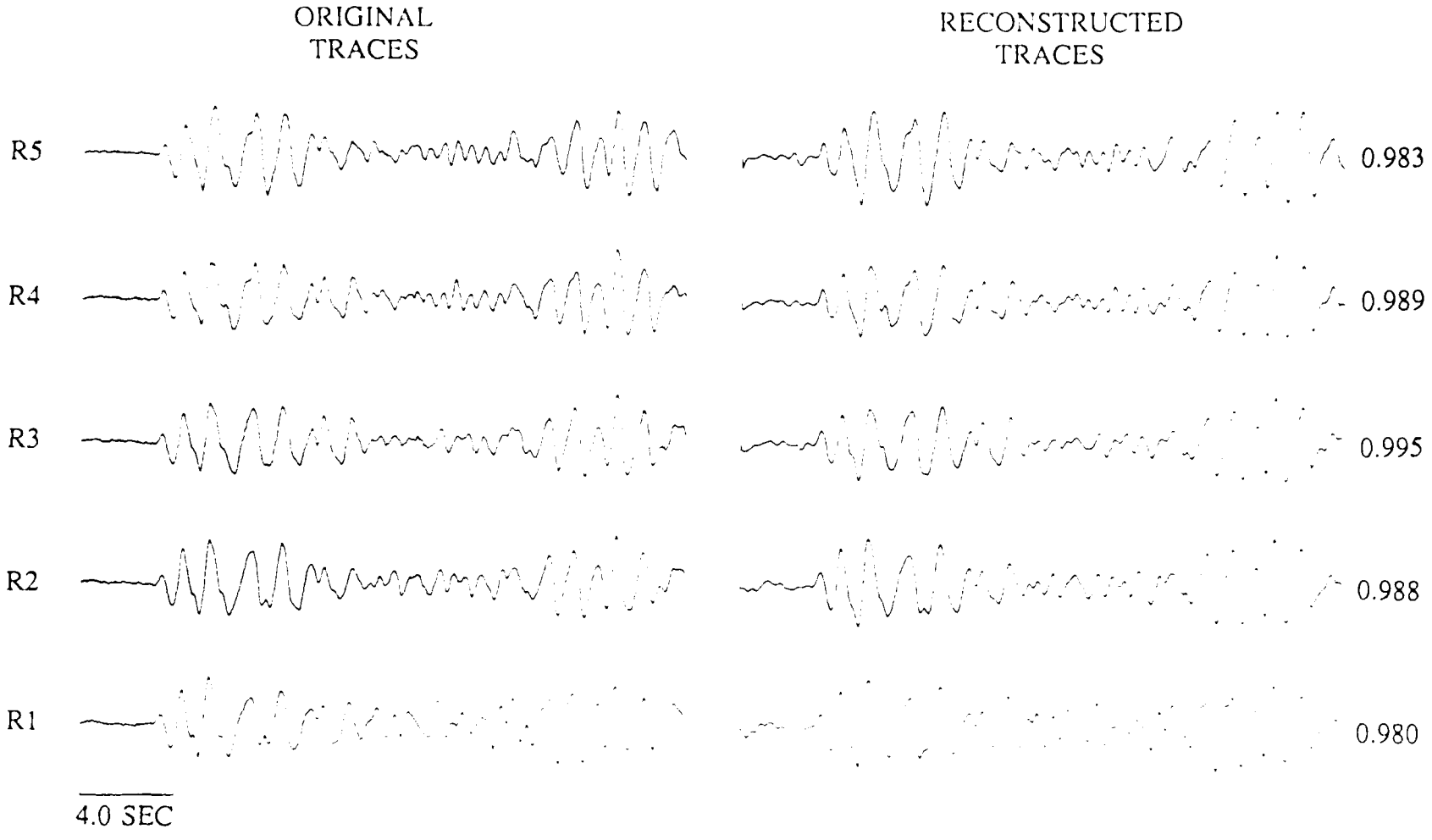

Figure 41. Examples of trace reconstructions (for event Cabrillo) at YKA as compared to original traces.

many studies. This event is not located at Yucca Flats but in a granite body north of it. Due to the short distance between Yucca Flats and the location of Piledriver, the recording site factors for Yucca Flats can also be expected to be applicable for Piledriver. The deconvolution for Piledriver it is relatively simple compared to those for the Yucca Flats events. Piledriver exhibits a double negative peak following the first positive arrival (P). The first of these is timed appropriately for the expected pP, though we do not have an explanation for the second negative peak.

Results for three-component data

The particle motions of teleseismic body waves are only in the first approximation linear for P and S. Even for simple layered structures of the crust the motion becomes elliptical in the most complex manner (Su and Dorman 1965) with prograde and retrograde motions in the various frequency bands. For realistic, three dimensional models of the near-station geology the motion becomes truly complex and three dimensional even for supposedly simple, linear P waves. While the first few cycles of the P wave are reasonably linear-elliptical in the plane of the azimuth of the arrival, the transverse component quickly builds up with time, approaching to a respectable fraction of the vertical and radial components in energy. It is a logical extension of the deconvolution work on multiple sites to approach the problem by treating each component of motion as a separate "site" in the deconvolution process. Each component will have a "site factor" in the frequency domain which characterizes the transformation of the motion due to local geology, these factors will depend, of course, on the slowness vector (azimuth-distance) of the P arrivals and may thus be used to recognize or characterize source regions of P waves.

The approach developed here is fundamentally different from practically all of the 3-component processing work being done recently (Christofferson et al 1986, Harris 1981)

instead of assuming a simply polarized wave appropriate to a halfspace, we plan to utilize the particle motion as it is, with all its complexities. A knowledge base of such characteristics may be accumulated observationally for a large number of source areas, without the need for understanding the detailed mechanism of the generation of complex particle motion. Although such an approach may be less practical presently, advances of computer technology will make it quite practical to store such information. We believe that source regions may be identified quickly and automatically by recognizing patterns of 3-component site factors rather than computing back-azimuths based on simplistic assumptions about polarization patterns. Any systematic deviations between the true azimuths and the back azimuths can be automatically accounted for in such schemes, as long as the master events used to derive the 3-component "site" factors are accurately located (possibly independently).

To test such concepts we have assembled a data base of four master events at the Kazakh test site as recorded at the RSTN station network. The deconvolved source time functions appear to be quite simple for these, mainly consisting of P and (presumably) pP arrivals as marked (Figure 42). The site impulse responses tend to be the most complex on the transverse components building up gradually with time, as expected, but simpler and impulselike on the vertical and radial components (Figure 43). Nevertheless, all the component "site" time functions seem to be much more complicated at RSCP and RSSD, two sites the geological structure under which have been shown to be complex by other studies (Owens et al 1986). Some raw data traces of these events are shown in Figure 44, and opposing them, we show the trace reconstructions for easy comparison. The good similarity of the original and reconstructed traces show that the "site" approach works well for three component data despite the larger variation of the back azimuths from the source region compared to seismic arrays, and that the complexities in particle motion can be reliably characterized by "component-site" transfer functions.

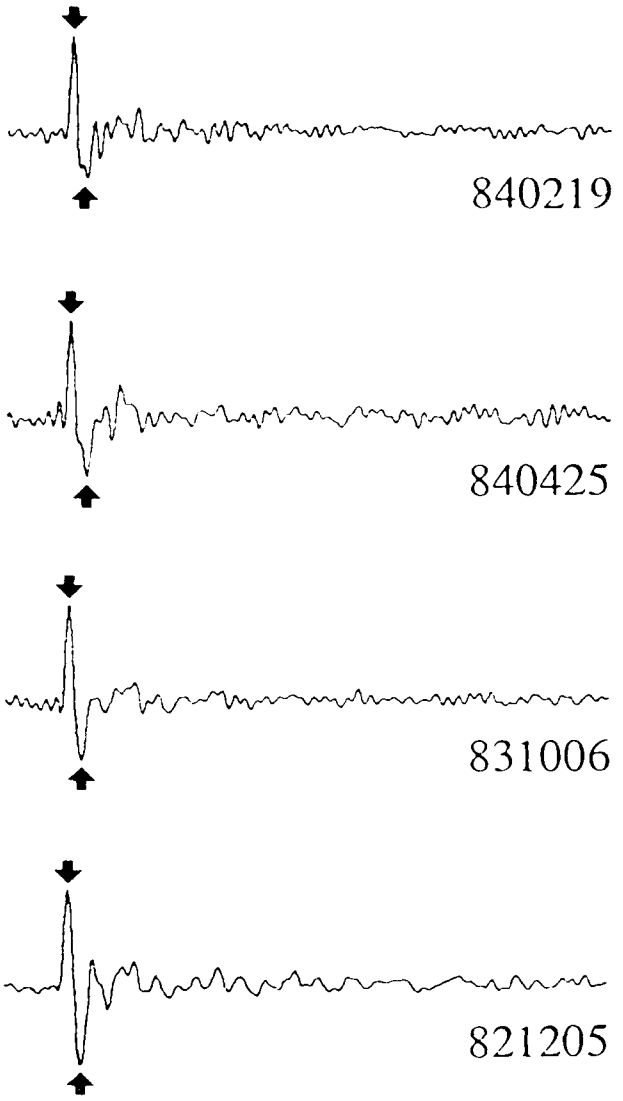

Figure 42. Source time function estimates for four E-EKTS events obtained from a data set from RSTN three component recordings. VSB wavelets have been recovered by deconvolutions. All of these show the prominent "pP" arrival.

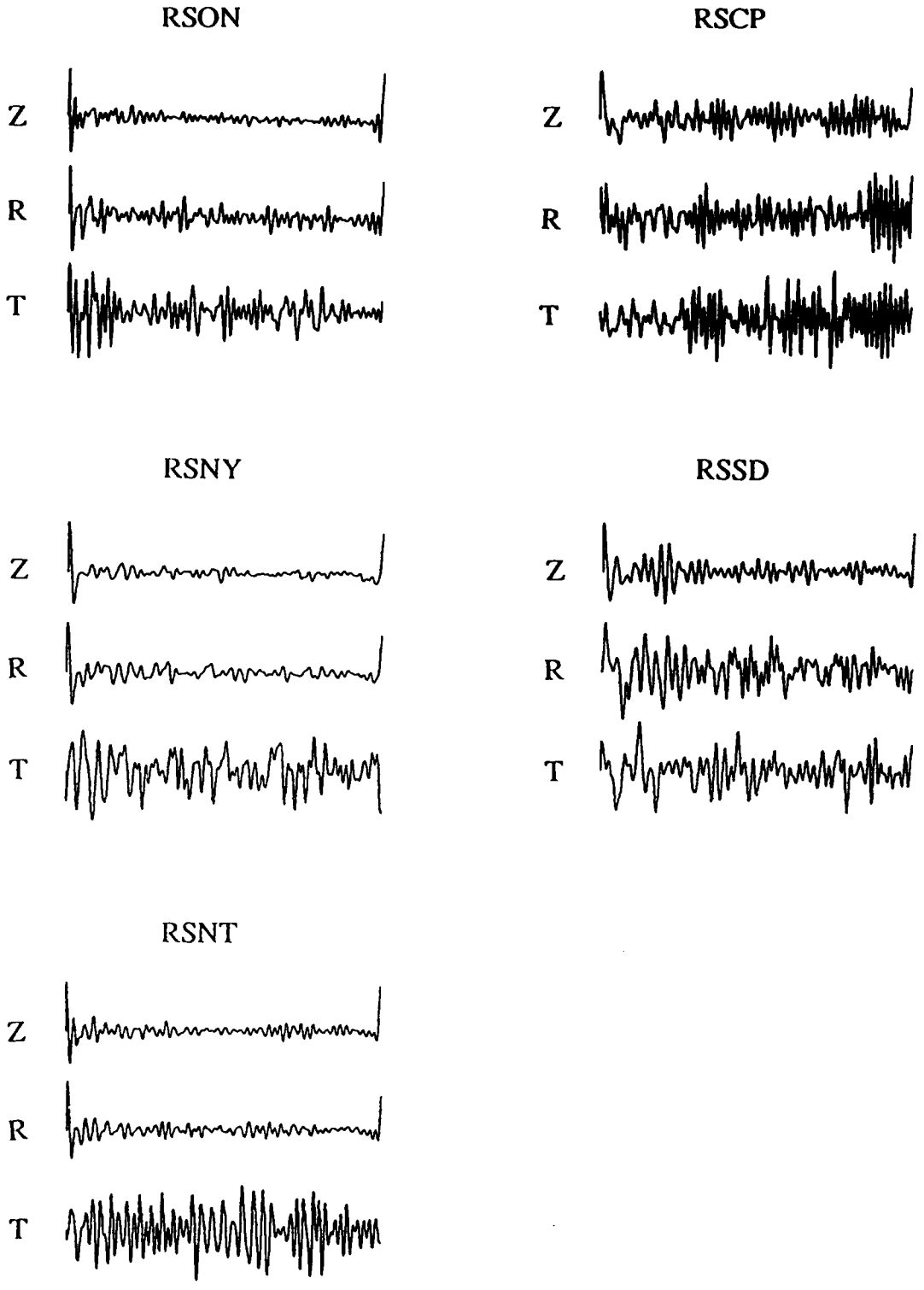

Figure 43. Site time function estimates for all components at the five RSTN stations. The RSCP and RSSD site functions are considerably more complex than those for RSON, RSNY and RSNT. This may be due to more complex geological structures at the former stations.

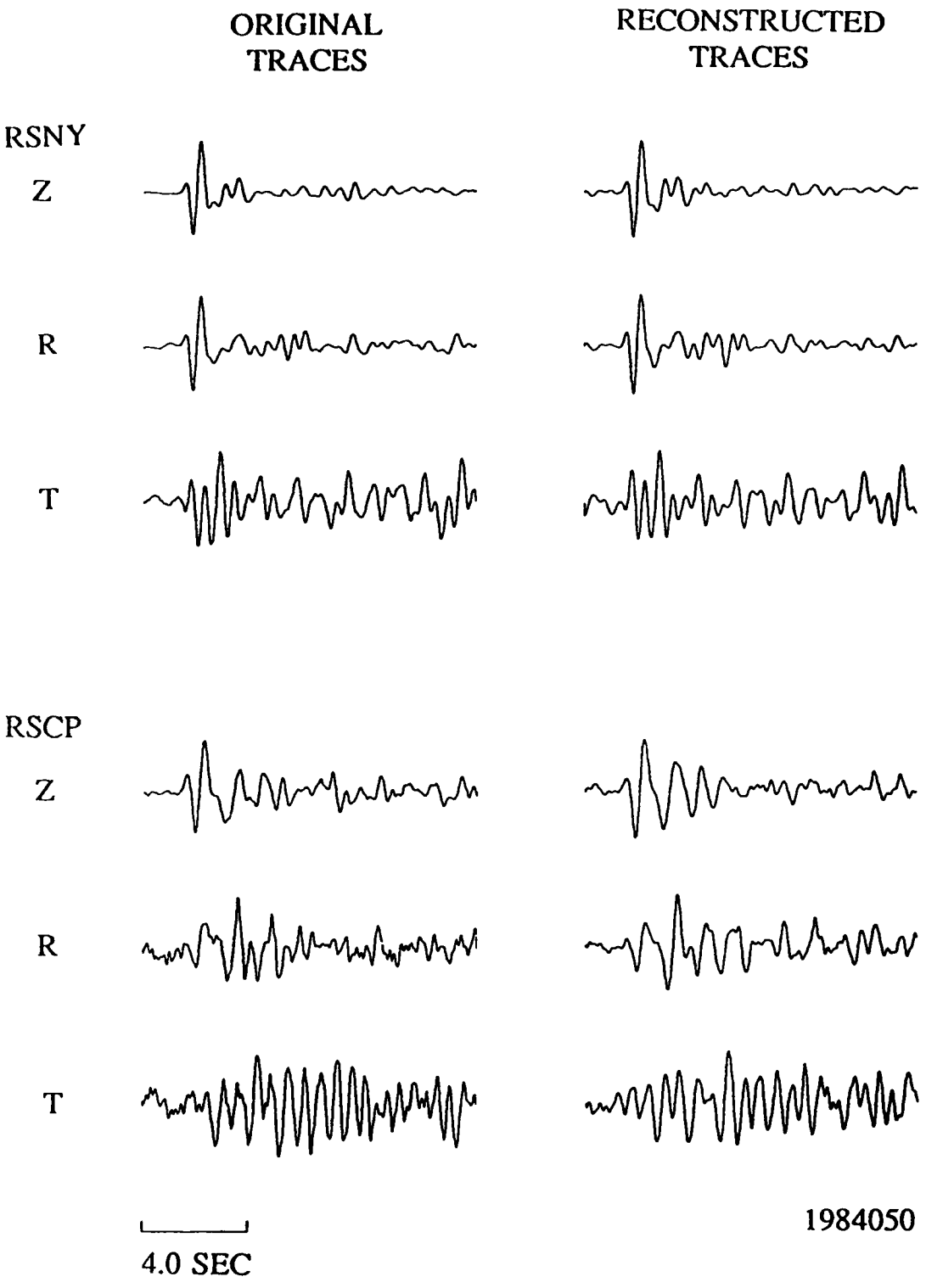

Figure 44. Original and reconstructed traces at three component RSTN stations for a E-EKTS event. These reconstructions are quite good considering the fact that the RSTN stations cover a wide area.

USE OF DECONVOLUTION RESULTS FOR YIELD ESTIMATION

From the above discussions it is apparent the the deconvolution method uses repeated averaging over sites and events in an iterative manner, while deconvolving the source and site factors as well as the factors (instrument, t* and source wavelet) assumed to be known. The basic idea is to average *waveforms* such that all traces are given an equal weight. In order to ensure this the whole process is started by equalizing all trace amplitudes by initial amplitude factors. This ensures that the largest event does not dominate the site factor estimates and that the site with the largest amplitude does not contaminate the source factor estimates. This way the traces with both the smallest and the largest absolute amplitudes can be reconstructed with about equal fidelity to the original waveforms. An inevitable consequence of this approach is that the absolute signal amplitudes become intractable through the process. The idea of waveform averaging, an essential ingredient of this deconvolution method, is in basic conflict with the preservation of the absolute signal amplitudes. To preserve the approximate equal weighting of the trace *waveforms* inside the program the t*, instrument and source wavelet amplitudes are all normalized, rather than scaled. In order to go back to absolute amplitudes we must relate the signal amplitudes or m_b to the deconvolution results through the absolute amplitudes measured for the set of traces originally entering the procedure.

A better measure of the event size may be constructed the following way; by dividing out the source and site time functions and instrument response in which the first positive peak is normalized to unity and a t* operator that is not normalized the result (properly limited in bandwidth to match the band used for the deconvolution) will be a simple impulsive waveform the log(amplitude) of which may be used as a new "m_b" parameter. The deconvolution of all these factors constitutes a set of corrections for site effects, pP, instrument and t^* with the absolute amplitude information in the original wave amplitudes restored. The absolute

amplification factors due to sites will still have to be averaged out in the absence of any absolute site amplitude reference levels in the data. During the continuation of this work we shall attempt to test this new magnitude measure.

CONCLUSIONS

Most of the ambiguities associated with the pP estimation methods proposed in the past are associated with the fact that, for most explosions, the simple P+pP model is not valid. This can be verified by analyses of interevent spectral ratios and the results of our multichannel deconvolutions. In addition, for single channels the site effects will also disguise any pP arrivals even if they are present. Therefore, most results concerning pP using the P+pP model, narrow band synthetics, cross-equalization and spectral fitting, can be shown to be invalid by broad-band analyses.

* C-EKTS explosion deconvolutions commonly show no or a poorly defined pP arrival. The radiation from the C-EKTS site seems to have strong azimuthal asymmetries as evidenced by the poor reconstructions of the original traces following joint deconvolutions of data from all arrays.

* E-EKTS explosions deconvolved appear to have relatively simple source functions with a direct P followed by a pP arrival with a time delay in the 0.3-0.6 sec range.

* Novaya Zemlya explosions show a complex late arrival instead of a well recognizable pP. YKA waveforms and deconvolutions are complex compared to deconvolutions at EKA and GBA.

* For Yucca Flats events we have obtained poor deconvolution results because of the extremely limited bandwidth of these signals and the extreme ringing at that test site. Piledriver deconvolutions at EKA show a simple waveform indicating two arrivals with negative polarity following P.

* The French nuclear explosions in the Sahara gave complex source functions with strong azimuthal variations.

* Application of the multichannel deconvolution technique to three component recordings indicates that the site response concept is applicable to 3-dimensional particle motion. This indicates that this approach can have application to three component processing.

* Reconstructions from the site and source time series and the source wavelets show excellent agreement with the original traces including fine details in the coda. The coda is partially due to both near site and source scattering.

FUTURE WORK

During the next year's work on this contract we shall continue our data analyses on additional data sets; the Swedish network, NORSAR will be also utilized in addition to the AWRE arrays. More data from NTS will be analyzed in addition to the Yucca Flats explosions. For Novaya Zemlya we shall seek data representing both the northern and southern tests areas.

To obtain a better understanding of the site functions we shall analyze 20 earthquakes and other events with azimuths centered at but different from those of the Kazakh and NTS test sites. This will enable us to test the sensitivity of site transfer functions to deviations in azimuth-slowness vector). The second year's work will also include the data analyses for Sinkiang explosions.

By studying the azimuthal asymmetries in the P wave radiation from various test sites and correlating them with previous studies of strain release light may be shed on the possible effects of such mechanisms on the short period P wave radiation and the m_b measurement. NTS and Kazakh are the most studied test sites with respect to strain release with numerous source mechanism solutions and F factor results which will be utilized.

By deconvolving the normalized reconstructions from the original traces as described above we shall test the new energy measure for explosion generated P waves provided by an integral of the resulting simple pulse. This new magnitude measure will be compared to actual yields (if known) or standard m_b. The result thus produced will be essentially corrected for site, attenuation and pP effects.

ACKNOWLEDGEMENTS

This work was supported by the Defense Advanced Research Projects Agency under contract MDA903-84-C-0289. The views and conclusions contained in this paper are those of the authors and should not be interpreted as representing the official policies, either expressed or implied, of the Defense Advanced Research Projects Agency or the U.S. government.

The authors gratefully acknowledge contributions of their coworkers, especially Drs. K. L. Mclaughlin and I. N. Gupta, who constantly contributed to this work by constructive criticism and useful ideas.

REFERENCES

Bache, T.C. (1982), Estimating the yield of underground nuclear explosions. *Bull. Seism. Soc. Am., 72,* S131-S168.

Bakun, W.H. and L.R. Johnson (1973). The deconvolution of teleseismic P waves from explosions MILROW and CANNIKIN, *Geophys. J. R. astr. Soc., 34,* 321-342.

Blandford, R.R., Cohen, T.J. and J.W. Woods (1973), An iterative approximation to the mixed-event processor. Technical Report *SDAC-TR-73-7,* Teledyne-Geotech, Alexandria, VA.

Burdick, L.J. and D.V. Helmberger (1979), Time functions appropriate for nuclear explosions. *Bull. Seism. Soc. Am., 69,* 957-974.

Christofferson, A., Husebye, E.S. and S.F. Ingate (1986), Wavefield decomposition using ML-probabilities in modelling single-site 3-component records. (Submitted to the Geophys. J. R. astr. Soc.)

Cohen, T.J. (1970). Source depth determinations using spectral estimation and cepstral analysis, *Geophys. J. R. astr. Soc., 20,* 223-231.

Cohen, T.J. (1975). Ps and pP phases from seven Pahute Mesa events, *Bull. Seism. Soc. Am., 65,* 1029-1032.

Cormier, V.F. (1982). The effect of attenuation on seismic body waves, *Bull. Seism. Soc. Am., 72,* S169-S200.

Dahlman, O. and H. Israelson (1977). *Monitoring Underground Nuclear Explosions,* Elsevier Scientific Publishing Company, Amsterdam.

Der, Z.A., McElfresh, T.W. and A. O'Donnell (1982), An investigation of the regional variations and frequency dependence of anelastic attenuation in the mantle under the United States in the .5-4 Hz band. *Geophys. J. R. A. S., 69,* 67-100.

Der, Z.A., R.H. Shumway, L.M. Anderson, T.W. McElfresh, and J.A. Burnetti (1983). Analysis of estimators for pP times and amplitudes, Technical Report *VSC-TR-83-17,* Teledyne Geotech, Alexandria, Virginia.

Der Z.A. and A.C. Lees (1985). Methodologies for estimating t*(f) from short period body waves and regional variations of t*(f) in the United States. *Geophys. J. R. A. S., 82,* 125-140.

Der, Z.A., McElfresh, T.W., Wagner, R. and J. Burnetti (1985), Spectral characteristics of P waves from nuclear explosions and yield estimation. *Bull. Seism. Soc. Am., 75,* 379-390.

Der, Z.A., R.H. Shumway, and A.C. Lees (1986a). Multichannel deconvolution of P waves at seismic arrays (to be published in the Bull. Seism. Soc. Am.).

Der, Z.A., Shumway, R.H., Lees, A.C. and E. Smart (1985), Multichannel deconvolution of P waves at seismic arrays. TGAL-85-4, Teledyne-Geotech, Alexandria, VA.

Douglas, A., Marshall, P.D. and J.B. Young (1986) The P waves from the Amchitka Island explosions (manuscript in preparation).

Filson, J. and C.W. Frasier (1972). Multisite estimation of explosive source parameters, *J. Geophys. Res., 77,* 2045-2061.

Greenfield (1971), Short period P wave generation by Rayleigh wave scattering at Novaya Zemlya. *J. Geophys. Res., 77,* 1988.

Harris (1981), recursive least squares with linear constraints. Proceedings of the IEEE Conference on Acoustics, Speech and Signal Processing, March 30,31 and April 1, 1981.

Hart, R.S., D.M. Hadley, G.R. Mellman, and R. Butler (1979). Seismic amplitude and waveform search, Technical Report *SGI-P-70-002,* Sierra Geophysics, Arcadia, California.

Israelson, H. (1983). Deconvolution based on source scaling applied to teleseismic signals, *FOA Rapport C 20514-T1,* Forsvarets Foskningsanstalt, Huvudavdelning 2, Stockholm, Sweden.

Jurkevics, A. and R. Wiggins (1984). A critique of seismic deconvolution methods, *Geophysics, 49,* 2109-2116.

Kemerait, R.C. and A.F. Sutton (1982). A multidimensional approach to seismic event depth estimation, submitted to a special issue of *Seismic Analysis and Discrimination,* Elsevier Publishing Co.

King and Calcagnile (1976), P-wave velocities in the upper mantle beneath Fennoscandia and western Russia, *Geophys. J. R. A. S., 46,* 407-432.

Lay, T., Arvesen, C.G., Burger, R.W. and L.J. Burdick (1984a). Estimating seismic yield and defining distinct test sites using complete waveform information, Technical Report *WCCP-R-84-04,* Woodward-Clyde Consultants, Pasadena, CA.

Lay, T., Burdick, L.J. and D.V. Helmberger (1984b). Estimating yields of the Amchitka tests by waveform intercorrelation. *Geophys. J. R. Astr. Soc., 78,* 181-207.

Levy, S. and P.K. Fullagar (1981). Reconstruction of sparse spike train from a portion of its spectrum and application to high resolution deconvolution, *Geophysics, 46,* 1235-1243.

Lundquist, G.M., G.R. Mellman and D.M. Hadley (1980). Relative receiver functions for three different array concepts, Technical Report *SGI-R-80-021.* Sierra Geophysics, Inc., Arcadia, California.

Marshall, P.D. (1972). Some seismic results from a worldwide sample of large underground explosions, *AWRE Report O 49/72,* AWRE, MOD(PE), Aldermaston, Berkshire, England.

Marshall, P.D., T.C. Bache, and R.C. Lilwall (1984). Body wave magnitudes and locations of Soviet underground explosions at the Semipalatinsk test site, *AWRE Report No. O 16/84,* AWRE, MOD(PE), Aldermaston, Berkshire, England.

Marshall, P.D. et al (1986). Report in preparation.

McLaughlin, K.L., L.M. Anderson, Z.A. Der, T.W. McElfresh, and A.C. Lees (1986a). Effects of local geologic structure on Yucca Flats, NTS, explosion waveforms: 2-dimensional finite difference calculations, Technical Report, *TGAL-86-4*, Teledyne Geotech, Alexandria, Virginia 22314.

McLaughlin, K.L., R.S. Jih, Z.A. Der, and A.C. Lees (1986b). The effects of near-source topography on explosion waveforms: teleseismic observations and linear finite difference calculations, *TGAL-86-03*, Teledyne Geotech, Alexandria, Virginia 22314.

McLaughlin, K.L., R.O. Ahner, and M.E. Marshall (1986c). Maximum likelihood event magnitudes and log (max/a) at the Novaya Zemlya and C-EKTS test sites, *TGAL-86-02*, Teledyne Geotech, Alexandria, Virginia 22314.

Mellman, G.R. and S.K. Kaufman (1981). Relative waveform inversion, *SGI-R-81-048*, Sierra Geophysics, Redmond, WA.

Mellman, G.R., S.K. Kaufman and W.C. Tucker (1984). Depth corrections for yield estimation of underground nuclear explosions, In *Basic Research in the VELA Program*, AFOSR review meeting, Santa Fe, New Mexico, May 7-9, 1984.

Mowat, W.M.H. and R.F. Burch (1977). Handbook for the stations which provide seismograms to the Blacknest Seismolotical Centre United Kingdom, *REF No. 44/47/29, Issue 2*, AWRE, MOD(PE), Aldermaston, Berkshire, England.

Mueller, R.A. and J.R. Murphy (1971), Seismic characteristics of underground nuclear detonations. *Bull. Seism. Soc. Am., 61*, 1675-1692.

Oldenburg, D.W. (1981). A comprehensive solution of the linear deconvolution problem, *Geophys. J. R. astr. Soc., 65*, 331-358.

Oldenburg, D.W., Levy, S. and K.P. Whittal (1981). Wavelet estimation and deconvolution, *Geophysics, 46*, 1528-1542.

Owens, T.J., Taylor, S.R. and G. Zandt (1986), Crustal structures at RSTN stations determined from inversion of broadband teleseismic P-waveforms. Lawrence Livermore National Laboratory, UCRL-95104. (Preprint).

Robinson, E.A. and S. Treitel (1980). *Geophysical Signal Analysis*, Prentice Hall, Englewood Cliffs, New Jersey.

Rodean, H.C. (1979). ISC events from 1964 to 1976 at and near the nuclear testing ground in eastern Kazakhstan, *UCRL-52856*, Lawrence Livermore Laboratory, Livermore, California 94550.

Shumway, R.H. (1984). Deconvolution of multiple time series, In *Statistical Analysis of Time Series*, Japan-U.S. joint seminar, Tokyo.

Shumway, R.H. and R.R. Blandford (1978). On detecting and estimating multiple arrivals from underground nuclear explosions, Technical Report *SDAC-TR-77-8*, Teledyne-Geotech, Alexandria, VA.

Shumway, R.H. and Z.A. Der (1985). Deconvolution of multiple time series, *Technometrics, 27*, 385-393.

Su, S.S. and J. Dorman (1965), The use of leaking modes in seismogram interpretation and in studies of crust-mantle structure. *Bull. Seism. Soc. Am., 55*, 989-1021.

von Seggern, D.H. and R.R. Blandford (1972). Source time functions and spectra for underground nuclear explosions, *Geophys. J. R. astr. Soc., 31*, 83-97.

Wiggins, R.A. (1978). Minimum entropy deconvolution, *Geoexploration, 16*, 21-35.

(THIS PAGE INTENTIONALLY LEFT BLANK)

DISTRIBUTION LIST
FOR UNCLASSIFIED REPORTS
DARPA-FUNDED PROJECTS
(Last Revised: 5 Jan 1987)

RECIPIENT	NO. OF COPIES
DEPARTMENT OF DEFENSE	
DARPA/GSD ATTN: Dr. R. Alewine and Dr. R. Blandford 1400 Wilson Boulevard Arlington, VA 22209-2308	2
DARPA/PM 1400 Wilson Boulevard Arlington, VA 22209-2308	1
Defense Intelligence Agency Directorate for Scientific and Technical Intelligence Washington, D.C. 20301	1
Defense Nuclear Agency Shock Physics Washington, D.C. 20305-1000	1
Defense Technical Information Center Cameron Station Alexandria, VA 22314	12
DEPARTMENT OF THE AIR FORCE	
AFGL/LWH ATTN: Dr. J. Cipar and Mr. J. Lewkowicz Terrestrial Sciences Division Hanscom AFB, MA 01731-5000	2
AFOSR/NPG ATTN: Director Bldg. 410, Room C222 Bolling AFB, Washington, D.C. 20332	1

AFTAC/CA 1
ATTN: STINFO Officer
Patrick AFB, FL 32925-6001

AFTAC/TG 3
Patrick AFB, FL 32925-6001

AFWL/NTESG 1
Kirtland AFB, NM 87171-6008

DEPARTMENT OF THE NAVY

NORDA 1
ATTN: Dr. J.A. Ballard
Code 543
NSTL Station, MS 39529

DEPARTMENT OF ENERGY

Department of Energy 1
ATTN: Mr. Max A. Koontz (DP-52)
International Security Affairs
1000 Independence Avenue
Washington, D.C. 20545

Lawrence Livermore National Laboratory 2
ATTN: Dr. J. Hannon and Dr. M. Nordyke
University of California
P.O. Box 808
Livermore, CA 94550

Los Alamos Scientific Laboratory 2
ATTN: Dr. K. Olsen and Dr. T. Weaver
P.O. Box 1663
Los Alamos, NM 87544

Sandia Laboratories 1
ATTN: Mr. P. Stokes
Geosciences Department 1255
Albuquerque, NM 87185

OTHER GOVERNMENT AGENCIES

Central Intelligence Agency 1
ATTN: Dr. L. Turnbull
OSI/NED, Room 5G48
Washington, D.C. 20505

U.S. Arms Control and Disarmament Agency 1
ATTN: Dr. M. Eimer
Verification and Intelligence Bureau, Rm 4953
Washington, D.C. 20451

U.S. Arms Control and Disarmament Agency 1
ATTN: Mrs. M. Hoinkes
Multilateral Affairs Bureau, Rm 5499
Washington, D.C. 20451

U.S. Geological Survey 1
ATTN: Dr. T. Hanks
National Earthquake Research Center
345 Middlefield Road
Menlo Park, CA 94025

U.S. Geological Survey 1
ATTN: Dr. R. Masse
Global Seismology Branch
Box 25046, Stop 967
Denver Federal Center
Denver, CO 80225

UNIVERSITIES

Boston College 1
ATTN: Dr. A. Kafka
Western Observatory
381 Concord Road
Weston, MA 02193

California Institute of Technology 1
ATTN: Dr. D. Harkrider
Seismological Laboratory
Pasadena, CA 91125

Columbia University 1
ATTN: Dr. L. Sykes
Lamont-Doherty Geological Observatory
Palisades, NY 10964

Cornell University 1
ATTN: Dr. M. Barazangi
INSTOC
Snee Hall
Ithaca, NY 14853

Harvard University 1
ATTN: Dr. J. Woodhouse
Hoffman Laboratory
20 Oxford Street
Cambridge, MA 02138

Massachusetts Institute of Technology 3
ATTN: Dr. S. Soloman, Dr. N. Toksoz, and Dr. T. Jordan
Department of Earth and Planetary Sciences
Cambridge, MA 02139

Southern Methodist University 1
ATTN: Dr. E. Herrin
Geophysical Laboratory
Dallas, TX 75275

State University of New York at Binghamton 1
ATTN: Dr. F. Wu
Department of Geological Sciences
Vestal, NY 13901

St. Louis University 2
ATTN: Dr. O. Nuttli and Dr. R. Herrmann
Department of Earth and Atmospheric Sciences
3507 Laclede
St. Louis, MO 63156

The Pennsylvania State University 1
ATTN: Dr. S. Alexander
Geosciences Department
403 Deike Building
University Park, PA 16802

University of Arizona 1
ATTN: Dr. T. Wallace
Department of Geosciences
Tucson, AZ 85721

University of California, Berkeley 1
ATTN: Dr. T. McEvilly
Department of Geology and Geophysics
Berkeley, CA 94720

University of California Los Angeles 1
ATTN: Dr. L. Knopoff
405 Hilgard Avenue
Los Angeles, CA 90024

University of California, San Diego 1
ATTN: Dr. J. Orcutt
Scripps Institute of Oceanography
La Jolla, CA 92093

University of Colorado 1
ATTN: Dr. C. Archambeau
CIRES
Boulder, CO 80309

University of Illinois 1
ATTN: Dr. S. Grand
Department of Geology
1301 West Green Street
Urbana, IL 61801

University of Michigan 1
ATTN: Dr. T. Lay
Department of Geological Sciences
Ann Arbor, MI 48109-1063

University of Nevada 1
ATTN: Dr. K. Priestley
Mackay School of Mines
Reno, NV 89557

University of Southern California 1
ATTN: Dr. K. Aki
Center for Earth Sciences
University Park
Los Angeles, CA 90089-0741

DEPARTMENT OF DEFENSE CONTRACTORS

Applied Theory, Inc. 1
ATTN: Dr. J. Trulio
930 South La Brea Avenue
Suite 2
Los Angeles, CA 90036

Center for Seismic Studies 2
ATTN: Dr. C. Romney and Mr. R. Perez
1300 N. 17th Street, Suite 1450
Arlington, VA 22209

ENSCO, Inc.
ATTN: Mr. G. Young 1
5400 Port Royal Road
Springfield, VA 22151

ENSCO, Inc. 1
ATTN: Dr. R. Kemerait
445 Pineda Court
Melbourne, FL 32940

Gould Inc. 1
ATTN: Mr. R. J. Woodard
Chesapeake Instrument Division
6711 Baymeado Drive
Glen Burnie, MD 21061

Pacific Sierra Research Corp. 1
ATTN: Mr. F. Thomas
12340 Santa Monica Boulevard
Los Angeles, CA 90025

Rockwell International 1
ATTN: B. Tittmann
1049 Camino Dos Rios
Thousand Oaks, CA 91360

Rondout Associates, Inc. 1
ATTN: Dr. P. Pomeroy
P.O. Box 224
Stone Ridge, NY 12484

Science Applications, Inc. 1
ATTN: Dr. T. Bache, Jr.
P.O. Box 2351
La Jolla, CA 92038

Science Horizons 2
ATTN: Dr. T. Cherry and Dr. J. Minster
710 Encinitas Blvd.
Suite 101
Encinitas, CA 92024

Sierra Geophysics, Inc. 2
ATTN: Dr. R. Hart and Dr. G. Mellman
11255 Kirkland Way
Kirkland, WA 98124

SRI International 1
ATTN: Dr. A. Florence
333 Ravensworth Avenue
Menlo Park, CA 94025

S-Cubed, A Division of 1
Maxwell Laboratories Inc.
ATTN: Dr. S. Day
P.O. Box 1620
La Jolla, CA 92038-1620

S-Cubed, A Division of
Maxwell Laboratories Inc.
ATTN: Mr. J. Murphy
11800 Sunrise Valley Drive
Suite 1212
Reston, VA 22091 — 1

Teledyne Geotech
ATTN: Dr. Z. Der and Mr. W. Rivers
314 Montgomery Street
Alexandria, VA 22314 — 2

Woodward-Clyde Consultants
ATTN: Dr. L. Burdick and Dr. J. Barker
556 El Dorado St.
Pasadena, CA 91105 — 2

NON-U.S. RECIPIENTS

National Defense Research Institute
ATTN: Dr. O. Dahlman
Stockholm 80, Sweden — 1

Blacknest Seismological Center
ATTN: Mr. P. Marshall
Atomic Weapons Research Establishment
UK Ministry of Defence
Brimpton, Reading RG7-4RS
United Kingdom — 1

NTNF NORSAR
ATTN: Dr. F. Ringdal
P.O. Box 51
N-2007 Kjeller
Norway — 1

OTHER DISTRIBUTION

To be determined by the project office — 9